VAGNER PASCUALINOTTO JUNIOR

FATIGUE LIFE ESTIMATION OF A NOTCHED COMPONENT USING FREQUENCY DOMAIN TECHNIQUE AND PROBABILISTIC LINEAR CUMULATIVE DAMAGE MODEL

São Paulo

2021

VAGNER PASCUALINOTTO JUNIOR

FATIGUE LIFE ESTIMATION OF A NOTCHED COMPONENT USING FREQUENCY DOMAIN TECHNIQUE AND PROBABILISTIC LINEAR CUMULATIVE DAMAGE MODEL

Revised Version

A dissertation submitted to the Polytechnic School of the University of São Paulo to obtain the degree of Master of Science.

Concentration Area:
Naval Architecture and Ocean Engineering

Supervisor: Prof. Dr. Diego Felipe Sarzosa Burgos

São Paulo

2021

Este exemplar foi revisado e corrigido em relação a versão original, sobre responsabilidade único do autor e com a anuência do seu orientador

São Paulo, 14 de outubro de 2021

Assinatura do Aluno: Vagner Pascualinotto Junior

Assinatura do Orientador: Diego Sarzosa Burgos

Catalogação-na-publicação

Pascualinotto Junior, Vagner
FATIGUE LIFE ESTIMATION OF A NOTCHED COMPONENT USING FREQUENCY DOMAIN TECHNIQUE AND PROBABLISTIC LINEAR CUMULATIVE DAMAGE MODEL / V. Pascualinotto Junior – versão corr.-- São Paulo, 2021.
111 p.

Dissertação (Mestrado) - Escola Politécnica da Universidade de São Paulo. Departamento de Engenharia Naval e Oceânica.

1.Fatigue Life Estimation 2.Cumulative Damage 3.Random Vibration 4.Power Spectral Density I.Universidade de São Paulo. Escola Politécnica. Departamento de Engenharia Naval e Oceânica II.t.

ACKNOWLEDGMENTS

First and above all, I thank God, for providing me with this opportunity.

My gratitude to my supervisor Prof. Dr. Diego Felipe Sarzosa Burgos for his support, guidance, tutoring and patience. A special thanks to my colleagues from Continental Brasil, Mr. Glenan Lago for the encouragement and Mr. Douglas Custodio for the support with the testing.

This dissertation is dedicated to my beloved wife Natalie Cuzziol Pascualinotto, for her unconditional support during the elaboration of this work, to my son Miguel Cuzziol Pascualinotto and my daughter Olivia Cuzziol Pascualinotto for being my source of inspiration.

ABSTRACT

Engineering structures are designed to withstand a variety of in service loading specific to their intended application. Random vibration excitation is observed in most of the structural components in the offshore, aerospace and automotive industries. Likewise, fatigue life estimation for structural components is fundamental for the verification of the design and assurance of the structural integrity throughout service. The linear cumulative damage model (Palmgren-Miner's rule) is still largely used for damage assessment, even though, its limitations are well-known. The scatter of fatigue testing data suggests that a probabilistic characterization of the material behavior is needed. In this work, the inherent uncertainties of the fatigue phenomenon as well as the influence of a geometrical discontinuity (notch) are explored in the fatigue life estimation of a structural component subjected to random vibration profiles. The fatigue life estimated using the methodology proposed in this work presented good agreement with testing results using both Lallane and Dirlik frequency domain counting methods. Lallane's method resulted in a 3% more conservative prediction than the average physical testing fatigue life, while Dirlik's method, resulted in an 8.4% higher predicted life for the most relevant load case.

Key words: Fatigue Life Estimation, Cumulative Damage, Random Vibration, Power Spectral Density

LIST OF FIGURES

LIST DE TABLES

LIST OF SYMBOLS

$[A\,]$:	Multiaxial Power Spectral Density input loading
CDF:	Cumulative Distribution Function
D_i:	Damage at a stress level *i*
$E[0]$:	Expected number of upward zero crossings
$E[P]$:	Expected number of positive peaks
f:	Frequency (Hz)
{P}:	Vector of external forces
FFT:	Fast Fourier Transform
FRF:	Frequency Response Function
f_{mean}:	Response PSD Mean Frequency
$[G]$:	Stress Response PSD matrix
$H(f)$:	Transfer Function
IFFT:	Inverse Fast Fourier Transform
k_f :	Fatigue Strength reduction Factor
k_t:	Elastic Stress Concentration factor
m_n:	n-th Spectral Moment
N_i :	Number of cycles to failure at a stress level *i*
n_i:	Number of cycles at a stress level *i*
$p(S_i)_{Dirlik}$	Dirlik's Probability Density Function
$p(S_i)_{Lallane}$	Lallane's Probability Density Function
$p(x)$:	Probability Density Function
PSD:	Power Spectral Density
PDF:	Probability Density Function
Q:	Quality Factor

$[Q]$	Dynamic Response Matrix
$R_{xx}(\tau)$:	Autocorrelation Function
rms:	Root Mean Square
S_i	Stress Amplitude *i*
$S_{yy}(f)$:	Power Spectral Density - Response
$S_{xx}(f)$:	Power Spectral Density – Excitation
TTF:	Time to Failure
$T_{exposure}$:	Exposure time under determined PSD profile
$\{u\}$	Displacement vector
x_{eff}:	Effective Distance
γ **:**	Irregularity Factor
ω_i**:**	Circular natural frequency (rad/s)
Ω_i**:**	Imposed circular frequency (rad/s)
σ_{ij}	Stress Response Tensor
σ_Φ:	Normal Stress oriented in the critical plane
$\{\Phi\}$	Mode Shape Vector
ζ:	Damping Ratio
μ_c:	Confidence Interval
μ_p:	Prediction Interval
χ:	Relative Stress Gradient

SUMMARY

1 INTRODUCTION

Engineering structures are designed to withstand a variety of in service loading specific to their intended application. Random vibration excitation is observed in most of the structural components in the offshore, aerospace and automotive industries. Likewise, fatigue life estimation for such components is fundamental to verify the design robustness assuring structural integrity throughout service.

Fatigue as a technical problem became evident around the middle of the 19th century, August Wöhler performed systematic fatigue tests of smooth and notched railway axles in the 1850s. In addition to the introduction of the S-N diagram, a plot of the number of cycles to failure at a given stress level, his work also led directly to the concept of a fatigue (or endurance) limit which represents the theoretical maximum cyclic load a material can withstand indefinitely without risk of fatigue failure [1].

Significant advances in the fatigue research were achieved with the mean stress effect studies by Gerber and Goodman, the development of fatigue safety diagrams by Haigh, investigation of reversed loading phenomena by Bauschinger, investigation of the notch effect on fatigue limit by Heyn, formulation of empirical laws to characterize fatigue limit by Basquin, the introduction of the crack growth energy balance by Griffith, life estimation under variable loading by Palmgren and the recognition of the statistical nature of fatigue by Weibull [1,2].

In the evaluation and prediction of the fatigue life of structures the role of mathematical and statistical models is crucial, due to the high complexity of the fatigue problem an efficient estimation of the corresponding parameters represents one of the most difficult challenges for the problem assessment, additionally, the possible shortage of data, which represents a common feature in the case of fatigue experimentation due to economic and/or time reasons.

Nonetheless, the fatigue damage assessment for components subjected to random excitation is an important concern in engineering. Fatigue damage evolves with the applied load in a cumulative manner which may lead to failure. Palmgren suggested the concept, which is known as the linear rule, Miner in 1945, first expressed the concept in mathematical form, where the measure of the damage is the cycle ratio with the assumption of constant work absorption per cycle (n_i) and characteristic amount of work absorbed at failure (N_i). The energy accumulation leads to a linear summation which at failure equals one, as shown in Equation (1). Despite of Palmgren-Miner's rule well-known limitations, such as, not

accounting for load sequence and interaction effects, it is still dominantly used in design due to its simplicity [3].

$$D_i = \sum_{i=1}^{k} \frac{n_i}{N_i} = 1 \quad (1)$$

The basic fatigue modeling for the parameter N_i consists of reproducing the fatigue behavior of materials under alternating stresses σ_a. Basquin's equation, presented in Equation (2) is a power law function representing fatigue life data using a linear function obtained in a log-log scale, its graphic representation is illustrated in Figure 1.

$$\sigma_a = A.(N_i)^B, \quad (2)$$

where A and B are constants that varies with the material.

Figure 1 - Basquin's S-N relationship in log-log scale

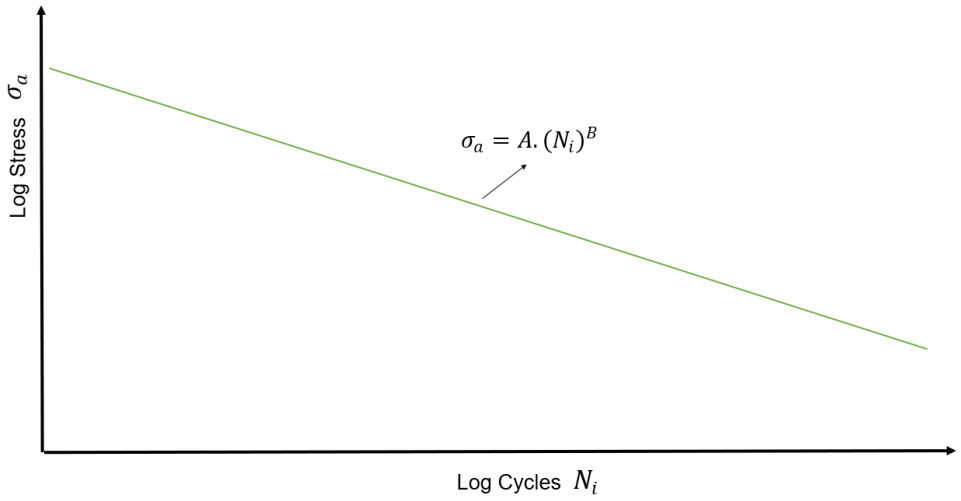

Source: Author

Due to the random characteristic of fatigue life, if several specimens were subjected to this type of tests with the same values of stress range and stress ratio, different fatigue lives would be observed.

An extension of this concept is the *p* quantile S-N curves, also called S-N-P curves, a generalization that relates the percentile of fatigue life to the applied stress or strain [4]. The percentile curves illustrate the variability of fatigue life, meaning that at p=0.5, 50% of the specimens fail above this curve and 50% below it. The percentile curves can also be used to

define design curves at any other percentile value, i.e p=0.01, where 1% of the failures (99% probability of survival) are expected to occur below this curve.

Figure 2a shows a fatigue test data due to a cyclic stress load, the percentiles curves are added to the raw testing data in Figure 2b.

Figure 2 - a) Fatigue test data on a semi-log plot due to constant alternating stress level b) Fatigue test data with percentiles curves

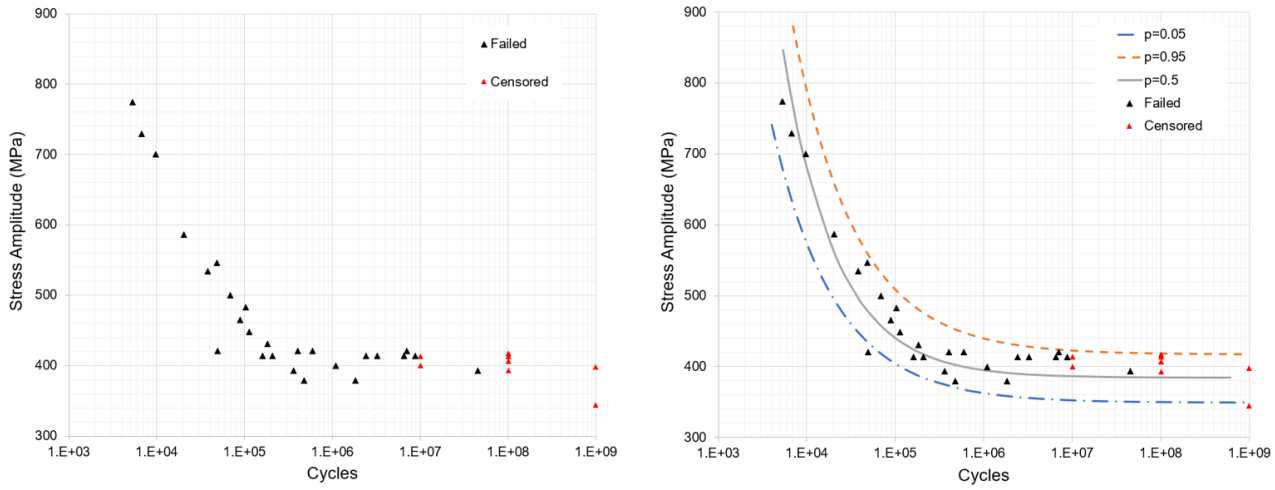

Source: Author, adapted from Pollak (2005)

Fatigue data on ferrous and titanium alloys reveal that specimens tested below a stress level are unlikely to fail. This limiting stress level called fatigue limit or endurance limit is observed by an accentuated curvature and an asymptotic behavior near the fatigue limit. Most nonferrous metals such as aluminum, copper and magnesium appear not to have a fatigue limit, the post endurance S-N slope for these materials gradually continues to drop.

For materials that exhibit fatigue limit, Nelson [5] fitted fatigue curves with non-constant standard deviation associated with each stress level utilizing maximum likelihood methods and modelled [6] the fatigue limited as a random parameter, where the test specimen would have different fatigue limits following a statistical distribution called “strength distribution”. Nelson’s work was the basis for the development of the Random Fatigue Limit (RFL) by Pascual and Meeker in [7]. The independent variable in a S-N test is the stress amplitude, the fatigue life distribution for a specific stress level is illustrated in Figure (3). The vertical distribution represents the variation of fatigue strength for a given life.

Figure 3 - Fatigue life and fatigue strength distributions

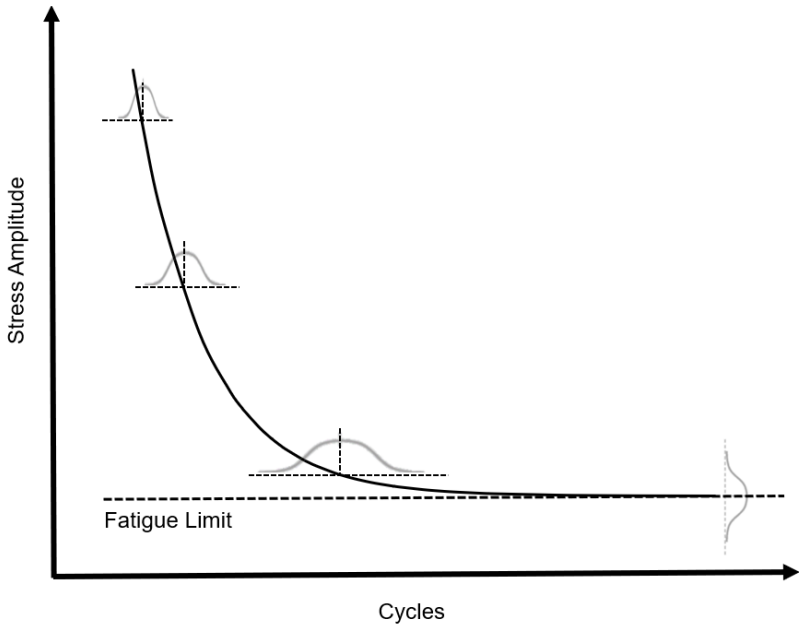

Source: Author

The fatigue damage is traditionally determined from time histories of loading, usually in the form of stress or strain. This approach is satisfactory but requires large time records to accurately describe a random loading process. Alternatively, a frequency domain approach has a significant advantage in terms of computational time when the finite element analysis is used. Random loading and responses are characterized using power spectral densities (PSDs).

1.1 OBJECTIVES

The goals of this study are twofold: a) to consider the statistical variation of the S-N fatigue curves into the assessment procedures for predicting fatigue life of critical structural components; b) to use the frequency domain approach to predict the fatigue life of a notched component. The final output of this study will be the definition of a robust and reliable methodology to study the fatigue response of any kind of structures using finite element analysis. The well-known time domain approach will be used to define benchmark solutions of the tested notched component.

The frequency domain approach offers great advantage in terms of calculation time, which can be used to solve much larger and complex problems using finite element analysis. Therefore, this work aims to review and identify modeling parameters that increase the accuracy of the results compared to the time domain reducing the differences commonly encountered in the literature. Teixeira [8] showed that the predicted fatigue life of a notched aluminum beam in the frequency domain being ~20% higher than the time domain estimation. Due to the scatter in fatigue testing results, probabilistic modeling of the S-N curves should be used to justify the difference.

The fatigue life of a 6061-T6 aluminum notched specimen is estimated for the combined load cases for two different vibration profiles. The total fatigue damage and life are estimated in both time and frequency domains for the different S-N curve percentiles, which are then compared to testing results.

2 STATE OF THE ART

2.1 INTRODUCTION TO FATIGUE

Fatigue as a technical problem became evident around the middle of the 19th century as a by-product of the industrial revolution.

ASTM E 1150 defines fatigue as the process of progressive localized permanent structural change occurring in a material subject to conditions that produce fluctuating stress and strains at some point or points and that may culminate in cracks or complete fracture after a sufficient number of fluctuations [9].

The idea that fatigue is a process is important to understand the multiscale nature of this phenomenon, as the size of material defects and cracks could be several orders of magnitude smaller than the structural component. Repeated constant or variable amplitude forces enable weak properties of the materials to become dominant, irreversible slip structures accumulation at the microscopic stress concentration sites (e.g. surface intrusions / extrusions), the different sizes and orientations of grains; small scratches and corrosion points at the surface; cavities, blisters, and microstructural defects revealing an extraordinary scatter in the fatigue testing data. As a result, the cycles to fracture for several parts or specimens will be very different [10].

Schijve [11] argued that in principle, it is correct to consider fatigue as a phenomenon characterized by microcrack initiation, crack growth and failure, however, this concept does not occur in the same way in all metallic materials.

The nature of the observed loading is very different from a constant fatigue amplitude S-N test, nonetheless, Schijves [11] and Fatemi and Yang [3] pointed out that for variable amplitude loading, Palmgren-Miner's rule, that predicts the fatigue life based on the S-N curve data, is still dominantly used in design. This is also observed in the standard for fatigue assessment in ship structures DNVGL-CG-0129 which also indicates the use of Palmgren-Miner's rule to estimate the damage accumulation in the structure [12].

2.2 OVERVIEW OF RANDOM VIBRATION FATIGUE MODELING VIA FINITE ELEMENT METHOD

The random vibration fatigue analysis can generally be accomplished in the time domain or in the frequency domain.

For the time domain or time series approach an adequate duration of the loading covering all random events is required, therefore, long time records of load data are needed. Figure (4) illustrates an example of a measured road load acceleration in all three-axis (X, Y and Z) of an automotive vehicle.

Figure 4 - Road load acceleration

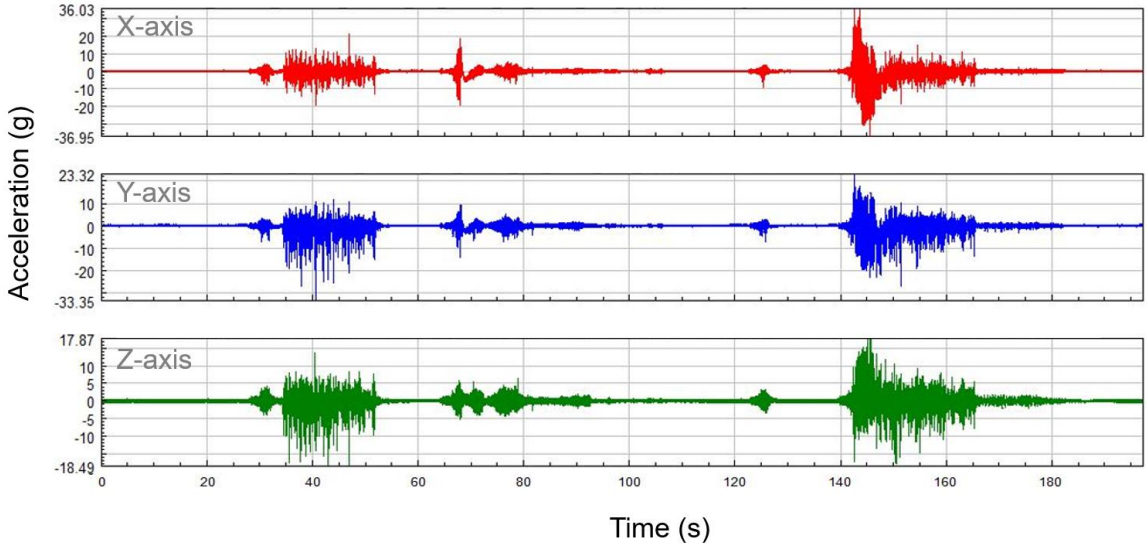

Source: Author

The fatigue life in the time domain is estimated by applying the time series load history to the component under evaluation, a transient structural analysis is performed to generate the stress histories at all discretized points of the structure, which are defined by the mesh size in the finite element modeling. Rainflow cycle counting and linear cumulative damage, per Palmgreen Miner's rule is applied to estimate the total damage and the fatigue life of the component. The general calculation procedure is illustrated in Figure (5).

Often, instead of the time series, the load is specified in its power spectral density (PSD) form, the time series load can be synthesized by performing an inverse fast Fourier transform (IFFT) for a specific time duration. This approach on long synthesized time histories is computationally expensive, therefore, the assumption that the data is ergodic, stationary

and Gaussian is required. Figure (6) illustrates the workflow of a synthesized time series approach.

Figure 5 - Fatigue life estimation - Time domain approach

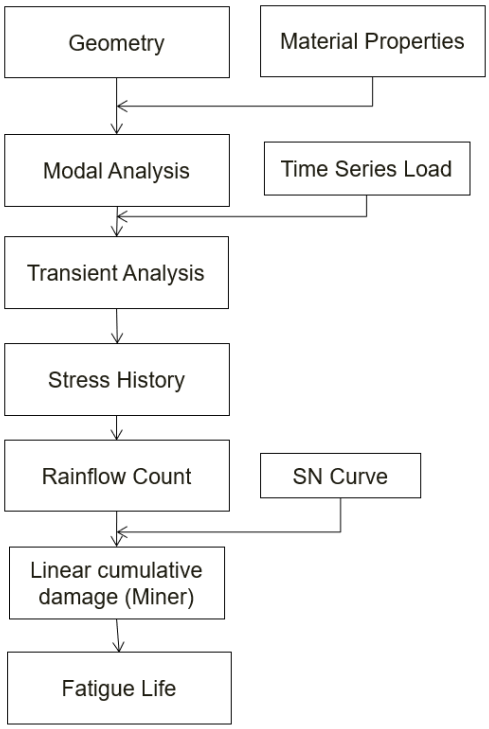

Source: Author

Figure 6 - Synthesized Time Series Approach

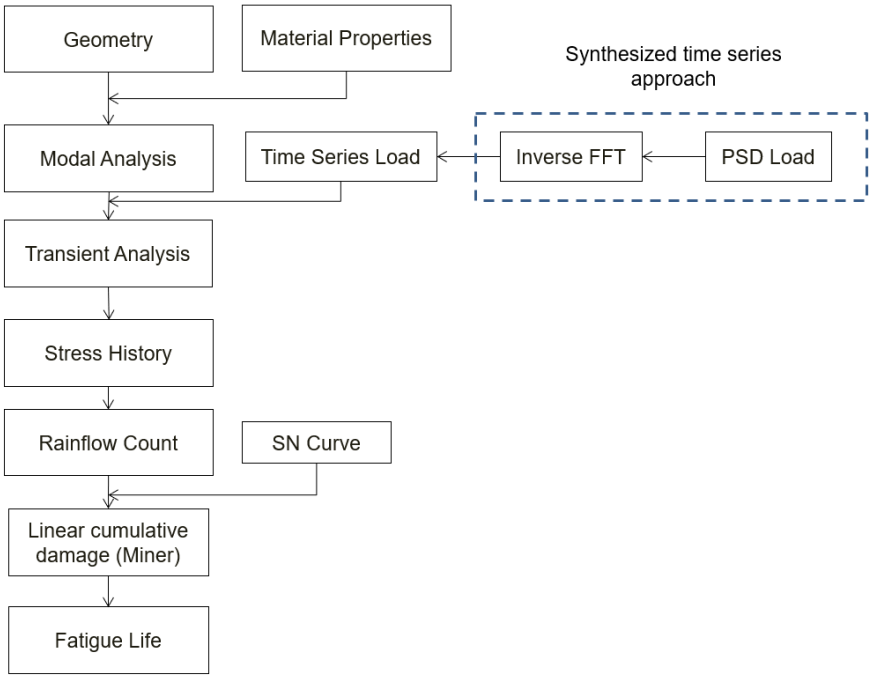

Source: Author

In the frequency domain workflow illustrated in Figure (7), the dynamic characterization of the discretized structure is made by its frequency response functions (FRFs), which are calculated based on a unit load excitation (e.g. for a PSD given in unit of acceleration g^2/Hz, the structure is harmonically excited with one (1) g acceleration at the correspondent excitation direction).

The PSD input load multiplies the square of FRFs stress tensor resulting in the stress response spectrum. The fatigue life is then estimated through the calculation of the spectral moments of the stress response spectrum, probability density function (PDF) and duration of the vibration profile. The obtained number of cycles that the structure is subjected is compared to the material S-N curves via linear cumulative damage.

The modal analysis is used in all procedures to determine the inherent dynamic characteristics of the structure by the identification of the natural frequencies and mode shapes, allowing the usage of modal superposition technique which is convenient to reduce calculation time when the finite element method is used.

Figure 7 - Fatigue life estimation - Frequency domain approach

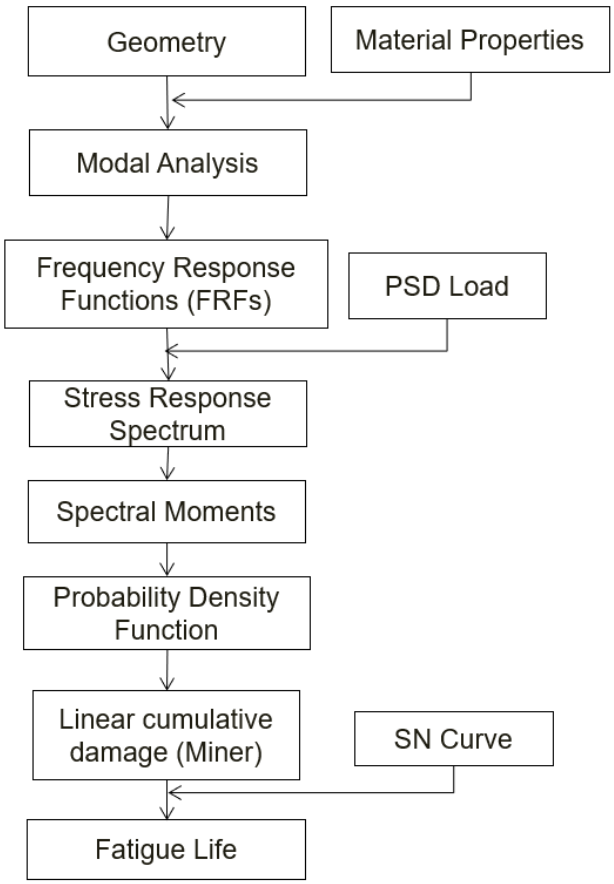

Source: Author

2.3 NOTCH EFFECTS IN FATIGUE

Notches are geometrical discontinuities which create a modification of the stress distribution around them, exhibiting a strong variation in stress gradient leading to a maximum stress at the tip of the notch tip. Notches, also referred as stress concentrators, are critical in the design and evaluation of mechanical components due to the local stress increase be significantly higher than the overall stress away from the discontinuity.

Figure (8) illustrates the changes in the structure stresses due to the presence of a notch. At the notch tip the stress is maximum, the net stress is defined at the reduced section of the component where the notch is located, and gross stress is the stress away from the influence of the notch.

Figure 8 - Definition of maximum, gross and net stresses due to the presence of a notch

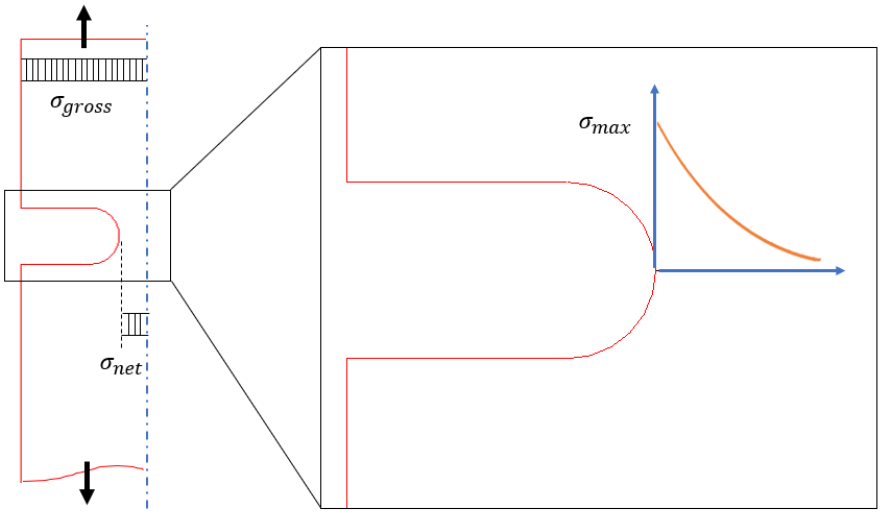

Source: Author, adapted from Pluvinage (2003)

The introduction of a notch in a component or structure is more detrimental than the consequence of the net section reduction [13]. Therefore, the following inequality can be defined as:

$$\sigma_{max} > \sigma_{net} > \sigma_{gross} \tag{3}$$

The local increase in stress can defined by the elastic stress concentration factor k_t by:

$$k_t = \frac{\sigma_{max}}{\sigma_{net}} \tag{4}$$

The elastic concentration factor can also be defined in terms of the gross stress by:

$$k_t = \frac{\sigma_{max}}{\sigma_{gross}} \tag{5}$$

Distinction must be made whether the net or gross stress is used in the determination of k_t.

Given that the maximum value of the stress concentration can be higher than the yield stress of the material, as consequence of plastic deformation at the notch tip, an elastic-plastic stress and strain concentration factors k_σ and k_ε relationship can be defined:

$$k_\sigma = \frac{\sigma_{max}}{\sigma_{net}} \; ; \; k_\varepsilon = \frac{\varepsilon_{max}}{\varepsilon_{net}} \tag{6}$$

Intuitively, the application of the elastic stress concentration factor as a reduction in the fatigue life of a component would be reasonable, as the increased stresses at the notch tip would lead to a reduced fatigue life. However, the experimental observations have shown that at the same endurance cycle, the notch stress controlling the fatigue life is not the maximum stress on the surface of the notch root, but an average stress acting over a finite volume of material at the notch root [13,14].

Notch effects in fatigue can be defined by the fatigue reduction factor k_f:

$$k_f = \frac{\Delta\sigma_s\,(N)}{\Delta\sigma_n\,(N)}, \tag{7}$$

where $\Delta\sigma_s$ and $\Delta\sigma_n$ are the stress amplitude for a smooth and for a notched specimen respectively at the same number of cycles to failure *N*. The use of the elastic stress concentration factor k_t results in over-conservative fatigue estimation compared to testing results, therefore, the following inequality can be defined [13].

$$k_f \leq k_t \tag{8}$$

The relationship between the elastic stress concentration factor (k_t) and the fatigue strength reduction factor (k_f) have been established by several models which are classified in three different categories depending on the assumptions used:

1) Models using empirical relationships and based on the concept of an average stress over a given distance.

2) Models based on the value of stress giving rise to a non-propagating short crack initiated from a notch.

3) Models based on the localization of fatigue damage in an effective volume.

Peterson's model [15] assumes that fatigue failure occurs when the stress, over a certain distance, is equal to or greater than the fatigue limit of a smooth specimen, an experimental relation using the concept of notch sensitivity that depends on material and geometry has been defined. A comprehensive review of the different models is presented by Pluvinage [13].

Based on the assumption that the fatigue failure requires a physical volume to occur, Pluvinage [13] presented a method named volumetric approach. The volumetric approach is a macro-mechanical method that uses elastic-plastic distribution and stress gradient evolution to predict the fatigue reduction factor k_f, based on the idea of fatigue damage accumulation in a specific region near notch tip. The fact that the fatigue tests are generally affected by a large scatter indicates that the stress distribution near the notch tip is different between specimens and consequently the first derivative of the stress distribution function, thereafter, a relative stress gradient can be defined as:

$$\chi = \frac{1}{\sigma_{xx}(y)} \frac{d\sigma_{xx}(y)}{dx} \tag{9}$$

The fatigue process volume is the high stressed region ahead of the crack or notch tip. Assuming a cylindrical fatigue process volume, where the height of the cylinder equals the thickness of the specimen, the cylinder diameter corresponds to an effective distance x_{eff} which in the volumetric approach is defined when the minimum of the relative stress gradient occurs. As the volumetric approach [13] assumes that all stress points in the process volume play a role in the fatigue process, the contribution of each point is weighted by the stress gradient and distance between the stressed point and notch tip. The stress gradient considers the influence of the loading mode, geometry and scale effect.

The fatigue strength reduction factor k_f, according to the volumetric approach is then defined as:

$$k_f = \frac{1}{y_{eff}\ \sigma_{net}} \int_0^{x_{eff}} \sigma_{xx}(y)(1 - y\chi)dx\ , \tag{10}$$

where $\sigma_{xx}(y)$ is the fatigue crack opening stress.

The elastic-plastic crack opening stress distribution and the relative stress gradient near the notch tip are shown in Figure (9).

Figure 9 - Elastic–plastic fatigue crack opening stress distribution

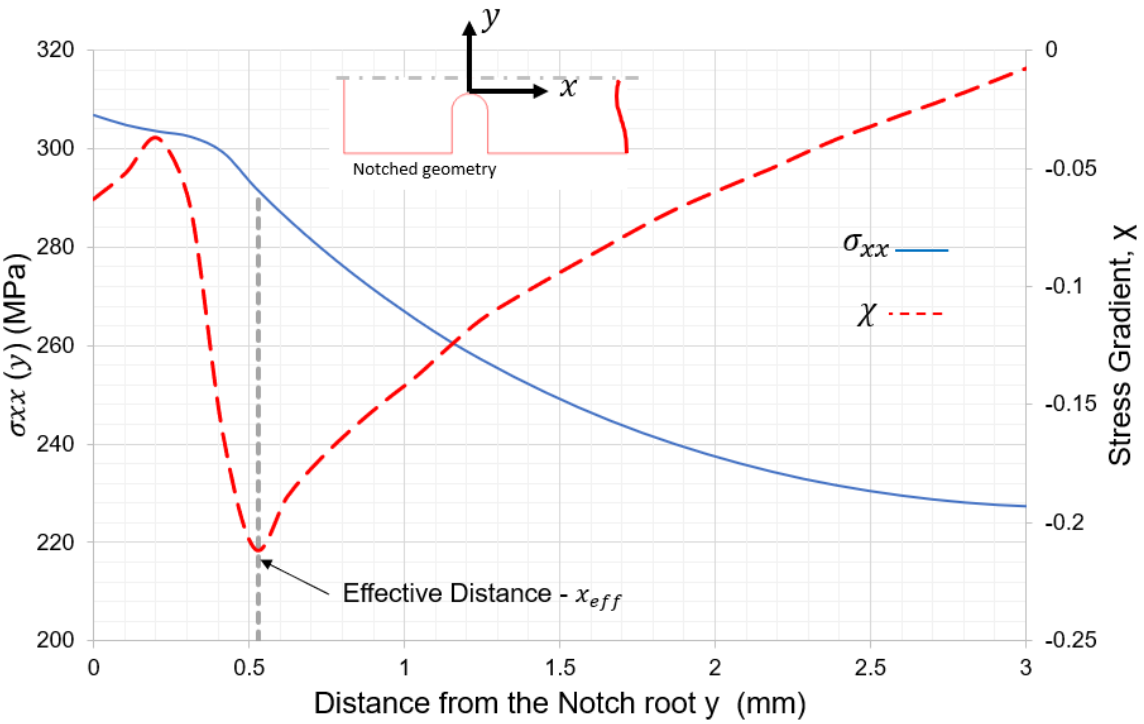

Source: Author

In the volumetric approach, the notch strength reduction factor is calculated by application of specimen material properties and its geometrical features via finite element analysis. The inflection point of the stress gradient is observed when the elastic-plastic behavior of the material is considered, therefore, the effective distance can be calculated for an applied load that exceeds the material yielding. The notch strength reduction factor is applied to the reference fatigue curve for a smooth specimen to obtain the notched or corrected fatigue curve.

The volumetric approach could also be applied when the smooth specimen results are not available but another notched specimen with same material, specimen geometry and different notch feature exists [16].

2.4 LINEAR STRUCTURE DYNAMIC RESPONSE CHARACTERIZATION

The dynamic behavior characterization of a component or structure can be determined both in time and frequency domains. In the time domain, it involves a complicated and often lengthy transient analysis. In frequency domain the transfer function relates the amplitude of the input (force, acceleration, moment) to the amplitude of the output stress for each frequency. The frequency response functions (FRFs) are determined by the modes and natural frequencies which the structure vibrates.

The vibration modes or mode shapes are an inherent property of the component/structure determined by the material properties (mass and stiffness) and boundary conditions. Each mode is defined by a natural (modal or resonant) frequency and a mode shape.

In linear systems a multiple-degree-of-freedom systems can be described by:

$$[M]\{\ddot{u}\} + [C]\{\dot{u}\} + [K]\{u\} = \{P\}, \tag{11}$$

where: $[M]$ is the global mass matrix, $[C]$ the global damping matrix, $[K]$ the global stiffness matrix, $\{u\}$ the displacement vector, $\{\dot{u}\}$ and $\{\ddot{u}\}$ are the first and second derivatives of $\{u\}$ respectively, $\{P\}$ is the vector of external forces.

A class of linear systems is the linear time invariant systems (LTI – Linear Time Invariant) is shown in Figure (10), the dynamic response characteristic of this system is represented by its Frequency Response Function (FRF) $H\,[(f)]$.

Figure 10 - Linear Time Invariant Dynamic System.

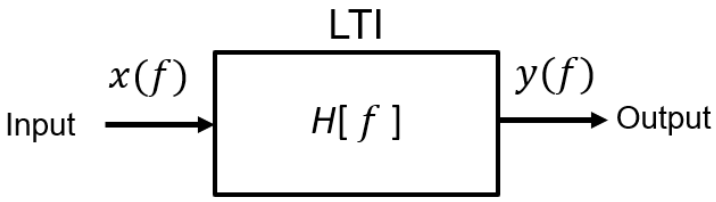

Source: Author

The single input x, single output y relationship for a linear system H, in terms of Fourier transforms are:

$$Y(f) = H(f)\,X(f), \tag{12}$$

where X, Y are the Fourier transform of the variables x and y. The FRF is generally a complex-valued quantity that can be represented in terms of magnitude and an associated phase angle. The ratio of the output amplitude and the input amplitude is equal to the gain factor $H(f)$ of the system, and the phase shift between the output and input is called phase factor $\theta(f)$ of the system.

$$H(f) = |H(f)|e^{-i\theta(f)} \tag{13}$$

The evaluation of the phase change can be used to identify areas of maximum response, which are critical to the structural integrity assessment of the structures under fatigue loading.

2.4.1 MODAL ANALYSIS

Let the dynamic behavior of structural systems be described briefly. Considering an undamped system with no external forces, Equation (11) can be reduced to Equation (14) with natural circular frequencies (ω_i) defined by Equation (15).

$$[M]\{\ddot{u}\} + [K]\{u\} = \{0\}, \tag{14}$$

$$\omega_i = 2\pi f_i \tag{15}$$

Assuming a harmonic oscillation, described by Equations (16) and (17):

$$\{u\} = \{A\}.sen(\omega_i t + \theta_i) \tag{16}$$

$$\{\ddot{u}\} = -\omega_i{}^2\{A\}.sen(\omega_i t + \theta_i) \tag{17}$$

Substituting Equations (16) and (17) into Equation (14):

$$[M] - \omega_i{}^2\{A\}.sen(\omega_i t + \theta_i) + [M]\{A\}.sen(\omega_i t + \theta_i) = 0 \tag{18}$$

$$\{A\}.sen(\omega_i t + \theta_i)\{[K] - \omega_i{}^2[M]\} = \{0\} \tag{19}$$

Equation (19) is satisfied if either $\{A\}.sen(\omega_i t + \theta_i) = \{0\}$ known as trivial solution, which implies no vibration to the system or if the determinant of the matrix $[K] - \omega_i{}^2[M] = \{0\}$. This is an eigenvalue problem which may be solved up to *m* values of ω^2 and *m* eigenvectors. From Equation (19) one obtains:

$$det\{[K] - \omega_i{}^2[M]\} = \{0\} \tag{20}$$

The eigenvectors $\{\Phi\}$ are the vibration modes and the eigenvalues are the natural frequencies associated each vibration mode [17].

2.4.2 MODAL COORDINATES AND MODE SUPERPOSITION METHOD

Mode-superposition or modal superposition technique uses the natural frequencies and mode shapes of a linear structure to characterize the dynamic response of a structure to a transient or steady excitation [17].

In this technique the structure displacement is written as a linear combination of the mode shapes. From the modal analysis, the eigenvectors $\{\Phi\}$ are computed. The displacement vector can then be expressed by:

$$\{u\} = \sum_{i=1}^{n} \{\Phi_i\}\, y_i \tag{21}$$

where $\{u\}$ is the displacement vector, $\{\Phi\}$ is the mode shape vector, y_i is the modal amplitude (modal coordinates), *n* is the number of modes and i represents the mode number. The modal coordinates can be thought as scale factors of each mode.

Substituting Equation (21) in Equation (14):

$$[M]\sum_{i=1}^{n}\{\Phi_i\}\,\ddot{y}_i + [C]\sum_{i=1}^{n}\{\Phi_i\}\,\dot{y}_i + [K]\sum_{i=1}^{n}\{\Phi_i\}\,y_i = \{P\} \tag{22}$$

Multiplying both sides of Equation (22) by the typical mode shape $\{\Phi_j\}^T$ one obtains:

$$\{\Phi_j\}^T[M]\sum_{i=1}^{n}\{\Phi_i\}\,\ddot{y}_i + \{\Phi_j\}^T[C]\sum_{i=1}^{n}\{\Phi_i\}\,\dot{y}_i + \{\Phi_j\}^T[K]\sum_{i=1}^{n}\{\Phi_i\}\,y_i = \{\Phi_j\}^T\{P\} \tag{23}$$

Considering the orthogonal condition of the natural modes:

$$\{\Phi_j\}^T [M]\{\Phi_i\} = 0 \ \ for\ i \neq j \tag{24}$$

$$\{\Phi_j\}^T [K]\{\Phi_i\} = 0 \ \ for\ i \neq j \tag{25}$$

The mode-superposition method, only allows Rayleigh or constant damping, thus:

$$\{\Phi_j\}^T [C]\{\Phi_i\} = 0 \ for\ i \neq j \tag{26}$$

Applying these properties into Equation (23), only the *i=j* terms remain:

$$\{\Phi_j\}^T [M]\{\Phi_j\}\ddot{y}_j + \{\Phi_j\}^T [C]\{\Phi_j\}\dot{y}_j + \{\Phi_j\}^T [K]\{\Phi_j\} y_j = \{\Phi_j\}^T \{f\} \tag{27}$$

Let $[\underline{M}]$ be the generalized or the matrix of modal masses, $[\underline{C}]$ the generalized or matrix of modal damping, $[\underline{K}]$ be the generalized or matrix of modal stiffness and $\{\underline{P}\}$ be the generalized or matrix of modal forces. Assuming a single degree of freedom oscillator, one obtains:

$$[\underline{M}] = \{\Phi_j\}^T [M]\{\Phi_j\} = 1\ (normality\ condition) \tag{28}$$

$$[\underline{C}] = \{\Phi_j\}^T [C]\{\Phi_j\} = 2\zeta_j \omega_j \tag{29}$$

$$[\underline{K}] = \{\Phi_j\}^T [K]\{\Phi_j\} = \omega_j{}^2 \tag{30}$$

$$\{\underline{P}\} = \{\Phi_j\}^T \{P\} = f_j \tag{31}$$

Where ζ_j is the fraction of critical damping for mode *j*, ω_j is the natural circular frequency of mode *j* and f_j is the force in modal coordinates.

Substituting Equations (28), (29), (30) and (31) into Equation (27) one obtains:

$$\ddot{y}_j + 2\zeta_j \omega_j \dot{y}_j + \omega_j{}^2 y_j = f_j \tag{32}$$

While in Equation (11) the system dynamics is described in terms of the geometric displacements $\{u\}$ in global coordinates, Equation (32) describes the system equation of motion in modal coordinates, since *j* represents any mode, Equation (32) has the same

number of uncoupled equations as the number of unknows y_j. A comprehensive description of the method to obtain $\ddot{y}_j$, $\dot{y}_j$ and y_j can be found in [17].

Substituting y_j in Equation (21) the modal coordinates are converted back into geometric displacements and the individual modal responses are superimposed to obtain the system response. The advantage of solving uncoupled system in modal coordinates is that the computationally expensive matrix algebra is performed in the solution of the system natural frequencies and modes, optimizing the calculation under transients and harmonic responses to obtain the system FRFs.

2.5 TIME DOMAIN APPROACH

2.5.1 TRANSIENT ANALYSIS

Transient structural analysis determines the dynamic response of a structure over time. One can obtain the time-dependent results such as displacement, strain, stress, and reaction force of the structure under time-dependent loads by solving the equation of motion of a multiple-degree-of-freedom system [17].

The transient analysis can be performed using implicit or explicit solvers. The main difference between the two methods is the time of the transient events. For random vibration problems, the structure is exposed to time-varying load for long periods of time, thereafter, implicit solvers are used.

Due to the second-order time derivatives in Equation (11), time integration methods are needed. Newmark method and Hilber-Hughes-Taylor (HHT) method are generally used in implicit transient analyses. The implicit solver iterates the next step result with the current step result and the next unknown result, which must be obtained through an iteration process. A detailed description of Newmark' s and HHT methods can be found in [17].

The transient stress response tensor $\sigma_{ij}(t)$ obtained from the transient analysis can be written as:

$$\sigma_{ij}(t) = \begin{bmatrix} \sigma_{xx}(t) & \sigma_{yy}(t) & \sigma_{zz}(t) & \sigma_{xy}(t) & \sigma_{yz}(t) & \sigma_{xz}(t) \end{bmatrix} \quad (33)$$

Rainflow cycle counting method is used to obtain the number of cycles for each stress amplitude. At each stress amplitude level, the fatigue damage is then computed by the ratio of the number of cycles that the structure is subjected and the number of cycles from the material S-N curve. A stress combination method (e.g critical plane, absolute maximum

principal, maximum principal) is used to reduce the stress tensor to a scalar value, the detailed description of the method is presented in chapter 2.6.3 of this work.

2.5.2 RAINFLOW CYCLE COUNTING

The response of the structure is the starting point for any fatigue analysis. In the time domain this is usually expressed in terms of strain or a stress time signal, where the amplitude and mean values are the key parameters in a stress cycle.

Matsuishi and Endo [18] initially proposed the rainflow cycle method to count the cycles of the half-cycles of strain time signals, where the counting process is based on the stress-strain behavior of the material. Other methods such as level crossing, range-pair, range-mean, all attempt to reduce a random sequence of peak valleys to a set of equivalent constant amplitude cycles allowing the application of a cumulative damage. Lallane [19] presented a detailed description of several counting methods including the rainflow.

Rainflow cycle counting identifies from a variable amplitude stress or strain history the number of cycles with different range and mean values (or maximum and minimum), those events are important for the fatigue analysis because they are identified as potentially damaging the structure. The following values associated with each cycle may be used in subsequent fatigue calculations:

- Maximum value of the cycle: S_{max}
- Minimum value of the cycle: S_{min}
- Range of stress: $S_{range} = S_{max} - S_{min}$
- Stress amplitude: $S_{amp} = \frac{S_{range}}{2}$
- Mean stress: $S_{mean} = \frac{S_{max} + S_{min}}{2}$

Once the rainflow cycles are counted, a useful way of visualizing the information is through the histogram plot of the quantities. The range-mean comprehensively shows the number of cycles, stress range and mean stress contained in the time signal input as shown in Figure (11).

The rainflow histogram can also be represented by the number of cycles as function of the stress range (or stress amplitude) as illustrated in Figure (12).

Figure 11 - Rainflow Histogram - Range-Mean

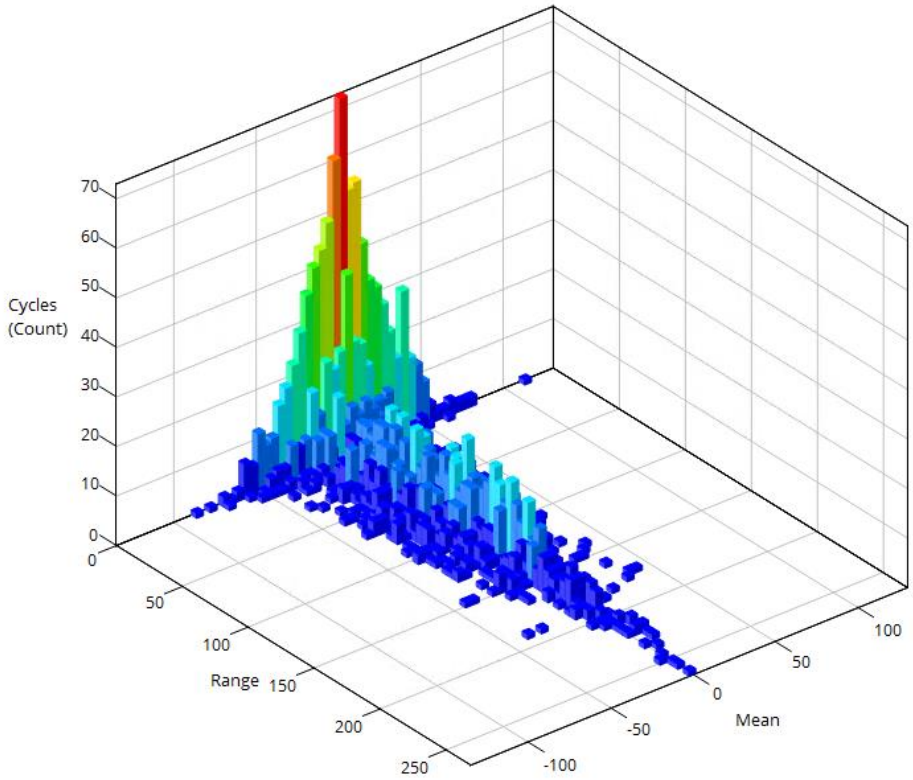

Source: Author

Figure 12 - Rainflow Histogram - Number of Cycles per Stress Range

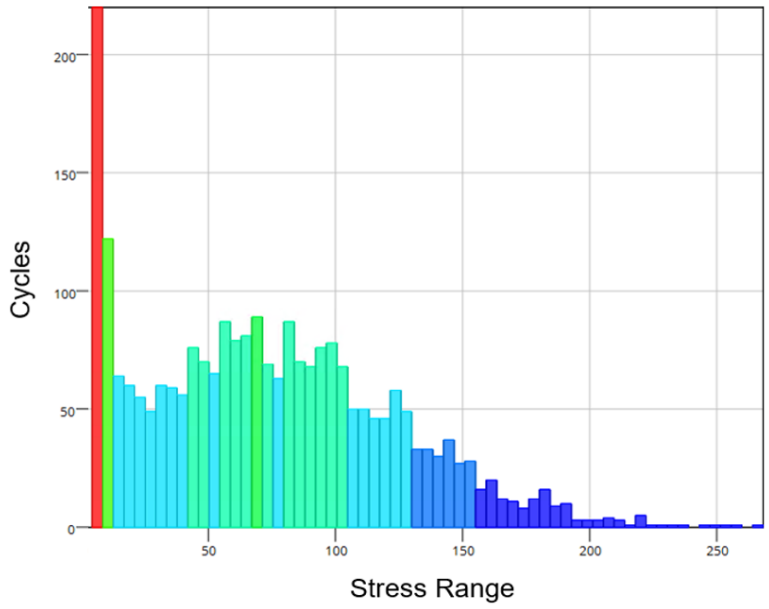

Source: Author

The representation of the cycles in a histogram brings clarity and enables a comprehensively evaluation of the structure response given the complexity of input excitation.

2.6 FREQUENCY DOMAIN APPROACH

2.6.1 HARMONIC RESPONSE

Harmonic analysis determines the steady-state response of a structure subjected to loads that vary harmonically with time. Considering the general equation of motion presented by Equation (11).

Assuming the force vector $\{P\}$ and displacement vector $\{u\}$, harmonic, not necessarily in phase, $\{u\}$ can be written as:

$$\{u\} = \{u_{max}\, e^{i\theta}\}\, \mathrm{e}^{\mathrm{i}\Omega \mathrm{t}}, \tag{34}$$

where: u_{max} is the maximum displacement, θ is the displacement phase shift and Ω is the imposed circular frequency.

Using complex notation equation (34) can be written as:

$$\{u\} = \{u_{max}\, (cos\theta + isin\theta\}\, \mathrm{e}^{\mathrm{i}\Omega \mathrm{t}} \tag{35}$$

$$\{u\} = (\{u_1\} + i\{u_2\})\, \mathrm{e}^{\mathrm{i}\Omega \mathrm{t}}, \tag{36}$$

where $\{u_1\} = \{u_{max}\, cos\theta\}$ is the real displacement vector, $\{u_2\} = \{u_{max}\, sin\theta\}$ the imaginary displacement vector, $u_{max} = \sqrt{{u_1}^2 + {u_2}^2}$ and $\theta = \tan^{-1}\frac{u_1}{u_2}$. Taking the time derivatives of $\{u\}$:

$$\{\dot{u}\} = i\Omega(\{u_1\} + i\{u_2\})\, \mathrm{e}^{\mathrm{i}\Omega \mathrm{t}} \tag{37}$$

$$\{\ddot{u}\} = -\Omega^2(\{u_1\} + i\{u_2\})\, \mathrm{e}^{\mathrm{i}\Omega \mathrm{t}} \tag{38}$$

Similarly, the force vector can be written as:

$$\{P\} = (\{P_1\} + i\{P_2\})\, \mathrm{e}^{\mathrm{i}\Omega \mathrm{t}}\,, \tag{39}$$

where $\{P_1\} = \{P_{max}\, cos\varphi\}$ is the real force vector, $\{P_2\} = \{P_{max}\, sin\varphi\}$ the imaginary force vector and φ is the force phase shift.

Substituting Equations (36), (37), (38) and (39) into Equation (11) one obtains:

$$[M]\left(-\Omega^2(\{u_1\} + i\{u_2\})\,\mathrm{e}^{\mathrm{i}\Omega t}\right) + [C]\left(i\Omega(\{u_1\} + i\{u_2\})\,\mathrm{e}^{\mathrm{i}\Omega t}\right) + [K]\left((\{u_1\} + i\{u_2\})\,\mathrm{e}^{\mathrm{i}\Omega t}\right) = (\{P_1\} + i\{P_2\})\,\mathrm{e}^{\mathrm{i}\Omega t} \quad (40)$$

Simplifying and grouping the similar terms, eliminating the time dependent term $\mathrm{e}^{\mathrm{i}\Omega t}$:

$$(-\Omega^2[M] + i\Omega[C] + [K])(\{u_1\} + i\{u_2\})\,\mathrm{e}^{\mathrm{i}\Omega t} = (\{P_1\} + i\{P_2\})\,\mathrm{e}^{\mathrm{i}\Omega t} \quad (41)$$

$$(\{u_1\} + i\{u_2\}) = (-\Omega^2[M] + i\Omega[C] + [K])^{-1}\{P_1\} + i\{P_2\} \quad (42)$$

The frequency response function (FRF) is computed by taking the transfer function of the linear system from Figure 10 (using natural circular frequency notation), where the inputs are the displacement vector $\{u\}$ and the output is the force vector $\{P\}$, from equation (42), one obtains $[H(\omega)]$ as:

$$[H(\omega)] = \frac{1}{(-\Omega^2[M] + i\Omega[C] + [K])} \quad (43)$$

Substituting Equations (28), (29) and (30) into Equation (43), $[H(\omega)]$ in modal coordinates can be written as:

$$[H(\omega)] = \frac{1}{\left(-\Omega^2 + i(2\zeta_j\omega_j) + (\omega_j)^2\right)} \quad (44)$$

The dynamic response matrix $[Q]$, containing the FRFs of the stress tensor calculated from the response displacements, external forces and material properties using finite element formulation is presented in Equation (45). Figure (13) illustrates an example of the FRFs of a given stress tensor.

$$[Q]_{nx6} = \begin{bmatrix} \sigma_{xx1}(f_i) & \sigma_{yy1}(f_i) & \sigma_{zz1}(f_i) & \sigma_{xy1}(f_i) & \sigma_{yz1}(f_i) & \sigma_{xz1}(f_i) \\ \vdots & \vdots & \vdots & \vdots & \vdots & \vdots \\ \sigma_{xxn}(f_i) & \sigma_{yyn}(f_i) & & \cdots & & \sigma_{xzn}(f_i) \end{bmatrix} \quad (45)$$

Figure 13 - FRFs of the stress tensor

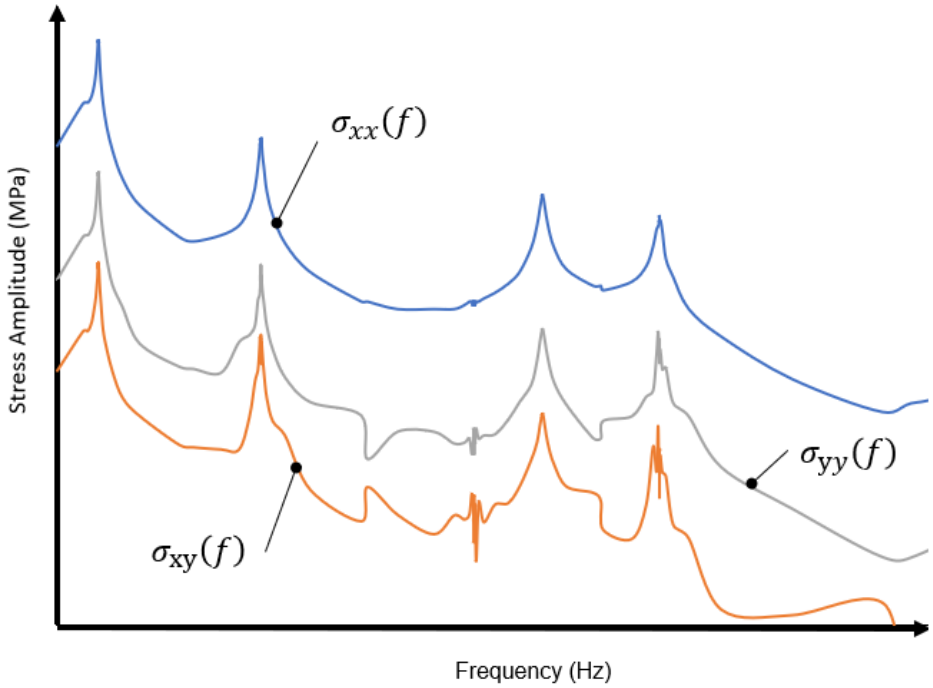

Source: Author

The FRFs describe the variation of the normal and shear stresses experienced by the structure given the input loading.

2.6.2 RANDOM VIBRATION

Any periodic time signal may be represented by the summation of a series of sinusoidal waves of various amplitudes, frequencies and phases, which is the basis of Fourier series expansion. The Fourier transform pair allows transformation between the time and frequency domains. The Fourier transform is defined as:

$$X(f) = \int_{-\infty}^{\infty} x(t) e^{-i2\pi ft}\, dt \tag{46}$$

and the inverse Fourier transform is:

$$x(t) = \int_{-\infty}^{\infty} X(f) e^{-i2\pi ft}\, dt \tag{47}$$

The autocorrelation function $R_{xx}(\tau)$ that defines how a signal is correlated to itself, with a time separation τ can be written as:

$$R_{xx}(\tau) = \int_{-\infty}^{\infty} x(t)x(t+\tau)dt = E[x(t)x(t+\tau)] \quad (48)$$

The autocorrelation function $R_{xx}(\tau)$ and the power spectral density S_{xx} are related by the Fourier transform pair as:

$$R(\tau) = \int_{-\infty}^{\infty} S_{xx}(f)e^{-j\omega t}\, d\omega \quad (49)$$

$$S_{xx}(f) = \int_{-\infty}^{\infty} R(\tau)e^{j\omega t}\, d\tau \quad (50)$$

The one-sided PSD $G_{xx}(f)$ defined for $0 \leq f \leq \infty$, can be written as:

$$G_{xx}(f) = 2S_{xx}(f) \quad (51)$$

The spectral density of narrow-band process is centered on a restrict range of frequencies, while for a wide-band process it extends over a broader range of frequencies.

By definition, a random time history cannot be periodic, however, if the time history is taken from an ergodic stationary Gaussian random process then it may be expressed in the frequency domain. A process is said to be stationary if the probability distributions of the ensemble are the same for all points in time. If the ensemble probability distribution function is Gaussian, then the process is known as a Gaussian random process.

A stationary process is called ergodic if the statistics taken from one sample are the same as those obtained for the ensemble. For nonstationary process, the statistics obtained from a sampled time history would not be representative of those of the whole random process as they would be continuously changing.

The PSD gives a statistical representation of a stationary random process in the frequency domain [20,21].

When the system is characterized by its FRFs and the input random excitation described by its PSD, the system stress response can be evaluated by “scaling” the PSD of the input signal(s) by the magnitude squared of the stress FRFs that can be written as:

$$G_{yy}(f) = |H_{xy}(f)|^2 G_{xx}(f) \tag{52}$$

Note that the square of the transfer function is necessary to keep the unit of the output consistent. Equation (52) in matrix form can be written as:

$$[G] = [Q]^T [A][Q], \tag{53}$$

where $[G]$ is the stress response PSD, $[A]$ is the input PSD excitation and $[Q]$ is the dynamic response matrix. Figure (14) illustrates the input PSD and the structure's response.

Figure 14 – Example of an input PSD - $[A]$ and the stress response PSD - $[G]$

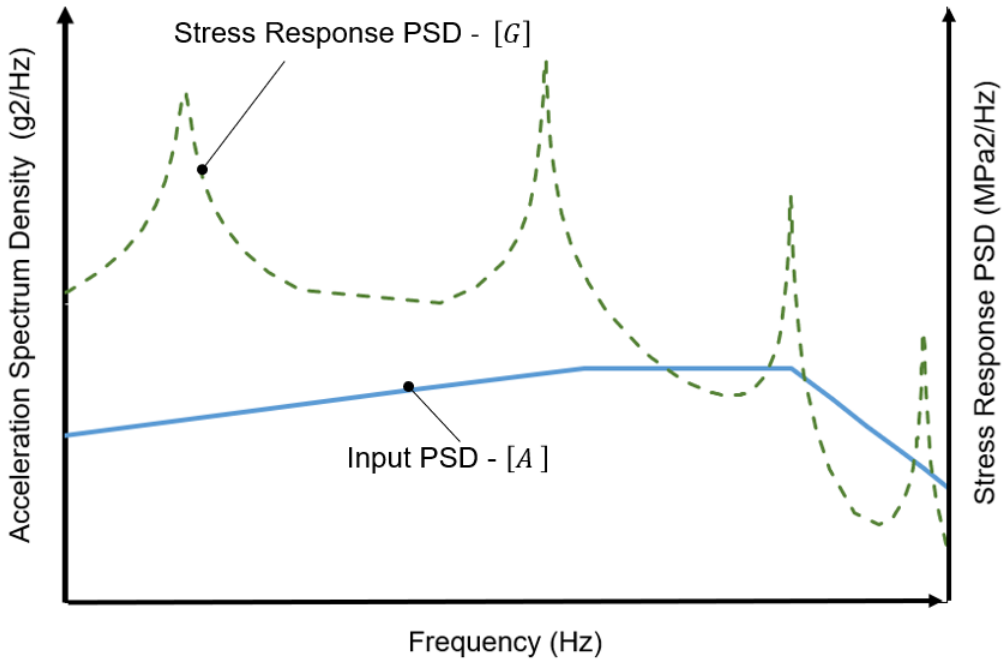

Source: Author

For a multi-PSD input (multiaxial loading), $[A]$ combines the auto PSDs on its main diagonal and the off-diagonal terms contain the Cross Power Spectral Densities (CPSDs) where the phase between pairs of loading sets is stored, the absence of cross spectrum information denotes no correlation between loading inputs.

For the general case of a multi-PSD input, $[A]$ can defined as:

$$[A]_{nxn} = \begin{bmatrix} PSD_{11} & \cdots & CPSD_{nn} \\ \vdots & \ddots & \vdots \\ CPSD_{1n} & \cdots & PSD_{nn} \end{bmatrix} \tag{54}$$

Usually in shaker tests one PSD is excited at each time in each specific axis (X, Y or Z), for this case the input PSD is given by A_{11}.

The acceleration *rms* (root mean square) of each PSD excitation provides a measure of the overall energy level associated to each individual excitation, and can be expressed as:

$$g_{rms_{PSD}} = \sqrt{\int_0^{+\infty} PSD(f)\, df}\,, \tag{55}$$

where the $\int_0^{+\infty} PSD(f)\, df$ is the area under the PSD curve. Assuming a zero-mean valued excitation, the *n*-th spectral moment of the stress response PSD matrix $[G]$ can be written as:

$$m_n = \int_0^{\infty} f^n G(f) df \; = \sum_{k=1}^{m} f_k^n G_k(f) \delta f \tag{56}$$

The spectral moments are typically used to identify the probability distribution function of the fatigue cycles used in the cycle counting methods. Rice [22] derived important relations for the distribution of peaks in a random signal, which provided the fundamentals to the fatigue estimation in the frequency domain. The expected number of upward zero crossings per unit time is given by:

$$E[0] = \sqrt{\frac{m_2}{m_0}} \tag{57}$$

The expected number of positive peaks per unit time (peak frequency) can be written as:

$$E[P] = \sqrt{\frac{m_4}{m_2}} \tag{58}$$

Figure (15) illustrates $E[P]$ and $E[0]$ for a given stress response signal.

Figure 15 - Representation of $E[P]$ and $E[0]$

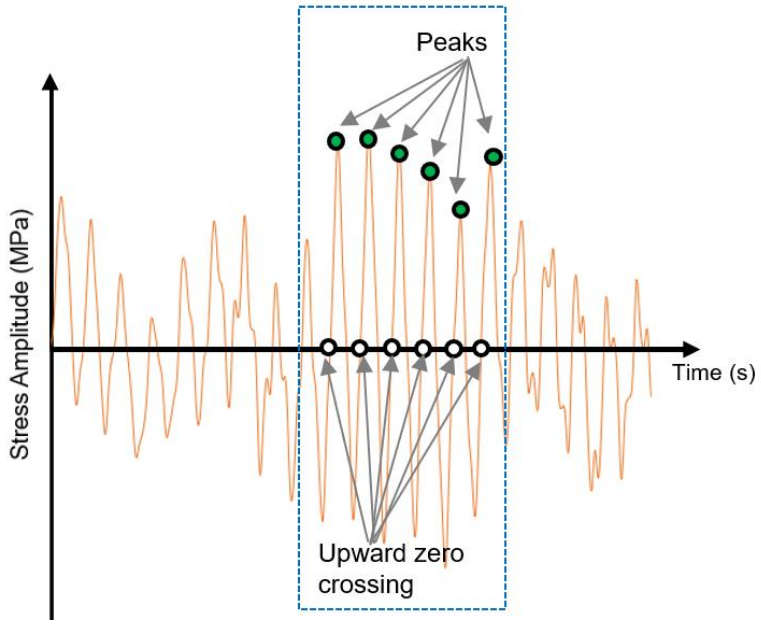

Source: Author

The irregularity factor γ or bandwidth parameter is defined as the ratio of number of crossings to number of peaks per unit time as per Equation (59), it is an important parameter to evaluate the concentration of the process near a central frequency. For a narrow band process $\gamma \rightarrow 1$, indicating that the number of peaks per second and zero crossing are similar. Bendat in [23] determined that the probability density function (pdf) of peaks for a narrow band signal follows a Rayleigh distribution.

$$\gamma = \frac{E[0]}{E[P]} = \sqrt{\frac{{m_2}^2}{m_0.m_4}} \tag{59}$$

The mean frequency is also defined as function of the spectral moments.

$$f_{mean} = \frac{m_1}{m_0}\sqrt{\frac{m_2}{m_4}} \tag{60}$$

The mean square amplitude of the time history is the area under the PSD curve and therefore the root mean square (RMS) is obtained by Equation (61).

$$A_{rms} = \sqrt{m_0} \tag{61}$$

2.6.3 STRESS COMBINATION METHOD - CRITICAL PLANE

To compare the resulting cycles to an S-N curve, the stress tensor $[Q]$ needs to be reduced to a scalar value. The stress tensor σ_{ij} can be expressed as:

$$\sigma_{ij} = \begin{bmatrix} \sigma_{xx} & \sigma_{xy} & \sigma_{zx} \\ \sigma_{xy} & \sigma_{yy} & \sigma_{yz} \\ \sigma_{zx} & \sigma_{yz} & \sigma_{zz} \end{bmatrix} \tag{62}$$

Considering that fatigue cracks initiate at free surfaces, in Figure (16) no normal or shear stress are applied to the root surface of the notch. Assuming an appropriate cartesian coordinate system where the Z-axis is normal to the free surface, the stress tensor is reduced to:

$$\sigma_{ij} = \begin{bmatrix} \sigma_{xx} & \sigma_{xy} & 0 \\ \sigma_{xy} & \sigma_{yy} & 0 \\ 0 & 0 & 0 \end{bmatrix} \tag{63}$$

Figure 16 - Surface resolution – Z as a surface normal

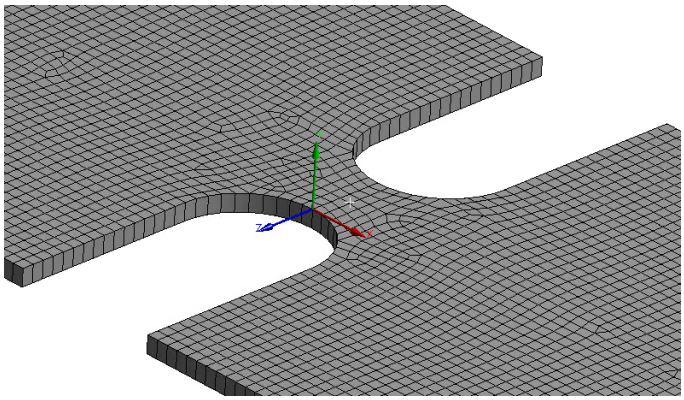

Source: Author

Stresses in this coordinate system can be assumed to be 2-D. In the critical plane stress combination method, the normal stress is calculated and rainflow counted in multiple planes. The critical plane is the plane with the highest predicted fatigue damage. The orientation of each plane is defined by the angle Φ with the local X-axis. The solution of normal stress for critical plane analysis can be defined as:

$$\sigma_{\Phi} = \frac{\sigma_{xx} + \sigma_{yy}}{2} + \frac{\sigma_{xx} - \sigma_{yy}}{2} \cos(2\Phi) + \sigma_{xy} \sin(2\Phi) \tag{64}$$

where Φ is defined at a specific angle resolution, e.g. every 10 degrees.

For a 3D case where the output stress PSD is defined by Equation (53) at each node of the finite element model, $[G(f)]$ is projected onto several selected planes, the plane that shows the largest 0^{th} spectral moment is defined as the critical plane. Figure (17) illustrates the orientation of a generic material plane Δ, a normal unit vector **n** can be defined through angles Φ and θ, where Φ is the angle between the local x**-** axis and the projection of the unit vector **n** on plan x-y. The angle θ is the angle between **n** and the z-axis. A new system of coordinates, **nab**, with origin in **O**, can be defined. Considering a generic direction **q** lying on the plane Δ and passing through point **O**. the angle between the direction **q** and the axis **a** is defined as α. The direction cosines vector $[d]$ is then defined as [24]:

$$d_{6x1} = \begin{bmatrix} \frac{1}{2}[sin(\theta)sin(2\Phi)cos(\alpha) + sin(\alpha)sin(2\theta)cos(\Phi)^2] \\ \frac{1}{2}[-sin(\theta)sin(2\Phi)cos(\alpha) + sin(\alpha)sin(2\theta)cos(\Phi)^2] \\ -\frac{1}{2}\, sin(\alpha)sin(2\theta) \\ \frac{1}{2}sin(\alpha)sin(2\Phi)cos(2\theta) - cos(\alpha)cos(2\Phi)\sin(\theta) \\ sin(\alpha)sin(\Phi)cos(2\theta) + cos(\alpha)sin(\Phi)\cos(\theta) \\ sin(\alpha)sin(\Phi)cos(2\theta) - cos(\alpha)sin(\Phi)\cos(\theta) \end{bmatrix} \tag{65}$$

Figure 17 - Normal **n** of material plane and the shear stress τ_q projected on Δ plane

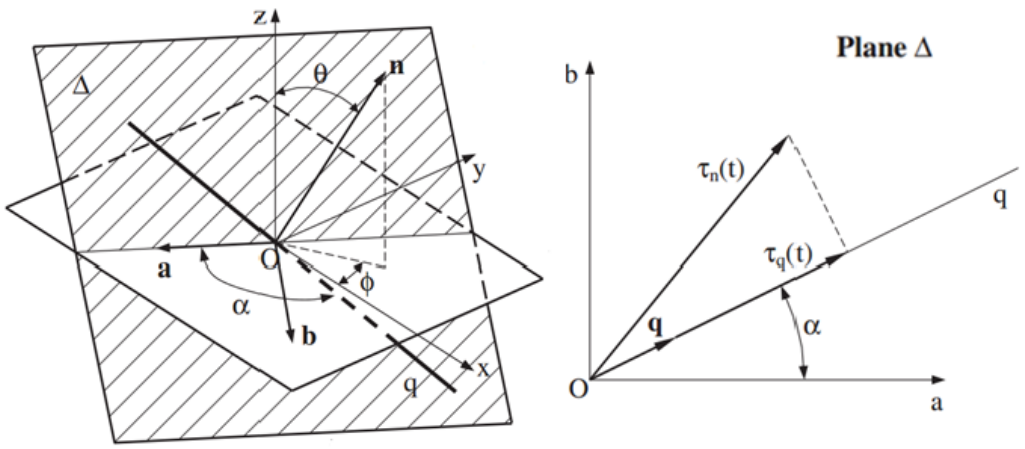

Source: Adapted from Teixeira (2014)

The shear stress as a function of frequency can be expressed by:

$$\tau_q(f) = d^T\,[G(f)]\,d \tag{66}$$

The spectral moments can be determined using Equation (66), by evaluating the shear stresses in the frequency range of interest [24].

2.7 SYNTHESIZED TIME SERIES FROM PSD SIGNAL

Time history signals are usually obtained from accelerometers or strain gages, the fatigue life in the time domain can be estimated from an acceleration time history using finite element transient analysis and rainflow cycle counting as previously described in section 2.5.

However, if the vibration profile is given in terms of the signal PSD, the time history can be synthesized using the inverse fast Fourier transform (IFFT) for a given time duration. This approach allows the creation of time history loads which can be used to compare fatigue calculation results obtained from the frequency domain.

A PSD does not have a unique time history because it discards the phase angle, which gives flexibility for shaker table tests for example, where the equipment can generate the time history considering the hardware characteristics inside a given tolerance [26].

The overall outline of the process to synthesize a time history from a PSD used in this work is illustrated in Figure 18, which is based on Quigley et al. [25] and Irvine [26].

A normally distributed white noise time history is generated and its fast Fourier transform (FFT) is obtained. The FFT is scaled according to the PSD magnitude per each constant frequency bandwidth Δf. Furthermore, the IFFT is used to obtain the time series of the scaled FFT signal. The obtained time series signal is scaled, so the g_{rms} of the synthesized signal matches the PSD input overall g_{rms} value.

Finally, the quality of the generated signal is verified by comparing the PSD of the synthesized time history with the original PSD input, an acceptance tolerance range must be defined as the duration of the time history also affects the accuracy of the synthesized curve.

Figure 18 - Synthesized time history from PSD input

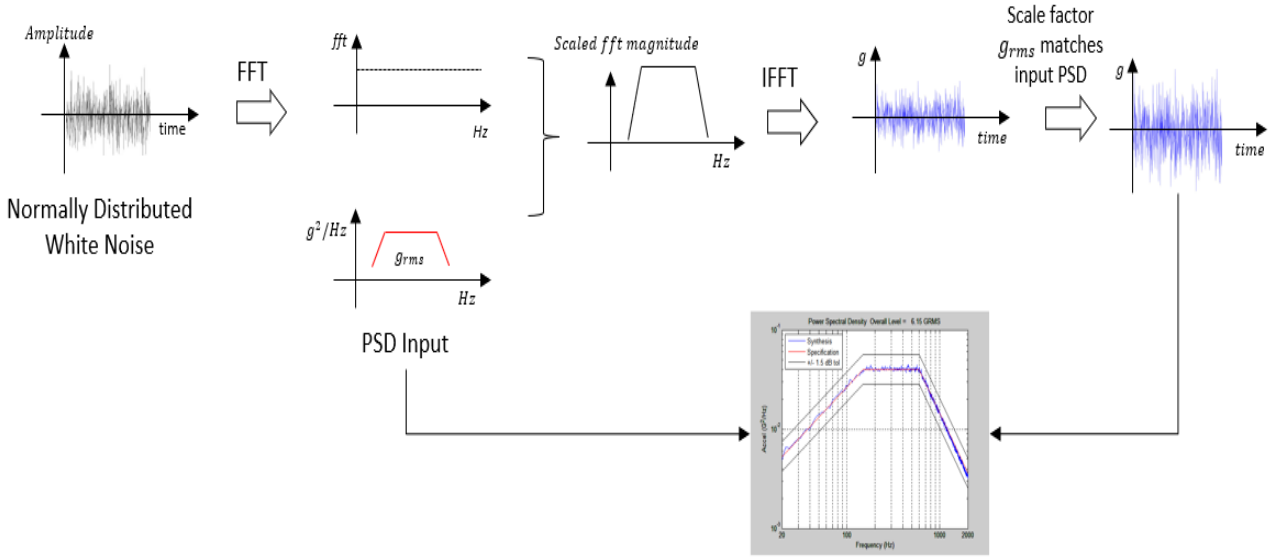

Source: Author, adapted from Quigley et al (2016) and Irvine (2020)

2.8 HALF POWER BANDWIDTH (3dB BANDWIDTH)

The half power bandwidth or 3dB bandwidth Δf of a resonance peak is defined as:

$$\Delta f = f_u - f_l, \tag{67}$$

where the lower and upper frequencies f_l and f_u are defined by:

$$|H(f_l)|^2 = |H(f_u)|^2 = \frac{1}{2}|H(f_{res})|^2 \tag{68}$$

The upper and lower frequencies are defined so that the power of $|H(f_{res})|$ has been halved in relation to the peak value of $|H(f_{res})|$. A quality factor Q is defined as the ratio between the center frequency f_{res} (resonance frequency) and the half power bandwidth as per Equation (69) [21].

The variables of the method are illustrated in Figure (19).

$$Q = \frac{f_{res}}{\Delta f} \tag{69}$$

Figure 19 - Half Power Bandwidth Method

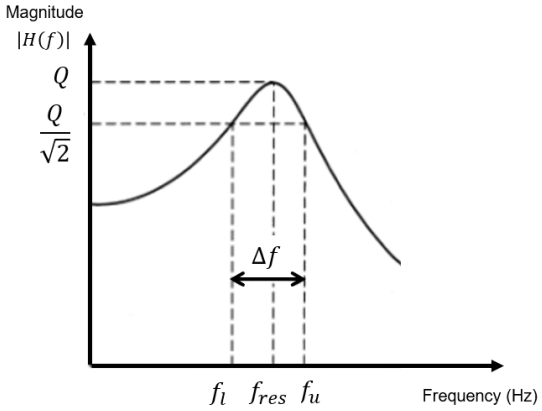

Source: Author

This method is used to determine the structure's damping ratio ζ. For small damping ratios (eg. ζ < 0.1), the damping ratio can be approximated by

$$\zeta \approx \frac{1}{2}\frac{\Delta f}{f} \approx \frac{1}{2}\frac{f_u - f_l}{f_{res}} \approx \frac{1}{2Q} \tag{70}$$

2.9 PROPORTIONAL OR RAYLEIGH DAMPING

Damping is the dissipation of energy from vibrating structure, generally in the form of heat. From the uncoupled equation of motion presented, Equation (32) implies a diagonal matrix of the modal damping $[C]$, otherwise, the modal superposition method would not be applicable, as the equations of motion would still be coupled. The concept of proportional damping is defined for the case where the damping matrix can be written as a linear combination of the mass and stiffness matrices, so it is simultaneously diagonalizable with $[M]$ and $[K]$.

The proportional or Rayleigh damping is defined as [27]:

$$[\mathrm{C}] = \alpha[M] + \beta[K]\,, \tag{71}$$

where α and β are real constants and represent the mass and stiffness proportional damping coefficients.

Modes of the Rayleigh damped systems preserves the simplicity of the real normal modes as in the undamped case solved in the modal analysis.

From the verification of measurement data using the half power bandwidth method, the damping ratios ζ_i and ζ_j can be determined, α and β can then be calculated as function of frequency range f_1 and f_2 as [27]:

$$\begin{bmatrix}\alpha\\ \beta\end{bmatrix} = \frac{2\zeta}{f_1 + f_2}\begin{bmatrix}f_1 f_2\\ 1\end{bmatrix} \tag{72}$$

Figure (20) illustrates the relationship between the mass and stiffness proportional terms as well as the damping ratio as function of frequency. The appropriate calculation of the Rayleigh damping coefficients is critical for the proper dynamic characterization of the structure.

Figure 20 - Mass and Stiffness proportional terms relation with Damping Ratio as function of Frequency

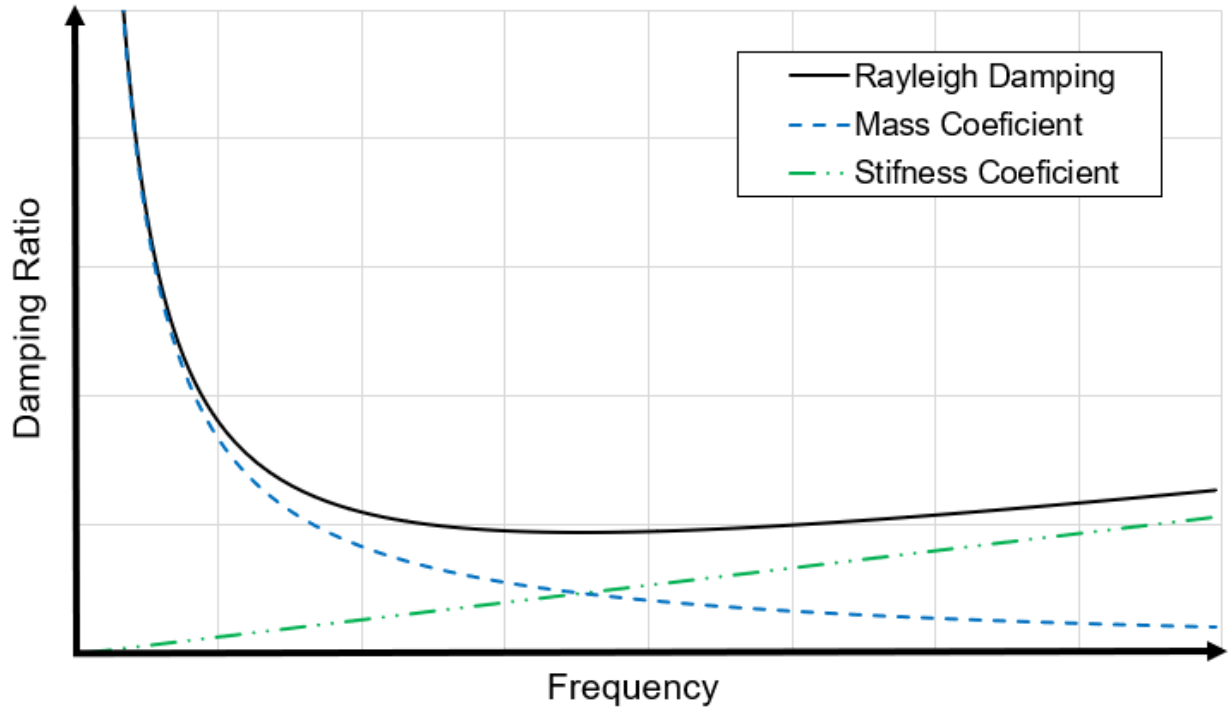

Source: Author

2.10 DISTRIBUTIONS AND PROBABILITY DENSITY FUNCTIONS

The distribution function of x or $F(x)$ (also referred as the cumulative distribution function – CDF) is defined as the probability of occurrence p of the variable x taking a value less than or equal to a .

$$F(x) = Prob\,[x \leq a] = p \tag{73}$$

The distribution function monotonically increased from $F(-\infty) = 0$ to $F(\infty) = 1$. The probability density function (PDF) is defined as

$$p(x) = \lim_{\Delta x \to 0} \left[\frac{Prob[x < x_j \leq x + \Delta x]}{\Delta x} \right] \tag{74}$$

The distribution function is related to the PDF by

$$F(x) = \int_{-\infty}^{x} p(\alpha)\, d\alpha \tag{75}$$

Two common PDFs are the Gaussian (or normal) PDF which for zero mean can be written as:

$$f_{norm}(x; \mu, \sigma) = \frac{1}{\sigma\sqrt{2\pi}}\, exp\left(\frac{-(x-\mu)^2}{2\sigma^2} \right) \tag{76}$$

and the Rayleigh, which PDF is shown below:

$$f_{ray}(x; \mu, \sigma) = \frac{x}{\sigma^2}\, exp\left(\frac{-x^2}{2\sigma^2} \right) \tag{77}$$

The Rayleigh function is useful studying the peak response of narrowband Gaussian signals.

The probability density can be written as $f\,(x; \theta)$ where f is the probability density of x, given a set of parameters θ. For the already presented normal distribution $\theta = (\mu, \sigma^2)$.

The joint probability $f\,(x, y; \theta)$ is the probability of x and y together as a pair, given a set of distribution parameters θ.

The marginal probability $f\,(x, y; \theta)$ is the probability of x, for all possible values of y, given the distribution parameters θ. The marginal probability is determined from the joint distribution of x and y by integrating over all values of y.

Conditional probability $f\,(x|y;\theta)$ is the probability of x by itself, given specific value of variable y, and the distribution parameters θ. If x and y represent events A and B, then:

$$P(A|B) = \frac{n_{AB}}{n_B} \tag{78}$$

where n_{AB} is the number of times both A and B occur, and n_B is the number of times B occurs. In general, the conditional probability of A given B is not the same as B given A.

A method to estimate the parameters θ of a probability distribution is the maximum likelihood estimation (MLE). The values of the parameters are estimated by maximizing the likelihood function, for a specific statistical model. If $x_1, x_2, \ldots . x_n$ are random variables normally distributed, Equation (76) can be written as:

$$f\,(x_1, \ldots, x_n|\mu, \sigma) = \prod_i^n \frac{1}{\sigma\sqrt{2\pi}}\, exp\left(\frac{-(x_i - \mu)^2}{2\sigma^2}\right) \tag{79}$$

The likelihood of the two parameters, μ and σ can be written as:

$$\mathcal{L}(\theta) \;=\; \mathcal{L}(\mu, \sigma) \;=\; -nlog\sigma \;-\; \frac{n}{2} log\; 2\pi \;-\; \frac{1}{2\sigma^2}\sum_{i=1}^{n}(x_i \;-\; \mu)^2 \tag{80}$$

Setting the derivative of the $\mathcal{L}(\theta)$ with respect to μ and σ to zero, the MLE values are obtained.

$$\frac{\partial \mathcal{L}}{\partial \mu} = \frac{1}{2\sigma^2}\sum_{i=1}^{n}(x_i \;-\; \mu) \;=\; 0 \tag{81}$$

$$\frac{\partial \mathcal{L}}{\partial \sigma} = -\frac{n}{\sigma} + \sigma^{-3}\sum_{i=1}^{n}(x_i \;-\; \mu)^2 \;=\; 0 \tag{82}$$

2.11 WIDEBAND RANDOM FATIGUE

The Palmgren-Miner linear cumulative damage rule was applied to narrow band random fatigue by Miles [28] in the mid 1950's. Miles extended the linear summation of damage to an integral of stress peaks scaled by the probability density function of stress peaks, which, for a narrow band random system, is a Rayleigh distribution. It is widely accepted the fact that the narrowband approximation, when applied to wideband process tends to overestimate the fatigue damage and was proved rigorously by Rychlik [29].

The difficulties to obtain stress time histories sufficiently long to reliably characterize the structures and the significant computational effort to calculate the transient stress responses to determine the rainflow cycle distributions has led to the development of frequency domain techniques. The seminal work by Rice [22] and research since has shown that the PDF of peak response can be determined from moments of the frequency domain response power spectral density (PSD) and that the peak PDF can be described by combination of a Gaussian and a Rayleigh PDF.

2.11.1 DIRLIK'S PROBABILITY DENSITY FUNCTION

In 1985, Dirlik developed an empirical closed form solution for the wide band random problem, the proposed PDF considered the sum of two Rayleigh distributions and one exponential distribution developed from an extensive Monte Carlo technique [30]. Although apparently more complicated than some alternative methods, it is only a function of the four moments of area of the PSD. This method has been found to be widely applicable and constantly outperforms all the other available methods considering the four moments of area of the PSD [31].

The Dirlik PDF model developed over the stress range is given by [30]:

$$p(S)_{Dirlik} = \frac{\frac{D_1}{Q_1} e^{\frac{-Z}{Q_1}} + \frac{D_2}{R^2} e^{\frac{-z^2}{2R^2}} + D_3 Z e^{\frac{-Z^2}{2}}}{2\sqrt{m_0}}, \tag{83}$$

where the parameters D_1, D_2, D_3, Q_1, R e Z are defined as function of the PSD moments as shown from Equation (84) through Equation (90).

$$x_m = \frac{m_1}{m_0}\sqrt{\frac{m_2}{m_4}} \tag{84}$$

$$D_1 = \frac{2(x_m - \gamma^2)}{1 + \gamma^2} \tag{85}$$

$$R = \frac{\gamma - x_m - {D_1}^2}{1 - \gamma - D_1 + {D_1}^2} \tag{86}$$

$$D_2 = \frac{1 - \gamma^2 - D_{1+}{D_1}^2}{1 - R} \tag{87}$$

$$D_3 = 1 - D_1 - D_2 \tag{88}$$

$$Q_1 = \frac{1.25(\gamma - D_{3+}D_2 R)}{D_1} \tag{89}$$

$$Z = \frac{S}{2\sqrt{m_0}} \tag{90}$$

Dirlik's PDF establishes the correlation between the stress response spectral density distribution and the rainflow cycle counts through the amplitude distribution. Moreover, the PSD being a static representation of the random process, requires as duration time parameter to properly model the damage experienced by the structure, this parameter is independent of the count method used, nonetheless, in a stationary process which the rainflow method is applied, the total number of cycles is a function of expected rate of peak occurrence $E[P]$ given in peaks per unit time multiplied by a time period $T_{exposure}$.

This relation gives a great computational advantage and flexibility for the calculation of fatigue life in the frequency domain, as the number of cycles for long periods of time, can simply be estimated by changing time parameter, which in the time domain would require the calculation of the entire load history.

Figure (21) illustrates Dirlik's PDF as a function of stress amplitude, which represents the probability of occurrence of a specific stress amplitude. The area under the curve is equal to a unit, as it represents all the possible stress amplitudes experienced by the structure. The number of cycles at a specific stress amplitude S_i is obtained for a given exposure time $T_{exposure}$ to a given vibration profile by Equation (91).

$$n_{i_{Dirlik}} = p(S_i)_{Dirlik}.dS.E[P].T_{exposure} \tag{91}$$

Figure 21 – Dirlik's pdf as function of the stress amplitude

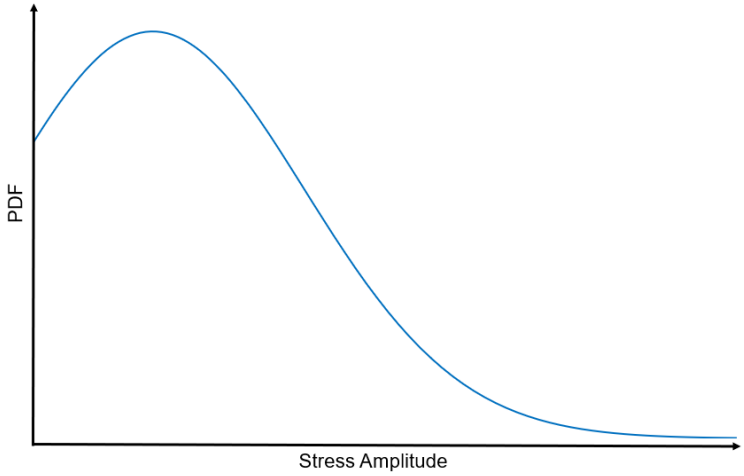

Source: Author

2.11.2 LALLANE'S PROBABILITY DENSITY FUNCTION

Lallane provides an analytical probability distribution based on Rice's distribution of peaks in a random signal. The probability density $p(S_i)_{Lallane}$ is a weighted sum of a Gaussian and Rayleigh distributions, with coefficients function of the irregularity factor.

Lallane's PDF model in [19] is given by:

$$p(S)_{Lallane} = \frac{\sqrt{1-\gamma^2}}{S_{rms}\sqrt{2\pi}} e^{-\frac{S^2}{2(1-\gamma^2){S_{rms}}^2}} + \frac{\gamma S}{2{S^2}_{rms}} e^{-\frac{S^2}{2{S^2}_{rms}}\left[1+erf\left(\frac{\gamma S}{S_{rms}\sqrt{2(1-\gamma^2)}}\right)\right]}, \quad (92)$$

where S_i is the stress range and $erf(x)$ is the Gauss error function given by:

$$erf(x) = \frac{2}{\sqrt{\pi}} \int_0^x e^{-t^2} dt \quad (93)$$

Similarly, to Dirlik's method, the number of cycles at a specific value of stress i are obtained for a given time of vibration duration, which can be written as:

$$n_{i_{Lallane}} = p(S_i)_{Lallane}.dS.E[P].T_{exposure} \quad (94)$$

2.12 S-N CURVES

Fatigue testing aims to identify the relationship between the resistance of a given material or structure subjected to cyclic loading. The results of a fatigue test are presented in graphs that relates the applied loading (e.g. force, stress, strain) and the number of cycles to failure.

The inherent variations in material properties, surface defects, manufacturing tolerances and testing conditions, result in an invariably scattered data. The characterization of the resistance to fatigue of material requires several test specimens tested at same and different loading conditions, therefore the fatigue data shall be described in a statistical manner. Since the work from August Wöhler performing systematic fatigue tests of smooth and notched railway axles in the 1850s, the classical approach to fatigue has focused on the plot of the number of cycles to failure for a given stress level, which is known as S-N diagram or S-N curve.

The percentile curves illustrate the variability of fatigue life, meaning that at p=0.5, 50% of the specimens fail above this curve and 50% below it, Figure (22) illustrates the fit of fatigue testing data using Basquin's model. The percentile curves can also be used to define design curves at any other percentile value.

Figure 22 - P-S-N curve following a Basquin model

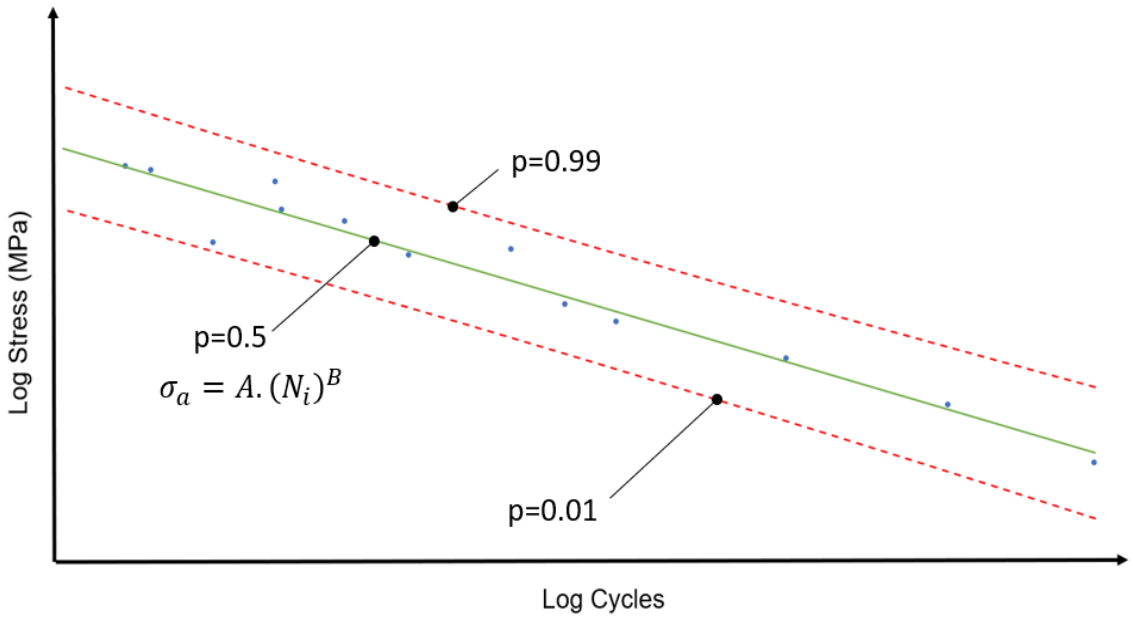

Source: Author

DNV-RP-C203 provides guidance to address uncertainties in fatigue life prediction.

A design S-N curve should provide 97.7% probability of survival. The design curves can be derived as mean minus two standard deviations. The mean curve is required to be estimated with at least 75% confidence. Two approaches are presented to derive a S-N design curve, named: Pure statistical approach and engineering approach. The main difference between the two approaches is the standard deviation of the test results which can be assumed to be the same as the standard S-N curves in the engineering approach and is "unknown" in the statistical approach. A detailed description of the statistical approach is presented in [12].

The standard approach in curve fitting assumes that the parameter plotted on the x-axis is the independent variable and the one plotted on the y-axis is the dependent variable. However, in the S-N diagram the dependent variable, number of cycles, is commonly presented in the x-axis. The best fit line through the data is estimated usually using the ordinary least squares (OLS) method. This method is based on choosing those values of the coefficients that minimize the sum of the squared deviations (residuals) of the observed values of $log\ N_i$ from those predicted by the fitted line [32].

Using the OLS method to estimate the mean curve giving a set of experimental data, the confidence interval must be defined. The linear regression in the log-log plot can be defined as:

$$y\ = a\ + bx\ + \epsilon \tag{95}$$

From testing data, the linear regression curve can be written as:

$$\hat{y}_i\ = a\ + bx_i\ , \tag{96}$$

where $\hat{y}_i$ is the value of y value predicted by the model at x_i and $\bar{x}$ and $\bar{y}$ are the average values of x and y.

$$b\ = \frac{\sum(x - \bar{x})\ (y - \bar{y})}{\sum(x - \bar{x})^2} \tag{97}$$

The error term is given by:

$$\epsilon_i = y_i - \hat{y}_i \tag{98}$$

The standard error of the estimate is defined as:

$$s_{xy} = s_y \sqrt{(1 - r^2)\frac{n-1}{n-2}}, \tag{99}$$

where n is the number of samples and s_y the standard deviation of y and r^2 is given by :

$$r^2 = \frac{\sum(\hat{y}_i - \bar{y})^2}{(y_i - \bar{y})^2} \tag{100}$$

The r^2 term represents the percentage of the variability of y that cannot be explained by the regression model.

The standard error of the confidence interval (CI) is given by:

$$s_{e_{CI\,i}} = s_{xy} \sqrt{\frac{1}{n} + \frac{(x_i - \bar{x})^2}{\sum(x_i - \bar{x})^2}} \tag{101}$$

Let S be a Student's t distribution defined as:

$$f(s) = \frac{\Gamma\left(\frac{\nu+1}{2}\right)}{\Gamma\left(\frac{\nu}{2}\right)} \frac{1}{\sqrt{\nu\pi}} \frac{1}{\left(1 + \frac{s^2}{\nu}\right)^{\frac{1+\nu}{2}}} \tag{102}$$

The function $f(s)$ returns the probability of observing a value of s from the Student's t distribution with ν degrees of freedom, $\Gamma(\cdot)$ is the gamma function. For a given significance level α, the inverse density $\alpha = \frac{1}{S}$, can be written as:

$$h(\alpha) = \frac{\Gamma\left(\frac{\nu+1}{2}\right)}{\Gamma\left(\frac{\nu}{2}\right)} \frac{1}{\sqrt{\nu\pi}} \frac{1}{\alpha^2\left(1 + \frac{1}{\alpha^2\nu}\right)^{\frac{1+\nu}{2}}} \tag{103}$$

The two values of $h(\alpha)$ which the two-tailed Student's t distribution is satisfied are defined as the critical values. Furthermore, the upper and lower intervals of $\hat{y}$ given the confidence interval μ_c and ν degrees of freedom can be defined as:

$$\hat{y}_{CI\ upper_i} = \hat{y}_i + h_{critical}(\alpha_{CI}|\nu)\, s_{e_i} \quad (104)$$

$$\hat{y}_{CI\ lower_i} = \hat{y}_i - h_{critical}(\alpha_{CI}|\nu)\ \ s_{e_i}\,, \quad (105)$$

where $\alpha_{CI} = 1 - \mu_c$

Similarly, the upper and lower percentile S-N curves (P-S-N), for a given prediction interval (PI) μ_p, are defined using the prediction interval standard error $s_{e_{PI}}$ as shown by Equations (106), (107) and (108).

$$s_{e_{PI_i}} = s_{xy}\sqrt{1 + \frac{1}{n} + \frac{(x_i - \bar{x})^2}{\sum(x_i - \bar{x})^2}} \quad (106)$$

$$\hat{y}_{PI\ upper_i} = \hat{y}_i + h_{critical}(\alpha_{PI}|\nu)\ \ s_{e_i} \quad (107)$$

$$\hat{y}_{PI\ lower_i} = \hat{y}_i - h_{critical}(\alpha_{PI}|\nu)\, s_{e_i}\,, \quad (108)$$

where $\alpha_{PI} = 1 - \mu_p$.

Equations (104) and (105) are used to validate the minimum interval where the mean curve (p=0.5) can be accepted which the DNV-RP-C-203 defines to be at least 75% confidence, whereas Equations (107) and (108) provide the framework to construct any other percentile curve defined by the prediction interval μ_p.

2.13 RANDOM FATIGUE LIMIT MODEL

When the material exhibits fatigue limit, there are two main considerations in modelling the relationship between the applied stress and fatigue life, first, the standard deviation of fatigue life decreases as the applied stress increases. Second, the curvature suggests the inclusion of a fatigue limit in the statistical model. The random fatigue-limit model describes features observed during experimental testing [7].

The fatigue life for each specimen *i* denoted by $\boldsymbol{N}$ at a stress level $\boldsymbol{S}$ can be modelled as:

$$\boldsymbol{ln(N_i) = \beta_0 + \beta_1 log(S_i - \gamma_{lim}) + \epsilon\,,\ \ S_i > \gamma_{lim},} \tag{109}$$

where $\boldsymbol{\beta_0}$ and $\boldsymbol{\beta_1}$ are fatigue curves coefficients, $\boldsymbol{\gamma_{lim}}$ is the fatigue limit of the specimen, $\boldsymbol{\epsilon}$ is the error term, which is a random life variable associated with the scatter from specimens which have same value for fatigue limit.

Let $\boldsymbol{V = log\ (\gamma_{lim})}$, then Pascual and Meeker in [7] assume $\boldsymbol{V}$ to have a probability density function given by:

$$\boldsymbol{f_V\left(v; \mu_{\gamma_{lim}}, \sigma_{\gamma_{lim}}\right) = \frac{1}{\sigma_{\gamma_{lim}}}\ \phi_V\left(\frac{v - \mu_{\gamma_{lim}}}{\sigma_{\gamma_{lim}}}\right)} \tag{110}$$

In Equation (110), $\boldsymbol{\mu_{\gamma_{lim}}}$ and $\boldsymbol{\sigma_{\gamma_{lim}}}$ are the location and scale parameters for the distribution of $\boldsymbol{\gamma_{lim}}$, respectively. $\boldsymbol{\phi_V}$ is either the standardized smallest extreme value (sev) or normal PDF.

Let $x = log\ (S)$ and $W = log\ (N)$. Then, for $V < x$ they assume that *W* given *V* has a PDF of the form:

$$\boldsymbol{f_{W|V}(\omega, \beta_0, \beta_1, \sigma, x, v) = \int_{-\infty}^{x} \frac{1}{\sigma}\ \phi_{W|V}\left\{\frac{\omega - \{\beta_0 + \beta_1 log\ [exp(x) - exp\ (v)]\}}{\sigma}\right\}} \tag{111}$$

In Equation (111), $\boldsymbol{\beta_0 + \beta_1 log\ [exp(x) - exp\ (v)]}$ acts as a location parameter and $\boldsymbol{\sigma}$ as a scale parameter, $\boldsymbol{\phi_{W|V}}$ is either the standardized smallest extreme value (sev) or normal pdf. The marginal PDF of *W* is given by:

$$\boldsymbol{f_W(\omega, x, \theta) = \int_{-\infty}^{x} \frac{1}{\sigma\sigma_{\gamma_{lim}}}\ \phi_{W|V}\left[\frac{\omega - \mu(x, v, \theta)}{\sigma}\right] \phi_V\left(\frac{v - \mu_{\gamma_{lim}}}{\sigma_{\gamma_{lim}}}\right) dv,} \tag{112}$$

where $\boldsymbol{\theta} = (\boldsymbol{\beta_0}, \boldsymbol{\beta_1}, \boldsymbol{\sigma}, \boldsymbol{\mu_{\gamma_{lim}}}, \boldsymbol{\sigma_{\gamma_{lim}}})$ and $\boldsymbol{\mu(x, v, \theta) = \beta_0 + \beta_1 log\,[exp(x) - exp\,(v)]}$. The marginal cumulative distribution function (CDF) of $\boldsymbol{W}$ can be written as:

$$\boldsymbol{F_W(\omega, x, \theta) = \int_{-\infty}^{x} \frac{1}{\sigma}\, \Phi_{W|V}\left[\frac{\omega - \mu(x, v, \theta)}{\sigma}\right] \phi_V\left(\frac{v - \mu_{\gamma_{lim}}}{\sigma_{\gamma_{lim}}}\right) dv,} \tag{113}$$

where $\boldsymbol{\Phi_{W|V}(\cdot)}$ is the cdf of $\boldsymbol{W|V}$. This statistical model is referred as random fatigue limit model (RFL).

There are no closed forms for the density and distribution functions which demands numerical evaluation.

2.13.1 MODEL PARAMETERS ESTIMATION

Pascual and Meeker in [7] used the maximum likelihood (ML) methods to estimate the parameters of the random fatigue-limit model. Statistics theory suggests that ML estimators, in general, have favorable asymptotic properties for large samples.

Let $\boldsymbol{N_p(s)}$ be the $\boldsymbol{p}$ quantile of the life distribution at stress level $\boldsymbol{S}$. The ML is estimated for $\boldsymbol{N_p(s)}$ for $\boldsymbol{p}$ = 0.05, 0.50 and 0.95 which are the percentile curves.

For the random fatigue-limit model defined previously with sample data $\boldsymbol{\omega_1 = \log(N_1)}, \ldots, \boldsymbol{\omega_n = \log(N_n)}$ at log stress levels $\boldsymbol{x_1, \ldots, x_n}$, respectively, the likelihood can be written as:

$$\boldsymbol{L\,(\theta) = \prod_{i=1}^{n} [f_W(\omega_i; x_i, \theta)]^{\delta_i} [1 - F_W(\omega_i; x_i, \theta)]^{1-\delta_i}}, \tag{114}$$

where $\boldsymbol{\delta_i = 1\ if\ \omega_i}$ is a failure and $\boldsymbol{\delta_i = 0\ if\ \omega_i}$ is a censored observation.

The function $\boldsymbol{L\,(\theta)}$ can be interpreted as being approximately proportional to the probability of observing $\boldsymbol{N_1, \ldots, N_n}$ for a given set of parameters $\boldsymbol{\theta}$. Generally, it is more convenient to write the log-likelihood function. Maximizing the log-likelihood function produces the same set of parameters as maximizing the likelihood function. The log-likelihood function is written as:

$$\boldsymbol{\mathcal{L}(\theta) = log[L(\theta)] = \sum_{i=1}^{n} \mathcal{L}_i(\theta)}, \tag{115}$$

where,

$$\boldsymbol{\mathcal{L}(\theta) = \delta_i log[f_W(\omega_i, x_i, \theta)] + (1 - \delta_i) log[1 - F_W(\omega_i, x_i, \theta)]}, \tag{116}$$

is the contribution of the $\boldsymbol{i}$ th observation. The ML estimate $\widehat{\boldsymbol{\theta}}$ of $\boldsymbol{\theta}$ is the set of parameters values that maximizes $\boldsymbol{L}(\boldsymbol{\theta})$ or $\boldsymbol{\mathcal{L}}(\boldsymbol{\theta})$.

An application of the RFL method is presented by Pollak in his PhD thesis [34] for the Titanium Alloy α-β Ti-6Al-4V.

For the distribution of the random variable $\boldsymbol{\gamma_{lim}}$, the Weibull distribution is an adequate choice for describing the skewed downward strength distribution of many engineering materials. The Weibull distribution introduces two parameters, the location parameter η and the scale parameter $\boldsymbol{\beta_2}$, which correspond to the location and scale parameters $\boldsymbol{\mu_{\gamma_{lim}}}$ and $\boldsymbol{\sigma_{\gamma_{lim}}}$ respectively, used in the RFL model.

Figure (23) illustrates the fit of the RFL model to the experimental data from [34]. The model parameters are shown in table 1:

Table 1 - RFL model parameters for data best fit

Parameter	Description	Value
β_0	S-N curve coefficient	4.95
β_1	S-N curve coefficient	-2.11
σ_ε	Std deviation in lognormal fatigue life	0.16
η	Weibull location parameter for fatigue limit	405
β_2	Weibull Scale parameter for fatigue limit	18

Figure 23 - RFL model applied to the α-β Ti-6Al-4V testing data showing the 0.05, 0.5 and 0.95 percentile fitting curves

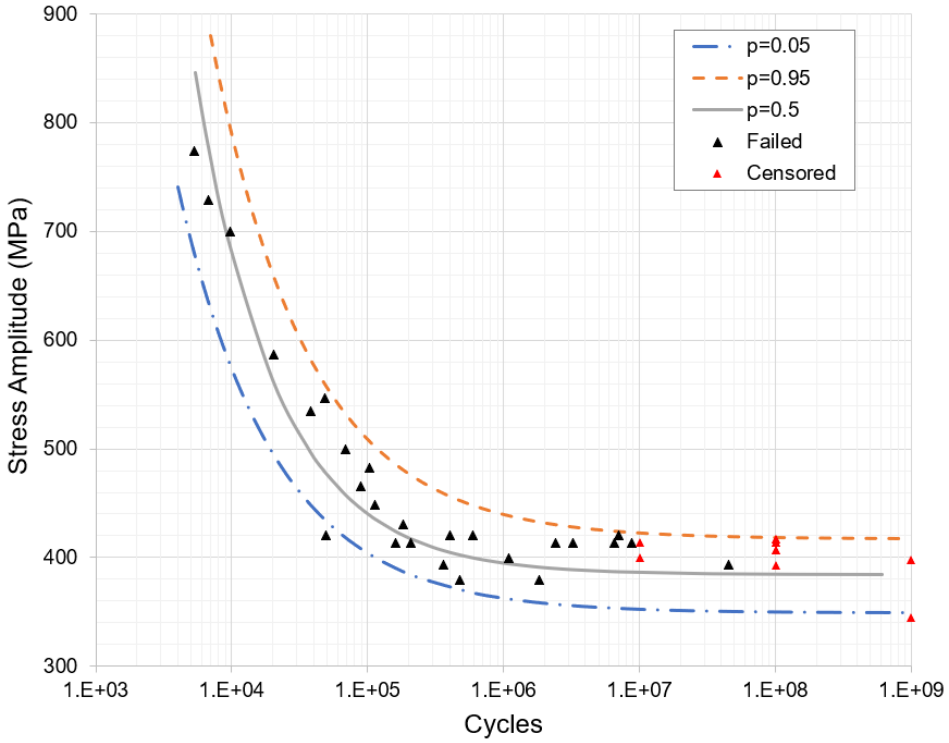

Source: Author

The fatigue data for the Titanium Alloy α-β Ti-6Al-4V reveals a significant curvature when the fatigue limit is approached. Basquin's model is no longer capable to model such behavior, thereafter, the RFL method expands the possibilities to properly model a wider range of materials specially in high cycle fatigue applications.

2.14 PROBABILISTIC LINEAR CUMULATIVE DAMAGE

The damage is calculated using generally the 50% percentile best fitted S-N curve using Equation (1), however, due to the scatter in the material data, a probabilistic linear cumulative is here proposed to characterize the variability of the damage estimation using the different percentile fatigue life curves. For materials that do not exhibit fatigue limit the percentiles curves could be estimated based on the OLS method and a defined prediction interval, for the case of materials that fatigue limit is observed, one could use RFL method to generate the percentile S-N curves.

Based on Palgren-Miner's equation the probabilistic linear cumulative damage is here defined as:

$$D_{p_x} = \sum_{i=1}^{k} \frac{n_i}{N_{i\,p_x}} \tag{117}$$

where p_x represents the percentile curve used for the damage estimation. The damage is now computed not only for the commonly used median percentile but for any confidence level interval of interest.

The fatigue life of the component expressed in Equation (117) is defined as number of repeats of the determined load or combination of loads which led the component to accumulate damage, therefore, a life greater than one means that the component will survive the subjected load requirement without failure. A value smaller than one is interpreted as the component is likely to fail before the test is completed.

$$Life_{\,p_x} = \frac{1}{D_{p_x}} \tag{118}$$

The time to failure (TTF) is estimated considering exposure time to the vibration profile and the damage associated to specific fatigue curve percentile as per Equation (119), which could also be defined in terms of life as shown by Equation (120).

$$TTF_{p_x} = \frac{T_{exposure}}{D_{p_x}} \tag{119}$$

$$TTF_{p_x} = T_{exposure}.Life_{\,p_x} \tag{120}$$

The time to failure is calculated based on the test duration, or repetitions of the random vibration excitation. The benefit of estimating the fatigue life using the different S-N curve percentiles is the understanding of how a specific material or manufacturing method could impact in the performance of the structure in service. Instead of a unique life value, the proposed method provides a range that is inherent to the scatter in fatigue testing.

Safety factors could also be added to the proposed modeling process, where design curves could be defined systematically based on pre-determined percentile curves.

The probabilistic linear cumulative damage model presented in Equation (117) has the flexibility to be applied independent of the method used to obtain the S-N curve percentiles, thereafter, allowing the usage of linear, bilinear, multilinear, hyperbolic, RFL, material modeling techniques.

Pascualinotto and Sarzosa discussed the application of the probabilistic linear cumulative damage using the RFL method described in 2.13 in [35].

3 MATERIALS AND METHODS

The fatigue life calculation in frequency domain offers great advantage in terms of calculation time compared to the time domain, enabling to solve much larger and complex problems using finite element analysis. However, due to statistical nature of the frequency domain method, the understanding of the parameters that influence most the fatigue prediction results is key to the reliable application of the method.

In [8] the predicted fatigue life in the frequency and time domains differed by approximately 20%, with the frequency domain result being more conservative. Observing the work from Castillo and Canteli in [4] and Pascual and Meeker in [7], the scatter of fatigue testing results suggests that the prediction of fatigue life must be made in a probabilistic manner.

The DNV-RP-C203 standard provides guidance to generate design curves to account for the testing scatter, considering the mean minus two standard deviations of the testing data. The suggested probability of survival is used in this work.

The fatigue life of a 6061-T6 notched aluminum specimen is estimated for the combined load cases of two different vibration profiles. The total fatigue damage and life are estimated in both time and frequency domains for the different S-N percentiles, the results are compared to experimental results.

3.1 FATIGUE LIFE ESTIMATION OF A NOTCHED 6061-T6 ALUMINUM COMPONENT

A notched 6061-T6 aluminum specimen illustrated in Figure (24) is subjected to two different vibration profiles applied in the Z axis direction, following the workflow shown in Figure (25). The first PSD profile was defined with a specific time duration, subsequently the component is subjected to a second PSD profile with an increased root mean square acceleration where the component was tested to failure. Based on the cumulative damage process, the objective of the first test is to pre-damage the structure. To evaluate the effects of the geometrical discontinuity in the fatigue life, a double notched specimen with 1.9mm wall thickness was defined.

Figure 24 - Specimen Design

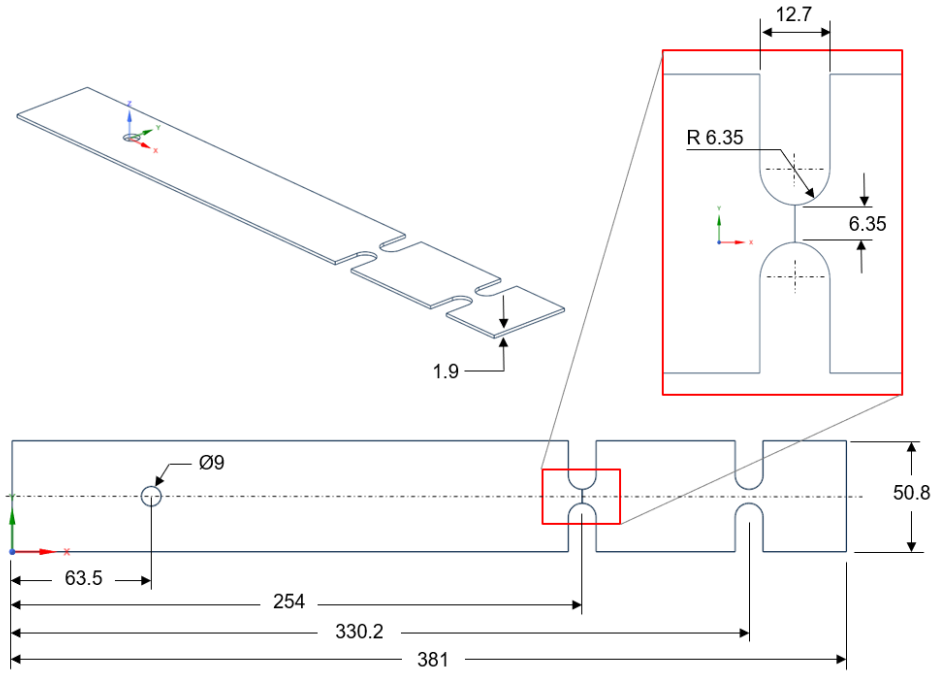

Source: Author

Figure 25 - Testing / Simulation workflow

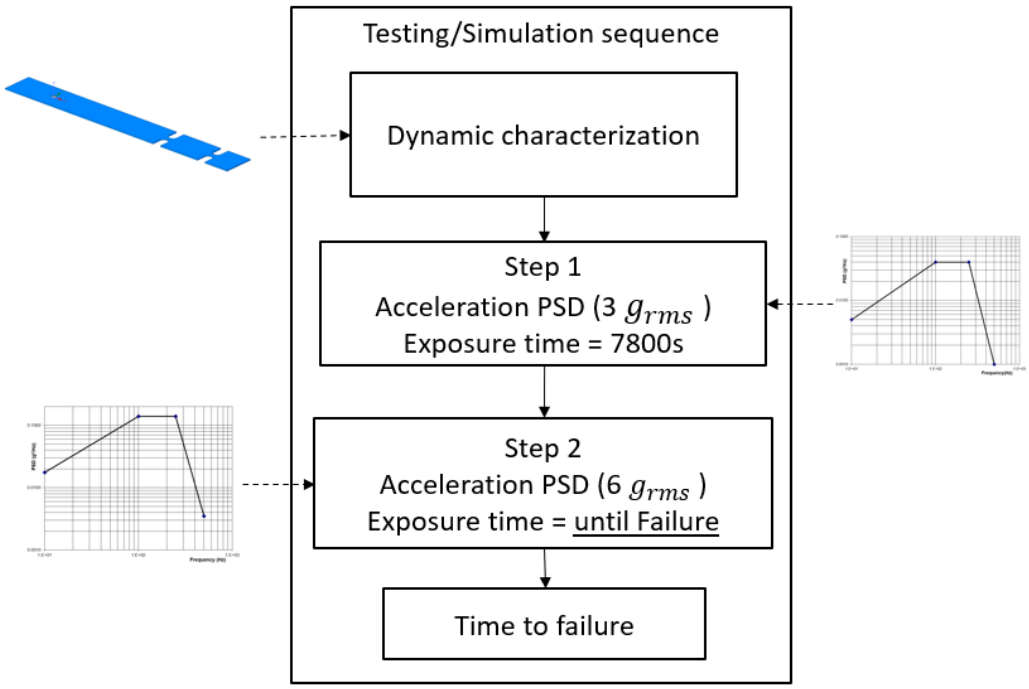

Source: Author

The material modeling took into consideration the engineering stress-strain curve and unnotched fatigue data from [36], the material data for the 6061-T6 aluminum are illustrated in Figures (26) and (27).

Figure 26 - 6061-T6 Aluminum – Engineering stress strain curve

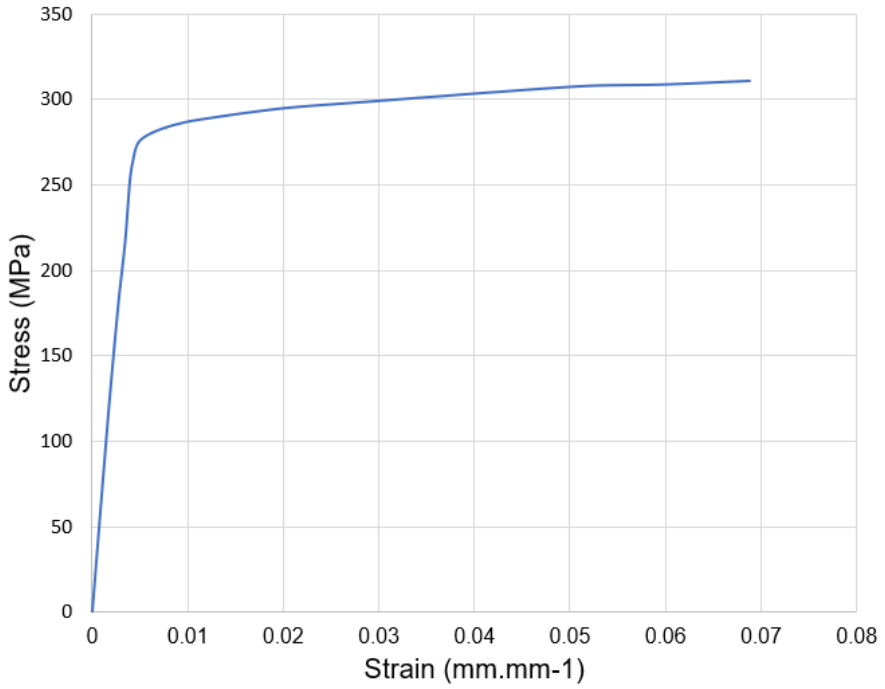

Source: Author

Figure 27 - 6061-T6 Aluminum - Unnotched Fatigue Data

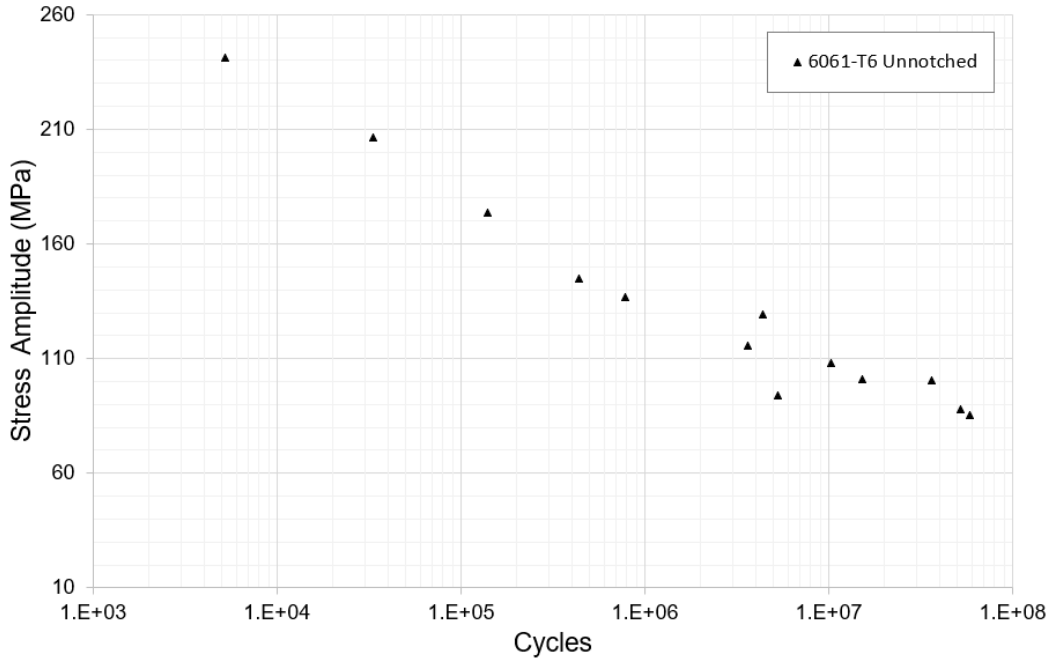

Source: Author

The fatigue strength reduction factor k_f is calculated using the volumetric approach to correct the S-N curve for the notched condition. Equations (121) and (122) following the local coordinate system in the numerical model as shown in Figure (28) can be written as:

$$k_{f_{model}} = \frac{1}{y_{eff}\ \sigma_{net}} \int_0^{y_{eff}} \sigma_{xx}(y)(1 - y\chi)dx \tag{121}$$

$$\chi_{model} = \frac{1}{\sigma_{xx}(y)} \frac{d\sigma_{xx}(y)}{dy} \tag{122}$$

Figure 28 - Crack opening direction - Y

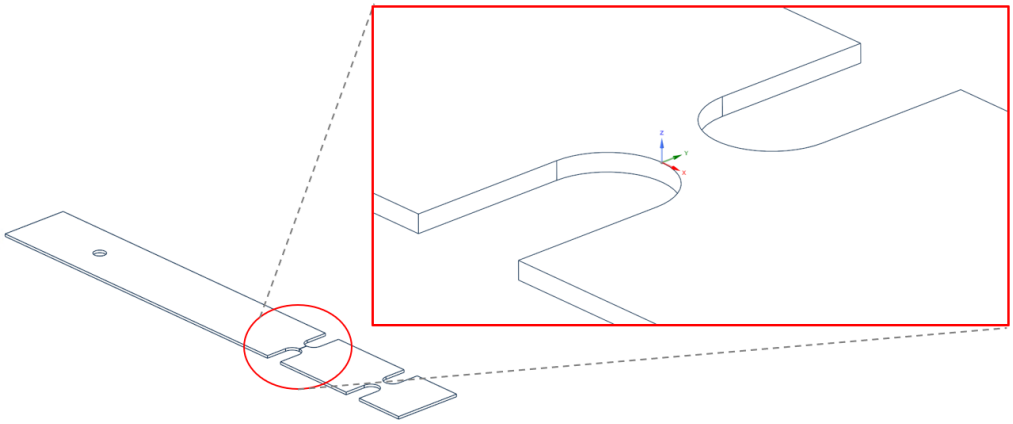

Source: Author

The crack opening stress is induced by the combined effect of a tensile and bending stress, a multilinear kinematic hardening plasticity model has been used to model the elastic-plastic behavior based on the stress-strain curve presented in Figure (26). A tensile displacement of 0.25mm and a moment load of 100N.mm were applied to the free end of the specimen to induce yielding at the root of the notch. The two loading conditions types were defined to correlate to the unnotched fatigue test which is generated through tensile loading and during the vibration test the specimen primarily undergoes bending loads.

A mesh independency study was carried out to properly capture the opening stress behavior near the notch tip. The determination of the mesh refinement was based not only on the stress value at the notch tip, but the behavior near the notch. The variation of the max stress at the notch root per the number of elements in the discretized finite element model is illustrated in Figure (29) for various mesh element sizes.

Figures (29) and (30) present the crack opening stress variation near the notch where five different element sizes were evaluated, 1mm, 0.5mm, 0.25mm, 0.125mm and 0.1mm. A

significant numerical difference is observed with 1mm element size, 0.5mm and 0.25mm have approximate solution values at the notch root compared to the smaller element sizes, however, as the volumetric approach uses the relative stress gradient, the stress distribution near the notch is relevant.

Figure 29 - Max stress at the notch root (y=0) per the number of elements in the finite element model

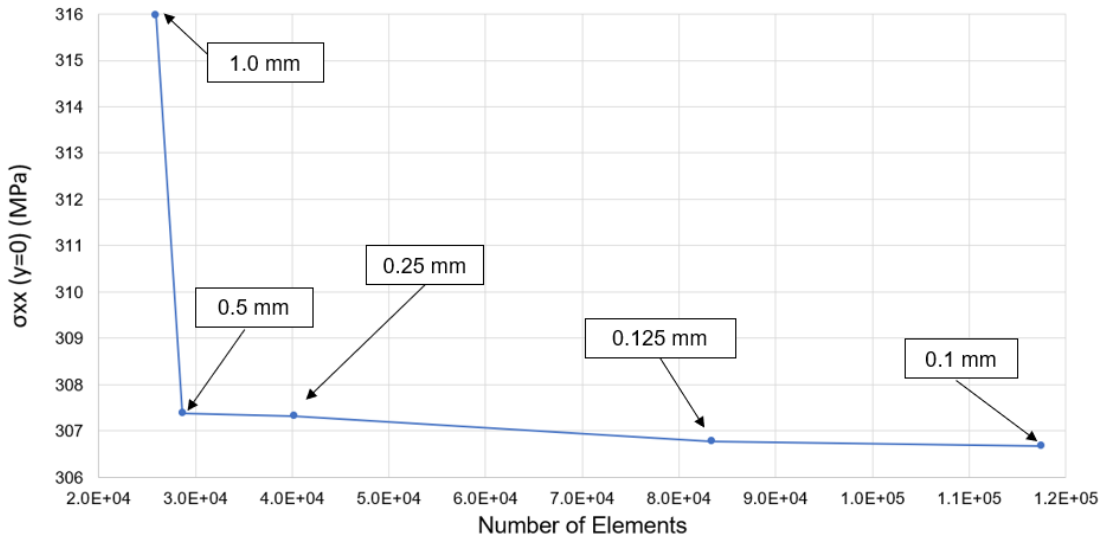

Source: Author

Figure 30 - Crack opening stress variation with the mesh element size refinement

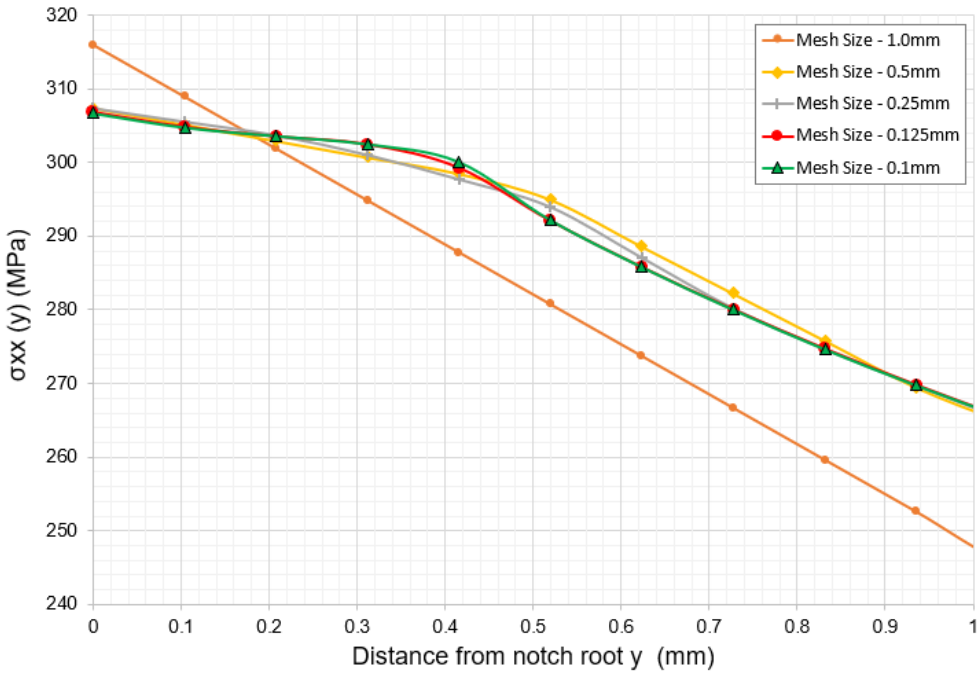

Source: Author

The stress solution for the element sizes 0.1mm and 0.125mm had an average variation of 0.1MPa from y=0 to y=1mm. After defining the size range where a minimum variation was expected the calculation time was also evaluated, as this choice would define the base model for the dynamic and fatigue analysis. The element size of 0.125mm has been selected based on the reduced computational time compared to the 0.1mm, the summary of the calculation time for the two elements sizes are shown in Table 2.

Table 2 - Calculation time for the refined element size at the notch area

Element Size (mm)	Calculation time
0.125	39 m 19s
0.100	2h 56m 52s

The model discretization with the mesh refinement at the vicinity of the notch to properly capture the stress gradient is illustrated in Figure (31). The crack opening stress $\sigma_{xx}(y)$ as function of the crack opening distance is shown in Figure (32).

Figure 31 - Numerical Model discretization – Mesh element size - 0.125mm

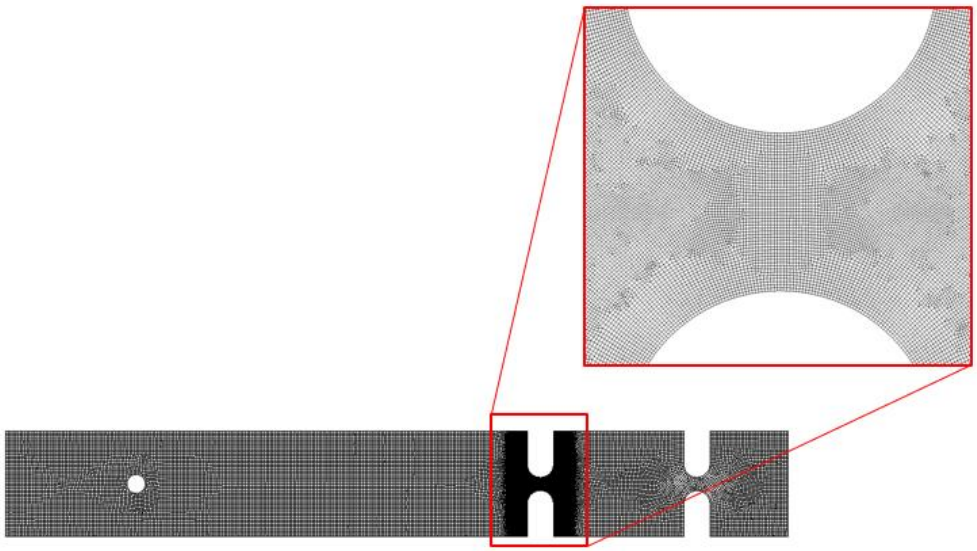

Source: Author

Figure 32 - Crack opening stress distribution near the notch

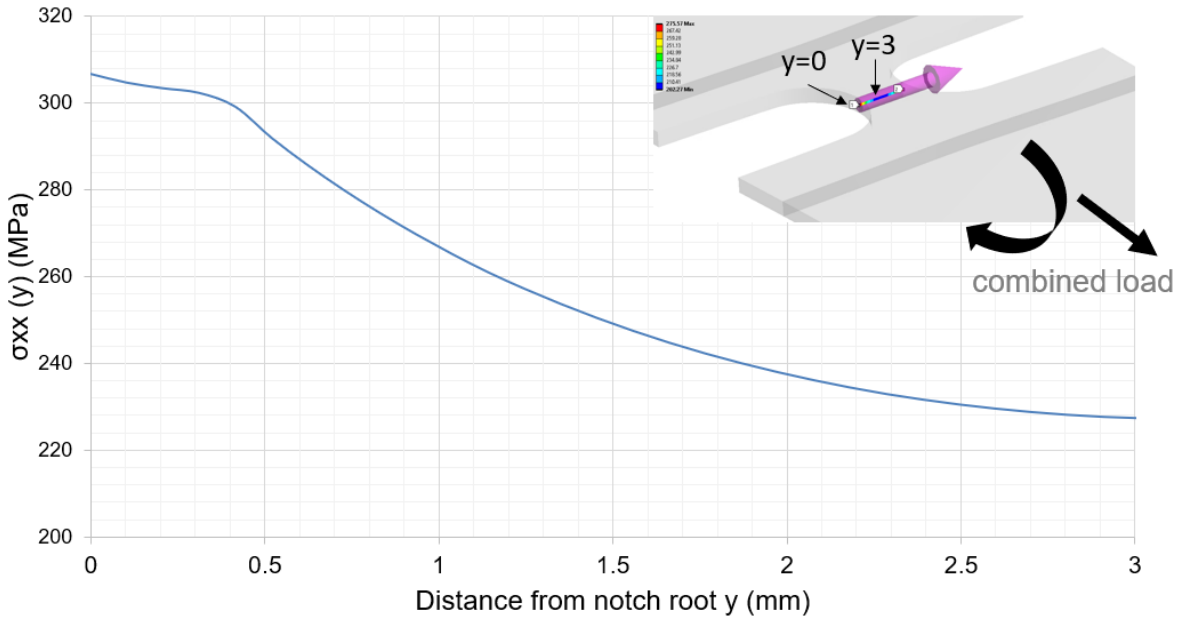

Source: Author

A MATLAB routine was created to calculate the relative stress gradient χ , the effective distance y_{eff} is determined graphically at the inflection point of χ as per Figure (33). The fatigue strength reduction factor of k_f=1.14 was obtained from Eq. (121).

Figure 33 - The elastic–plastic fatigue crack opening stress and relative stress distribution

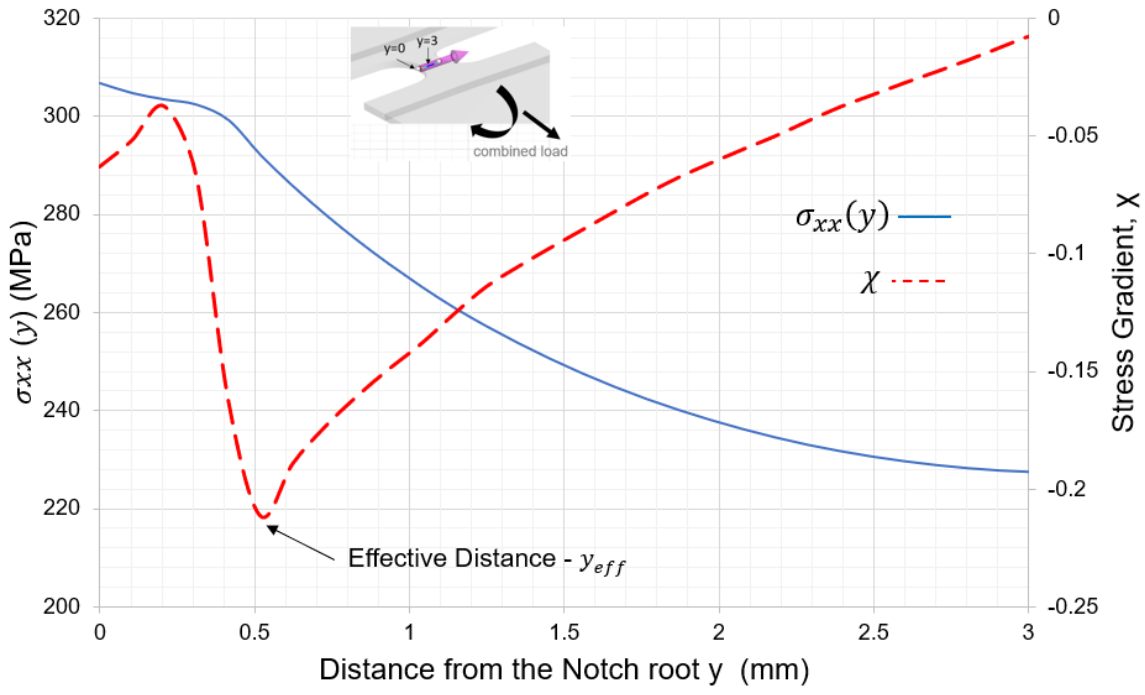

Source: Author

The plot of the raw fatigue unnotched data presented in Figure (27) considering the log number of stress as the independent variable and following the DNV-RP-C203 engineering approach recommendation is shown in Figure (34) which illustrates the fit of the data for the percentile curves p=0.01 and p=0.99. The prediction interval (PI) has been defined as 97.7% for a mean confidence interval (CI) of 95%. Table 3 presents a summary of the statistical parameters that define the confidence interval curves as well as the percentiles curves for the defined prediction interval.

Table 3 – Statistical parameters to define the percentile curves

Parameter	Description	Value
n	Number of tested samples	13
$\bar{x}$	Mean log of stress	2.09 MPa
s_{xy}	Standard error of predicted cycle value for each stress value in the regression	0.285
μ_{c}	Confidence interval	0.950
μ_p	Prediction Interval	0.977
ν	Degrees of freedom	11
$h_{critical}(\alpha_{CI}\|\nu)$	Student's t critical value for the given confidence interval	2.20 MPa
$h_{critical}\ (\alpha_{PI}\|\nu)$	Student's t critical value for the given prediction interval	2.69 MPa

Figure 34 - Unnotched fatigue raw data with 95% CI / 97.7% PI

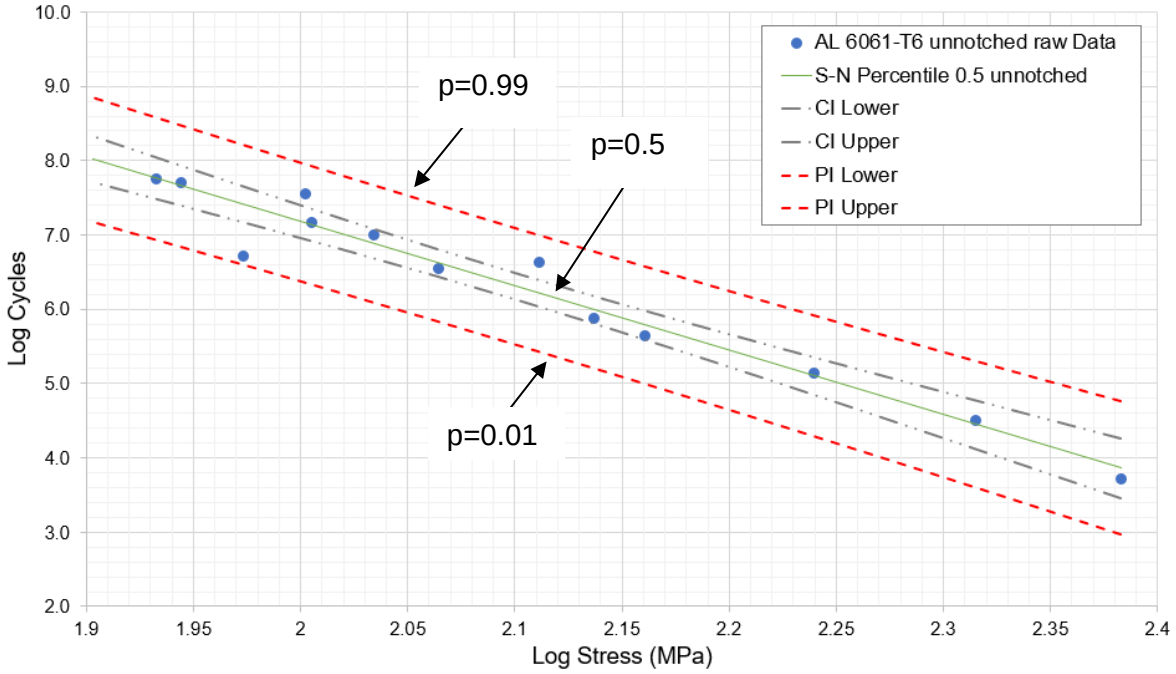

Source: Author

As expected, the percentile curves create an envelope that contains of all data points from testing, this is a better representation of the variation which reflects directly in the component fatigue life.

The fatigue strength reduction factor k_f is then applied to the unnotched S-N percentile curves. The corrected P-S-N curves in a log-log scale are illustrated in Figure (35).

It is noticeable the influence of the notch reducing the fatigue strength of the specimens that contain this type of geometric discontinuity. Due to time and economic constrains to generate fatigue data for all the different design possibilities, the presented method supports the identification of parameters that can affect the fatigue performance tailoring the decisions regarding testing scope.

Figure 35 - Corrected percentile S-N curves for k_f=1.14

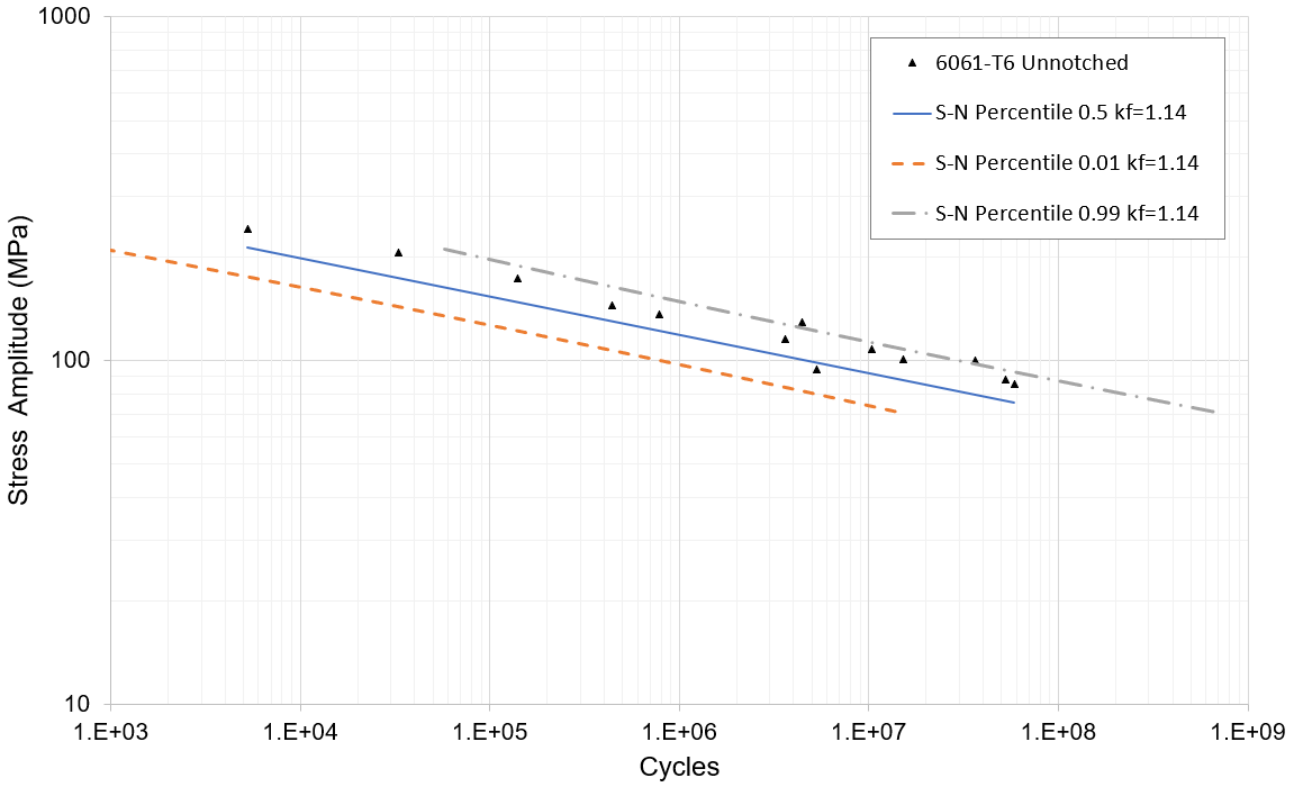

Source: Author

The probabilistic damage is then determined using the corrected P-S-N curves for the notched specimen.

The dynamic characterization of the structure was carried out by performing the modal analysis solving the natural frequencies and vibration modes of the structure. The boundary conditions were defined to emulate the fixation of the specimen in the shaker fixture. A fixed support was applied at the highlighted area in Figure (36). A shell model with the element formulation SHELL181 was used.

Figure 36 - Modal analysis boundary condition

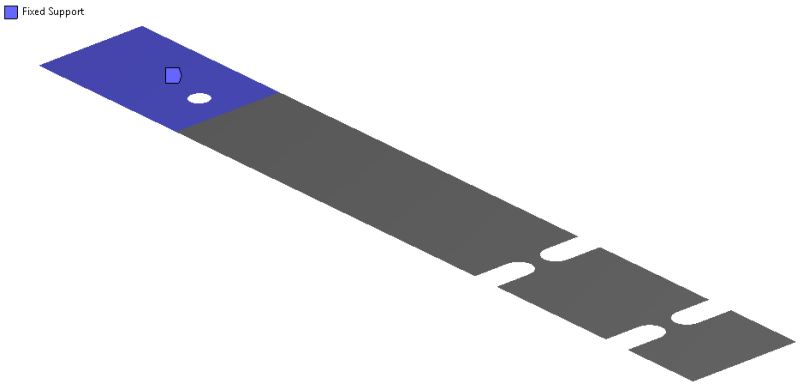

Source: Author

Seven modes are found in the frequency range up to 500Hz, which is the upper limit of the vibration profiles, natural frequencies are shown in Table 4:

Table 4 - Mode Shapes and Natural frequencies – AL 6061-T6

Vibration Mode	Natural Frequency (Hz)
1	17.29
2	85.49
3	174.98
4	203.73
5	252.86
6	440.11
7	453.81

Even though the upper frequency limit of the input vibration profile is 500Hz, the natural frequencies and modes for the FRFs were obtained considering a factor of two over the upper limit, thus 1000Hz.

The mode shapes are shown in Figure (37).

Figure 37 - Notched specimen vibration modes

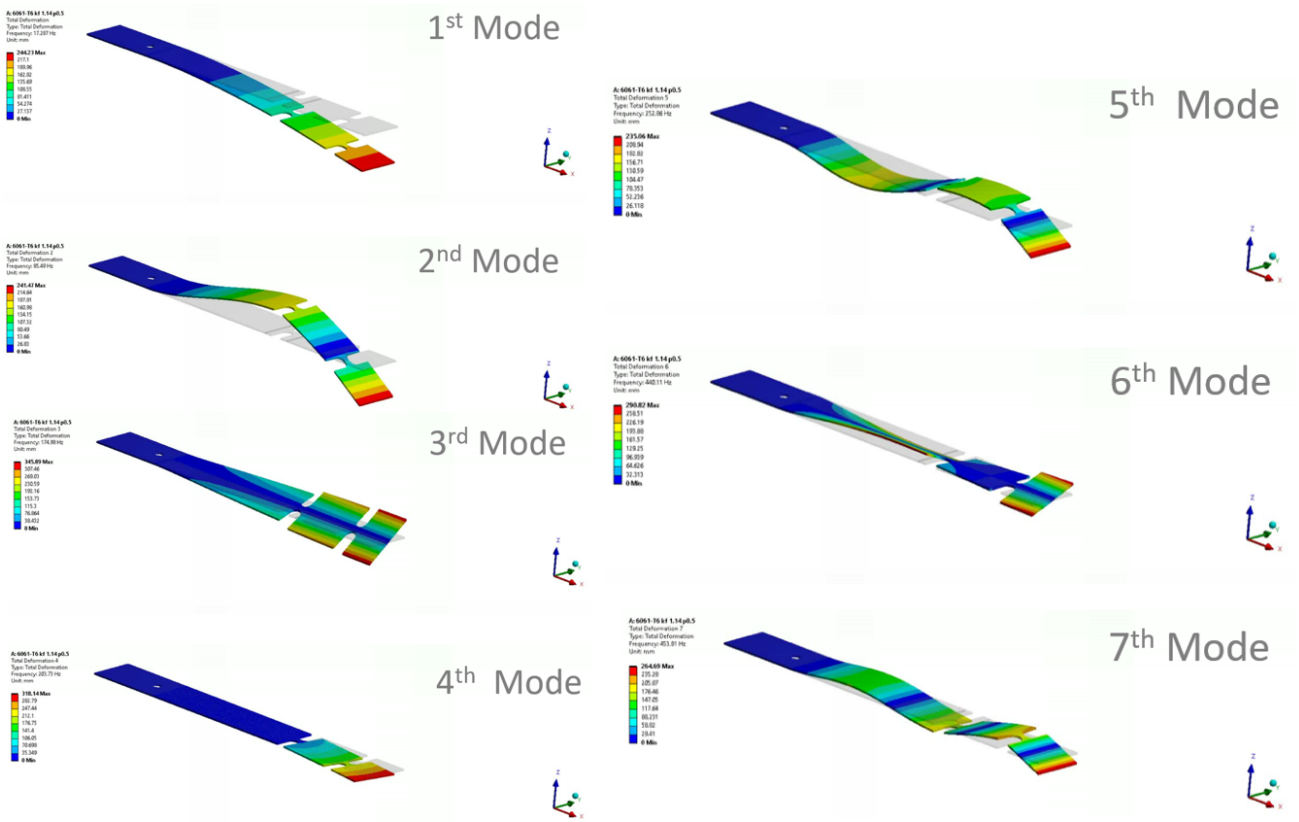

Source: Author

To properly define the transient response and obtain the FRFs, the damping must be defined, which is a very difficult parameter to obtain. When testing data is not available, a constant damping ratio is usually estimated based on previous experience with same or similar material or based on the information available in the literature. In this work the damping was modeled using the half power bandwidth method obtained from testing data, the results of a constant damping were also compared.

The machining of tested specimens and fatigue testing were carried out at the Continental Brasil Ind. Automotiva in Guarulhos-SP testing facility, as shown in Figure (38).

Figure 38 - Hardware used to conduct the vibration test

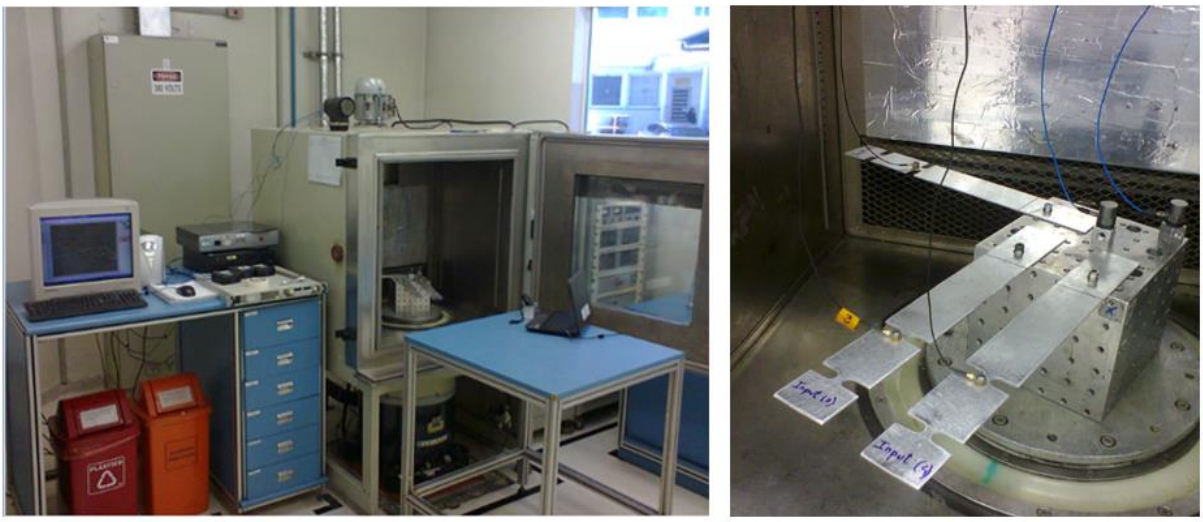

Source: Author

A DSA-4K - GW Gearing & Watson Electronics Limited electrodynamic shaker and three Bruel & Kjær DeltaTron 4519-003 accelerometers were used to excite and measure the acceleration responses at the notches on the test specimens when the specimens were subjected to the second vibration profile (Step 2) with 6 g_{rms} acceleration.

Normally, the input PSD profiles are created based on accelerometers time histories which are then converted to the frequency domain in the format of a PSD. In this work, the PSD profiles were defined to create a broad band excitation with stress responses below the yield point of the AL 6061-T6 material. The two profiles were created to illustrate the fact that fatigue phenomenon is cumulative, therefore, the first profile was defined under the hypothesis that the acceleration levels and exposure time would not be enough to create a fatigue failure. The PSD profiles were applied to the computational model to validate the premises.

The two acceleration spectrum densities applied during the test are shown in Figure (39).

Figure 39 - Step 1: 3.21g_{rms} and Step 2: 6 g_{rms}

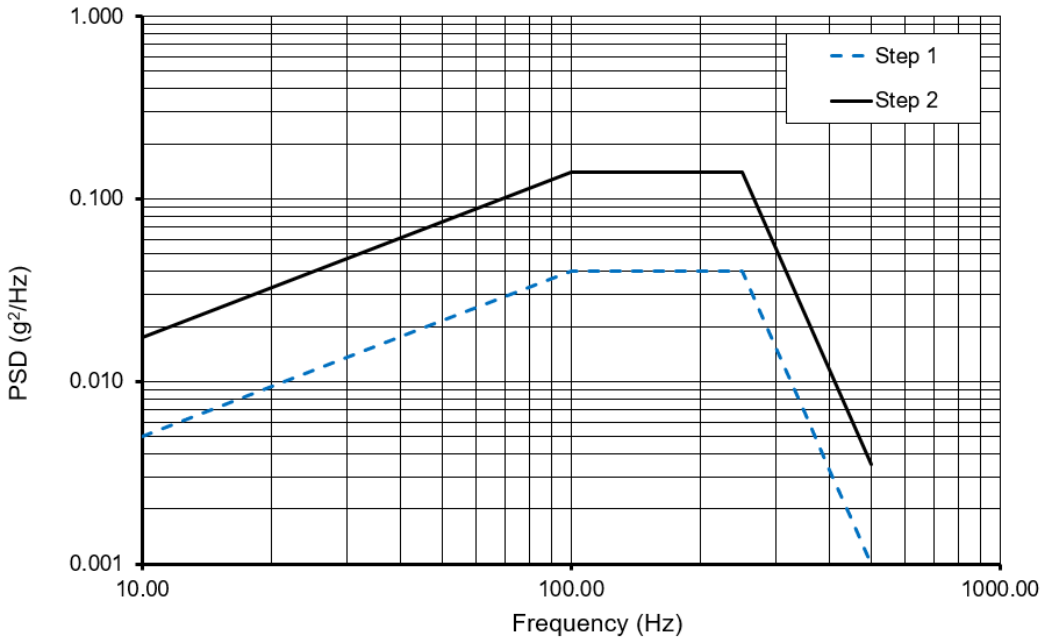

Source: Author

Due to an issue with one of the reading channels, the results of only two channels Input3 – Sample 1 and Input 4 – Sample 2 were available for analysis. The acceleration response spectrum densities (ASDs) of the two test specimens are shown in Figure (40). For each resonance peak the damping ratio ζ was calculated based on the quality factor *Q* using half power bandwidth method. The results of the damping ratios as function of frequency are illustrated in Figure (41).

Figure 40 - Acceleration Response spectrum - 6 g_{rms} input

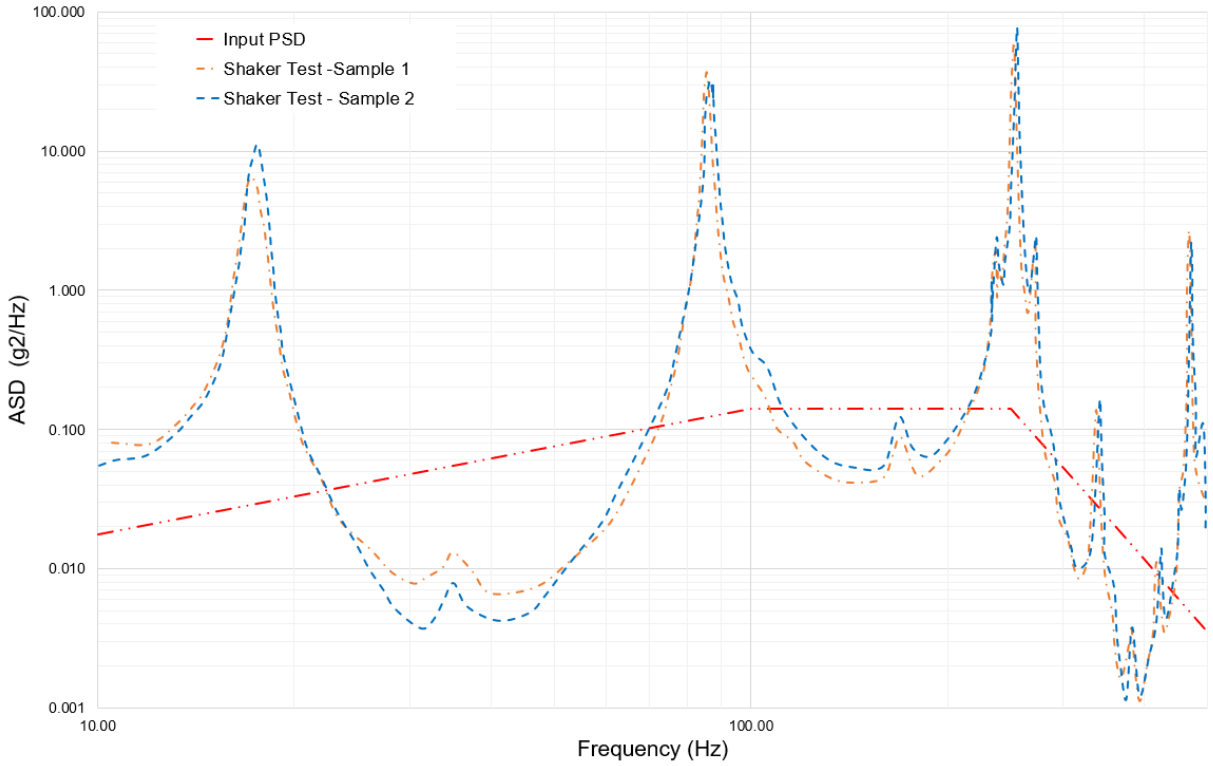

Source: Author

Figure 41 - Damping ratio ζ measured at the resonance peaks

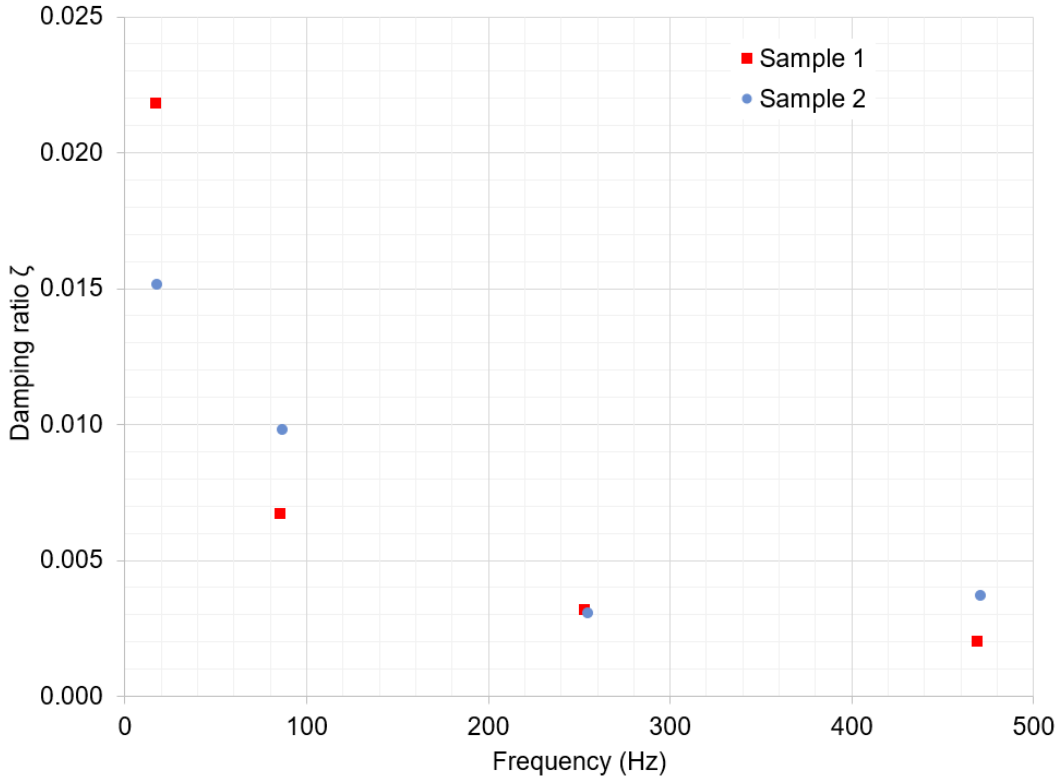

Source: Author

Clearly, the damping ratio is not constant but varies with frequency, thus, the Rayleigh damping model was employed. The definition of model parameters α, β , f_1 and f_2 was not only based on the fit to experimental results but also to the verification of the response for that set of parameters through a series of random vibration simulations. The set of parameters obtained for the Rayleigh damping model are listed in Table 5.

Table 5 – Rayleigh damping model parameters for data best fit

Parameter	Description	Value
f_1	Lower Frequency	125 Hz
f_2	Upper Frequency	1000 Hz
α	Mass proportional coefficient	4.1888
β	Stiffness proportional coefficient	8.49e-7
ζ	Damping Ratio	0.003

The fit of the damping ratio using Rayleigh's model compared to damping ratio obtained from testing is shown in Figures (42).

Figure 42 - Damping ratio fit to the measured data

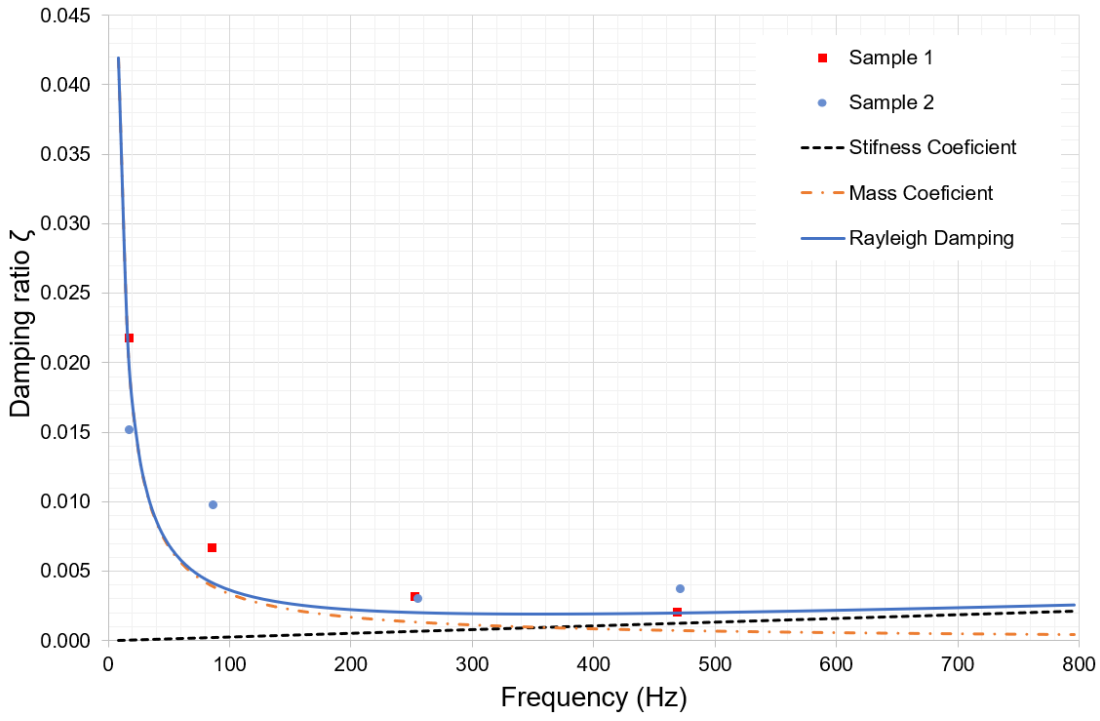

Source: Author

The simulated dynamic response using the Rayleigh's damping model is compared to the physical testing result in Figure (43).

Figure 43 - Acceleration response spectrum comparison between testing and simulation data

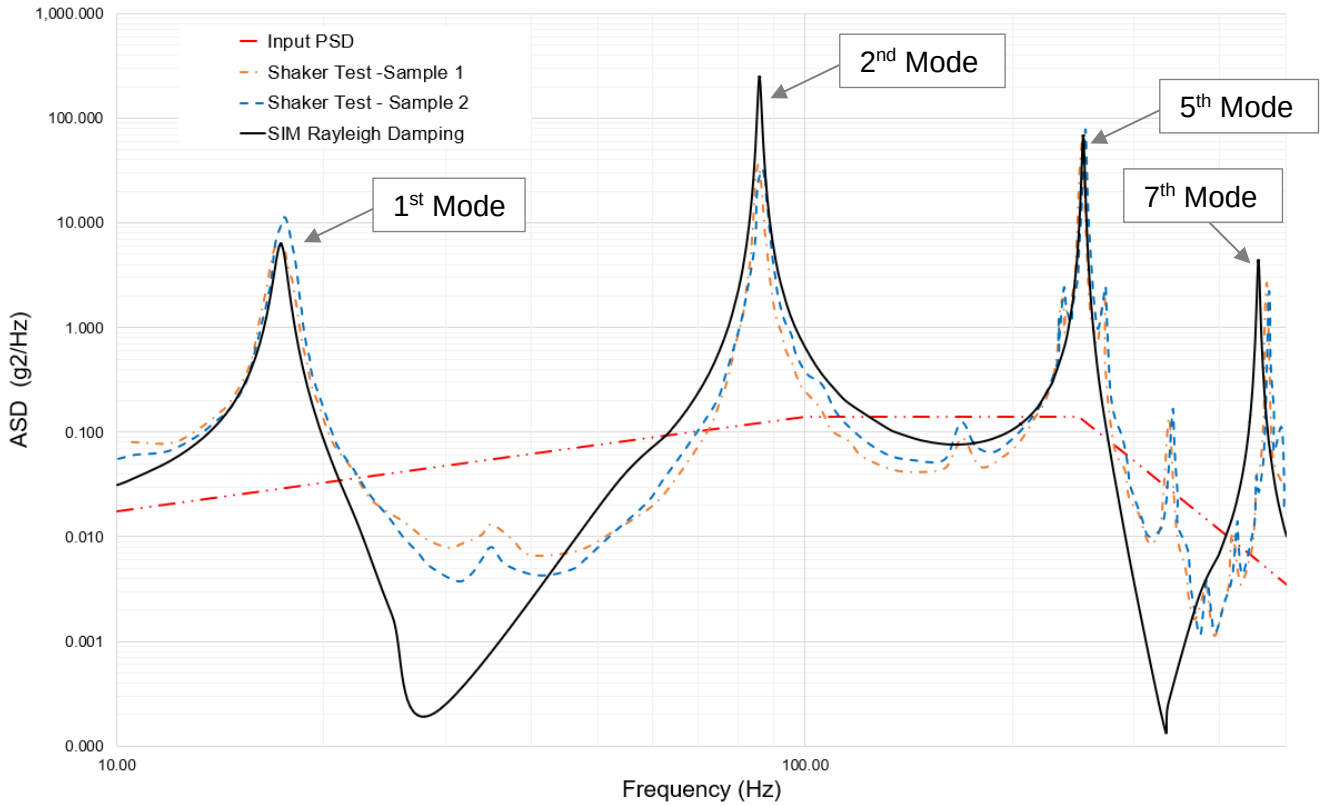

Source: Author

The simulated amplitudes are in good agreement with testing results for the first, fifth and seventh modes, a higher resonance amplitude is found at the second natural frequency in the numerical model. One hypothesis for the discrepancy could be related to the added mass of the accelerometer during the test, which could also be related to the shift in the natural frequency at the seventh mode.

The defined Rayleigh damping parameters were applied to dynamic analysis of the structure in both time and frequency domains.

3.1.1 TIME DOMAIN

Two acceleration time histories were synthesized following the acceleration spectrum densities specifications. Following the process described in Figure (18), the PSD of the synthesized time histories are compared to the original PSDs to ensure the quality of the synthesis. As the time signal is generated from a normally distributed white noise, the normality of the time signal is verified.

A tolerance range of +/-1.5 dB has been defined to evaluate the sampling parameters defined to synthesize the signal.

A summary of the statistics of the synthesized signals is given in Table 6. The synthesized time signals are shown in Figures (44) and (46). A comparison of the synthesized time histories and the original PSD specifications are illustrated in Figures (45) and (47). One can also observe that the acceleration amplitude histograms follow a normal distribution, these results were expected as the signals were synthesized from a normally distributed white noise as described in section 2.7.

Table 6 - Synthesized time histories statistics

Parameter	3.21 g_{rms}PSD	6 g_{rms}PSD
Time step	0.1907e-3 s	0.1907e-3 s
Sample rate	5243 samples/s	5243 samples/s
Overall accel rms	3.21g_{rms}	6g_{rms}
Max/Min accel. amplitude	15.2 g / -13.6 g	23.3 g / -23.9 g
Kurtosis	3.05	2.99

Figure 44 - Synthesized acceleration time history from the 3.21 g_{rms} PSD

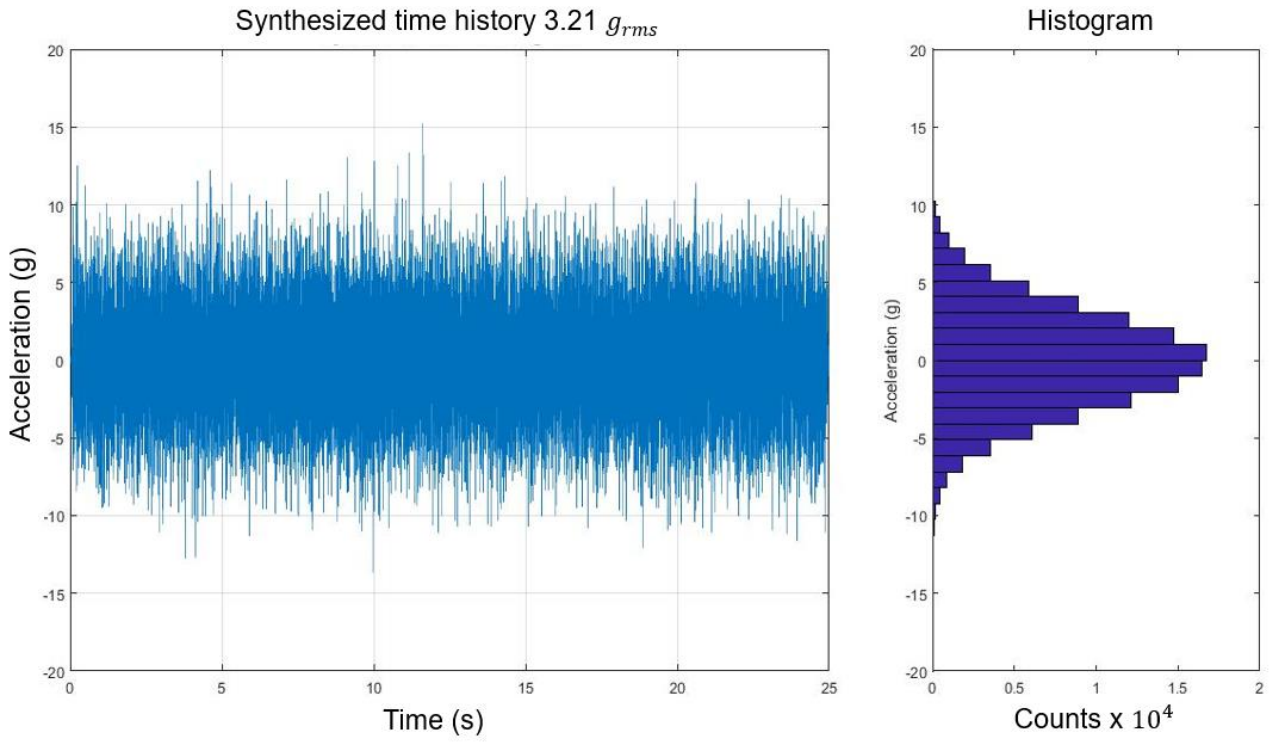

Source: Author

Figure 45 - Synthesized time signal PSD compared to original PSD spec from Step 1

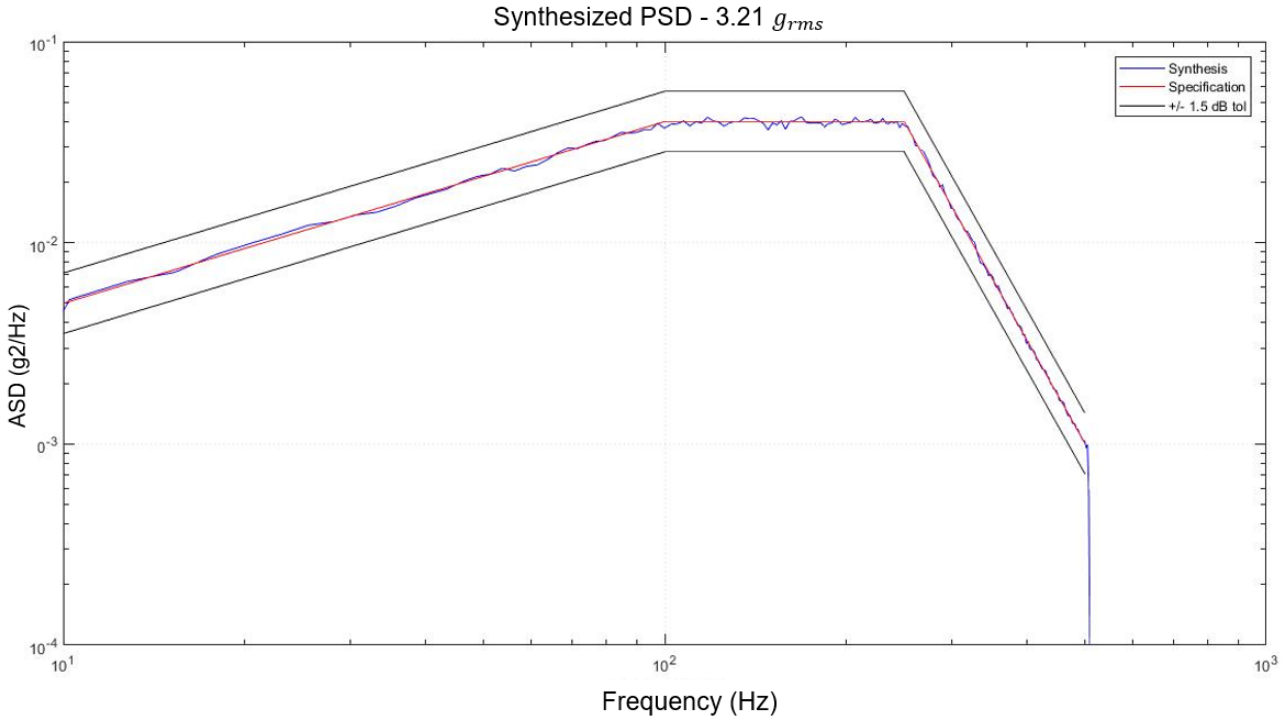

Source: Author

Figure 46 - Synthesized acceleration time history from the 6 g_{rms} ASD

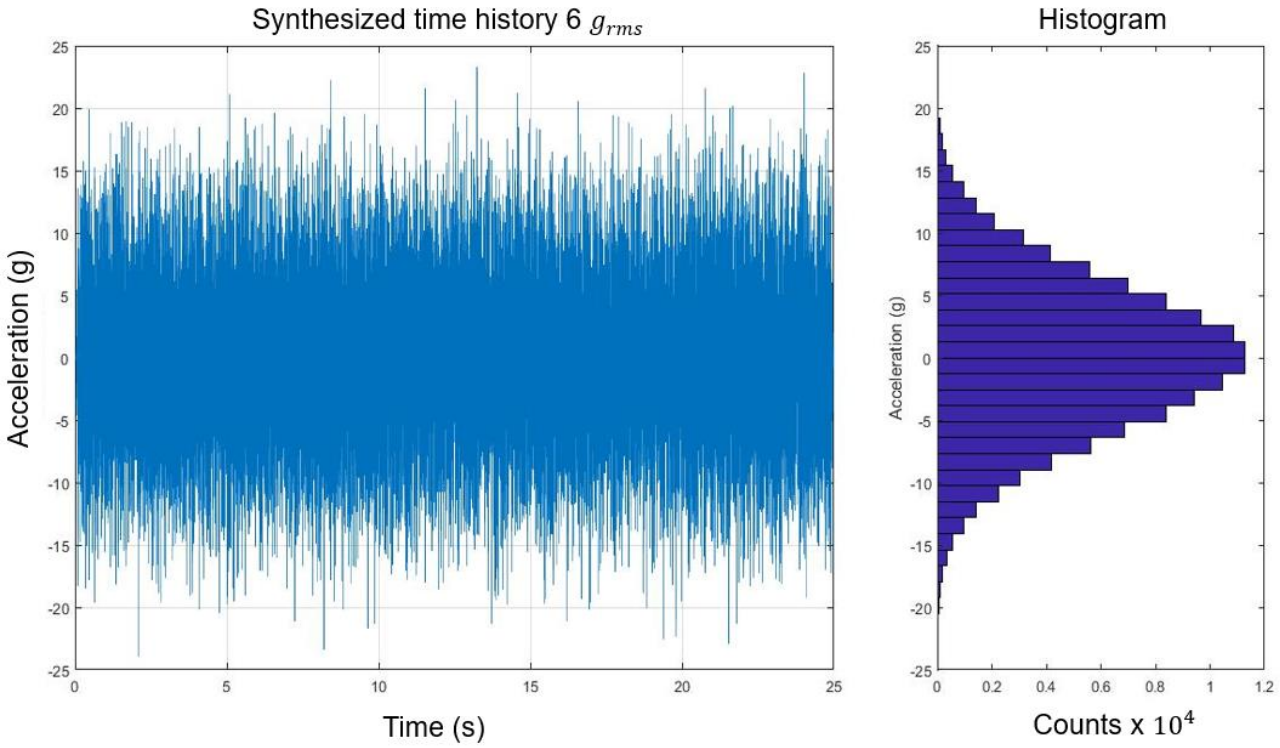

Source: Author

Figure 47 - Synthesized time signal PSD compared to original PSD spec from Step 2

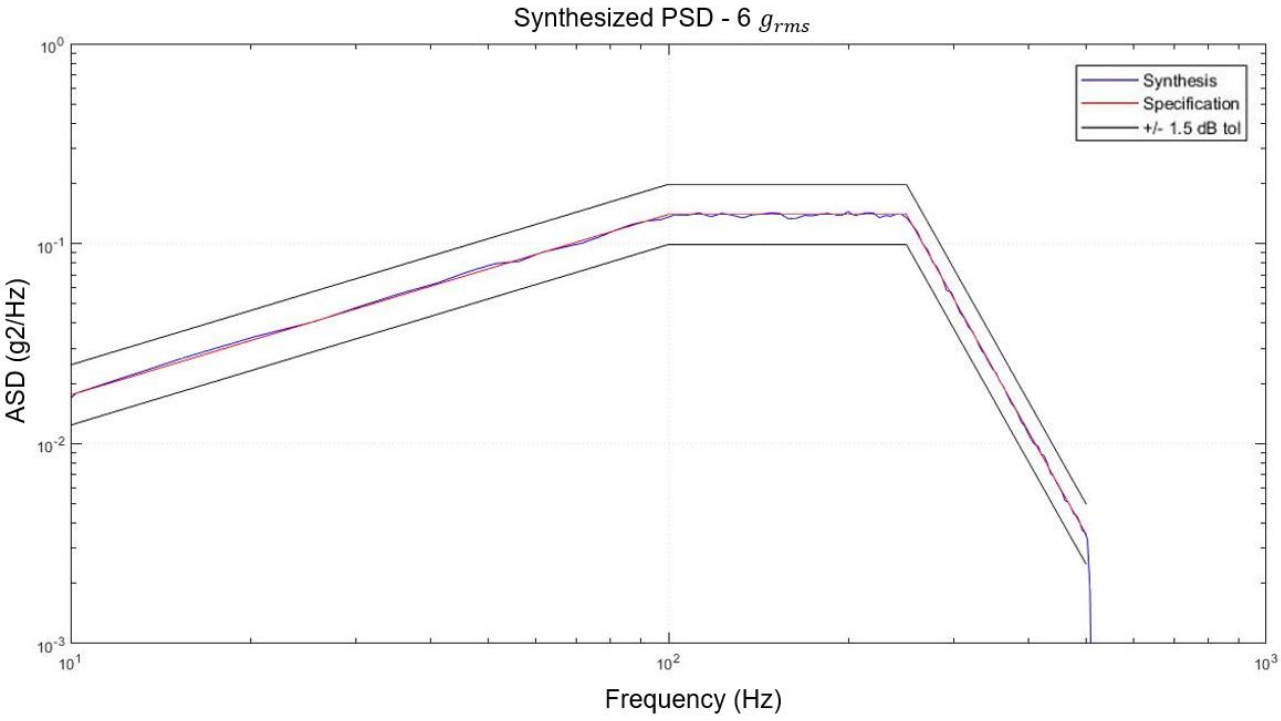

Source: Author

The synthesized acceleration time signals were applied as a transient base excitation to the notched specimen at the fixed support defined in the modal analysis, the Rayleigh damping was used. The time transient analysis is computationally expensive analysis as the stress response tensor is calculated for each time step (0.0001907s) which for the total signal length of 25s gives a total of 131,095 acceleration records. At the free surface the time transient stress tensor can be written as:

$$\sigma_{ij}(t) = [\sigma_{xx}(t) \quad \sigma_{yy}(t) \quad \sigma_{xz}(t)] \tag{123}$$

Figures (48) and (49) illustrate the time transient stress response for the two synthesized acceleration excitations at the notch root shown in Figure (50).

Figure 48 - Stress response measurement point

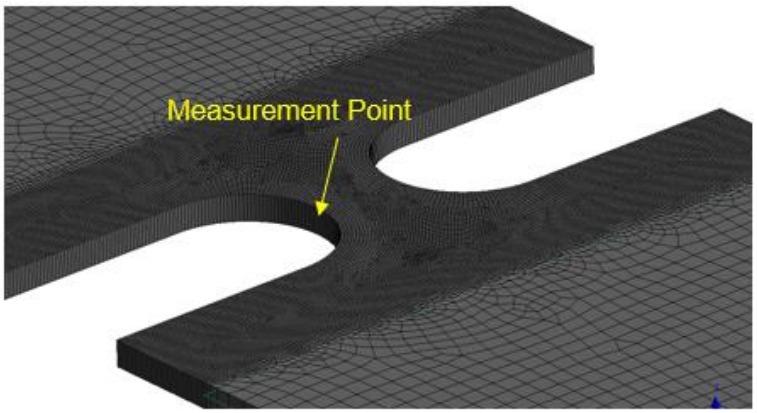

Source: Author

Figure 49 - Transient stress response - 3.21g_{rms} input

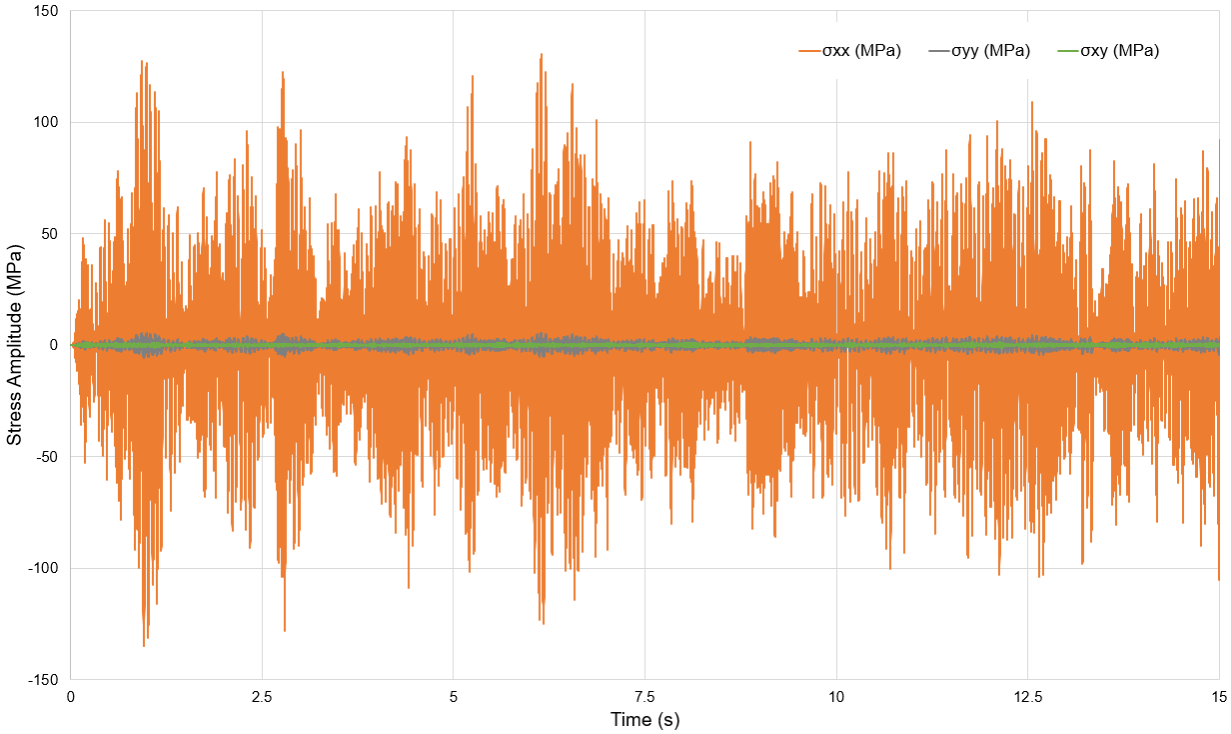

Source: Author

Figure 50 - Transient stress response - 6 g_{rms} input

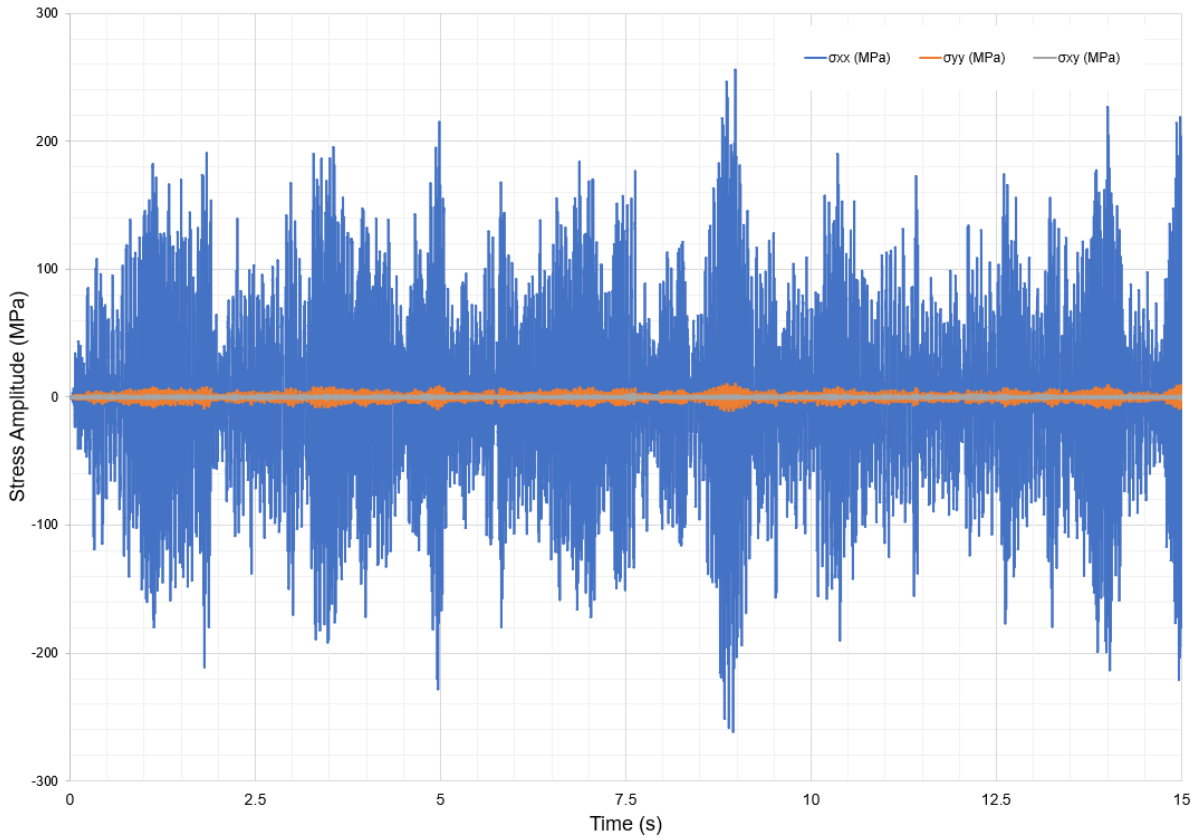

Source: Author

The stress response is predominantly uniaxial, σ_{xx} is significantly higher than σ_{yy} and σ_{xy}. A summary of the minimum and maximum stress amplitudes is presented in Table 7:

Table 7 - Min / Max transient stress amplitudes

Stress (MPa)	3.21 g_{rms}PSD	6 g_{rms}PSD
$\sigma_{xx_{min}} / \sigma_{xx_{max}}$	-135.2 / 130.4	-277.6 / 272.0
$\sigma_{yy_{min}} / \sigma_{yy_{max}}$	-5.6 / 5.4	-11.4 / 11.1
$\sigma_{xy_{min}} / \sigma_{xy_{max}}$	-1.3 / 1.4	-2.4 / 2.5

The number of cycles, given a defined stress range (or amplitude) can then be calculated using the rainflow cycle count algorithm. The component fatigue life can be predicted based on the linear cumulative damage estimated for a given S-N curve percentile.

For the two vibration profiles applied in sequence, the damage, life and time to failure can be expressed by:

$$D_{p_x} = \left(\sum_{i=1}^{k} \frac{n_i}{N_{i_{p_x}}}\right)_{Step\ 1} + \left(\sum_{i=1}^{k} \frac{n_i}{N_{i_{p_x}}}\right)_{Step\ 2} \tag{124}$$

$$Life_{p_x} = \left(\frac{1}{D_{p_x}}\right)_{Step\ 1} + \left(\frac{1}{D_{p_x}}\right)_{Step\ 2} \tag{125}$$

$$T_{failure_{p_x}} = \left(T_{exposure}.Life_{p_x}\right)_{Step\ 1} + \left(T_{exposure}.Life_{p_x}\right)_{Step\ 2} \tag{126}$$

3.1.2 FREQUENCY DOMAIN

The frequency response functions (FRFs) and the dynamic response matrix $[Q]$ are calculated from a unit acceleration harmonic base excitation. The dynamic response matrix is independent of PSD excitation and for the case being explored in this work, vibration in z-axis direction only, $[Q]$ can be written as a tensor:

$$[Q]_{1x6} = [\sigma_{xx}(f) \quad \sigma_{yy}(f) \quad \sigma_{zz}(f) \quad \sigma_{xy}(f) \quad \sigma_{yz}(f) \quad \sigma_{xz}(f)] \tag{127}$$

At the free surface the dynamic matrix can be reduced to the stress tensor:

$$[Q]_{1x6} = [\sigma_{xx}(f) \quad \sigma_{yy}(f) \quad \sigma_{xy}(f)] \tag{128}$$

Figures (51) illustrates the FRFs for the normal stresses $\sigma_{xx}(f)$, $\sigma_{yy}(f)$ and shear stress $\sigma_{xy}(f)$ measured at the notch root per Figure (48).

Figure 51 - FRFs measured at the notch root for a 1g base harmonic excitation

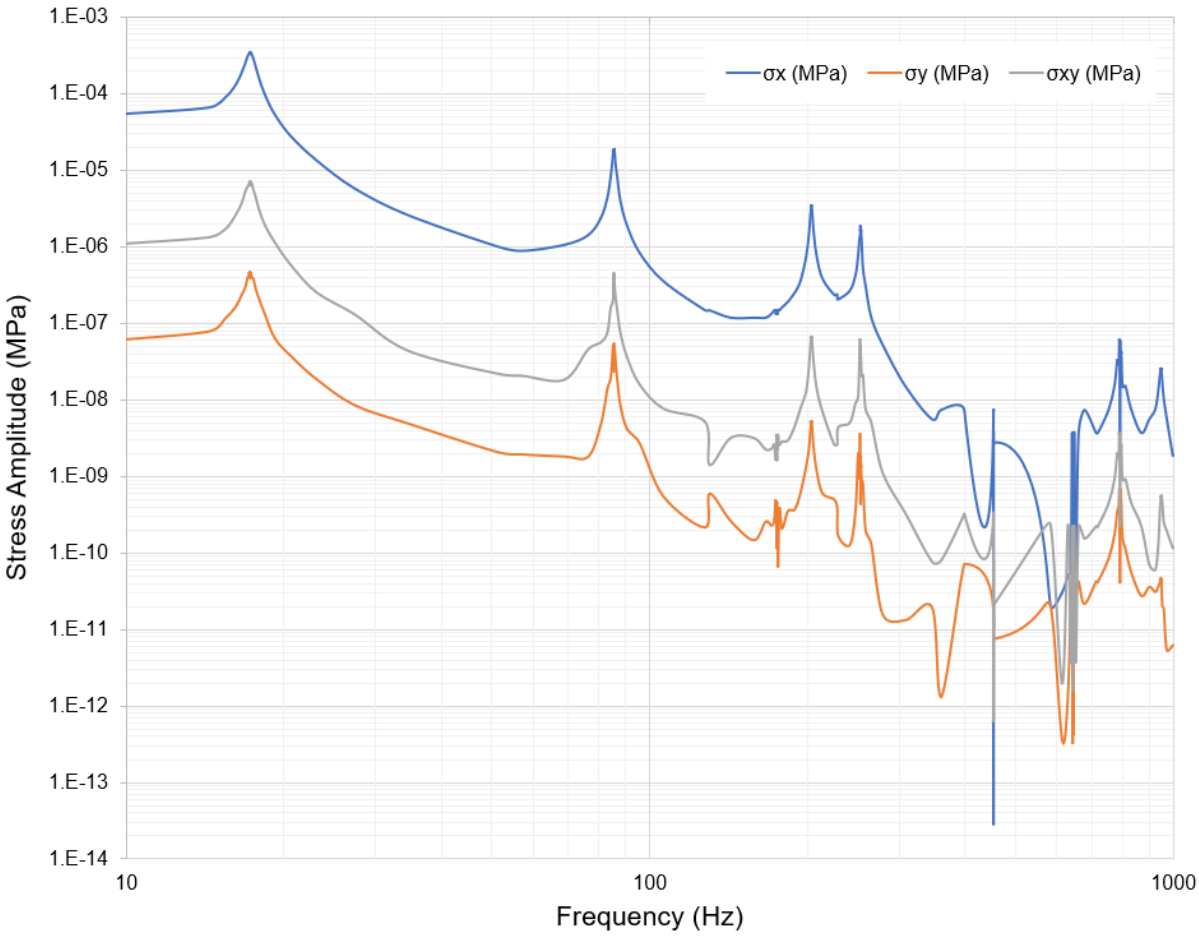

Source: Author

The FRFs show a predominantly axial stresses, with peak responses at the first and second modes. Shear stresses are significantly lower for the uniaxial excitation case. Furthermore, the response peaks up to 500Hz are observed at the modes 1, 2, 4 and 5. The vibration mode 3 in torsion is an antiresonance, thus not being evident on the FRF responses.

The unit harmonic base acceleration allows the direct application of Equation (53) to obtain the stress response PSD for the given input acceleration spectrum in the Z-axis can be written as:

$$[G]_{1x6} = [Q]_{1x6}{}^{T} [A]_{1x1} [Q]_{1x6}, \tag{129}$$

$$[A]_{1x1} = [PSD_z] \tag{130}$$

The critical plane method is used to combine the stress response PSD components, an embedded feature in Ansys - nCode was used to perform the stress combination. The resultant stress PSDs for the two input accelerations are shown in Figure (52).

Figure 52 - Stress Response PSD for both input PSDs

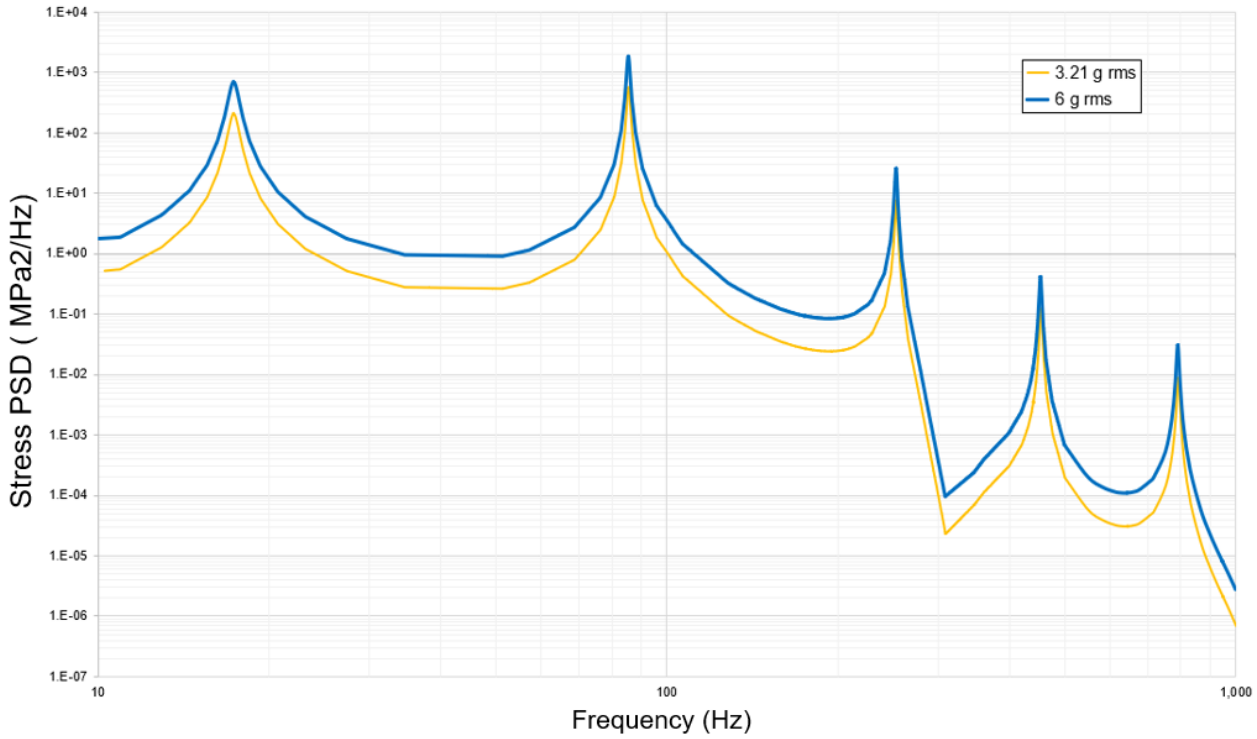

Source: Author

From the combined stress response PSD, number of cycles is then estimated based on the probability density function (Dirlik or Lallane), the input PSD exposure time and the expected number of positive peaks. The PSD has no time duration, as it is simply a representation of the frequency content and energy of the time signal, therefore, the total number of cycles must be scaled by the period that the structure is exposed to the vibration profile. Similarly, to the definition of the acceleration spectrum magnitudes, the time durations were defined to create a cumulative damage process in the first step not leading to failure, followed by a sufficient exposure time to the second profile leading to failure. The exposure time were defined as 7800s for the 3.21 g_{rms}PSD input and 2500s for the 6 g_{rms}PSD. The component fatigue life was estimated based on the linear cumulative damage calculated for the defined S-N curve percentiles.

4 RESULTS AND DISCUSSIONS

4.1 TIME DOMAIN

In the time domain, the number of cycles from the stress random response were obtained using the rainflow cycle count algorithm. The range-mean histogram of the number of cycles for each of the stress responses shown in Figures (53) and (54) considers only the data for 25s exposure. Thereafter, the number of cycles shown are scaled by a time factor to the match the number of cycles from testing for the damage calculation.

Figure 53 - Range-Mean Rainflow cycle count histogram for 25s of 3.21 g_{rms}PSD input

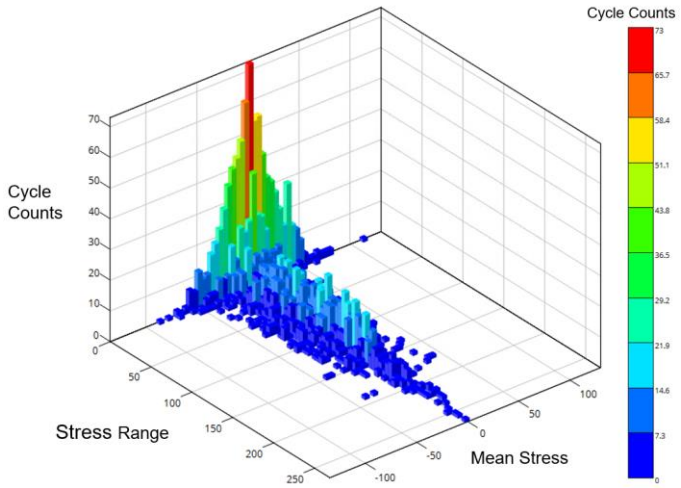

Source: Author

Figure 54 - Range-Mean Rainflow cycle count histogram for 25s of 6 g_{rms}PSD input

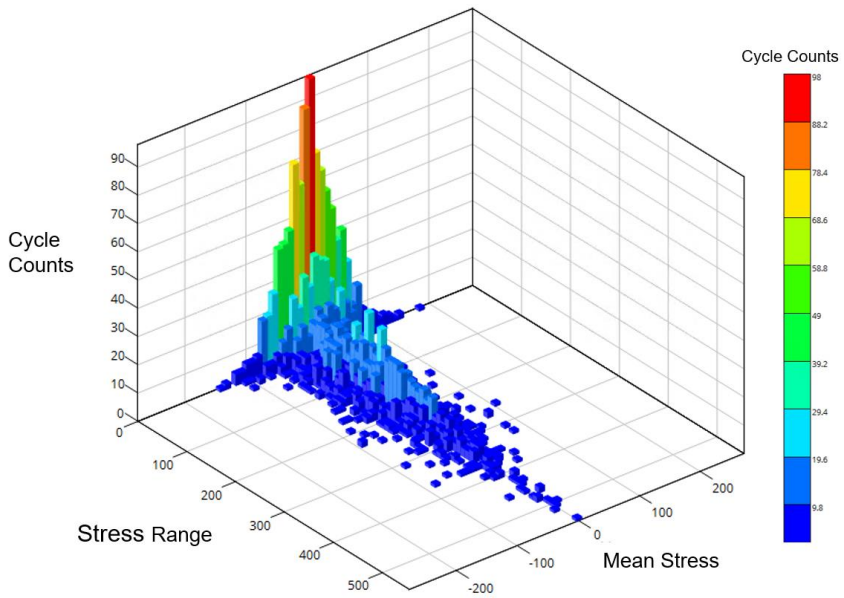

Source: Author

Another comprehensive representation of the rainflow data is through the so called *From-To* histogram illustrated in Figure (55) where the number of cycles is given by the colored bar chart (z-axis). In the *From -To* representation, *From* represents the stress level that the cycle originates from, whereas the *To* represents the stress level that the cycles finishes, the cycle counts represents the number of times that a particular From -To cycle occurs. In a tensile cycle there is a positive mean, the diagonal from lower left to upper right represents stress range close to zero line, thus not producing significant damage, conversely, the diagonal from upper left to lower right is the zero-mean line, it represents the most damaging cycles due to their very large range.

Figure 55 - *From-To* rainflow cycle histogram (a) 25s of 3.21 g_{rms}PSD input and (b) 25s of 6 g_{rms}PSD input

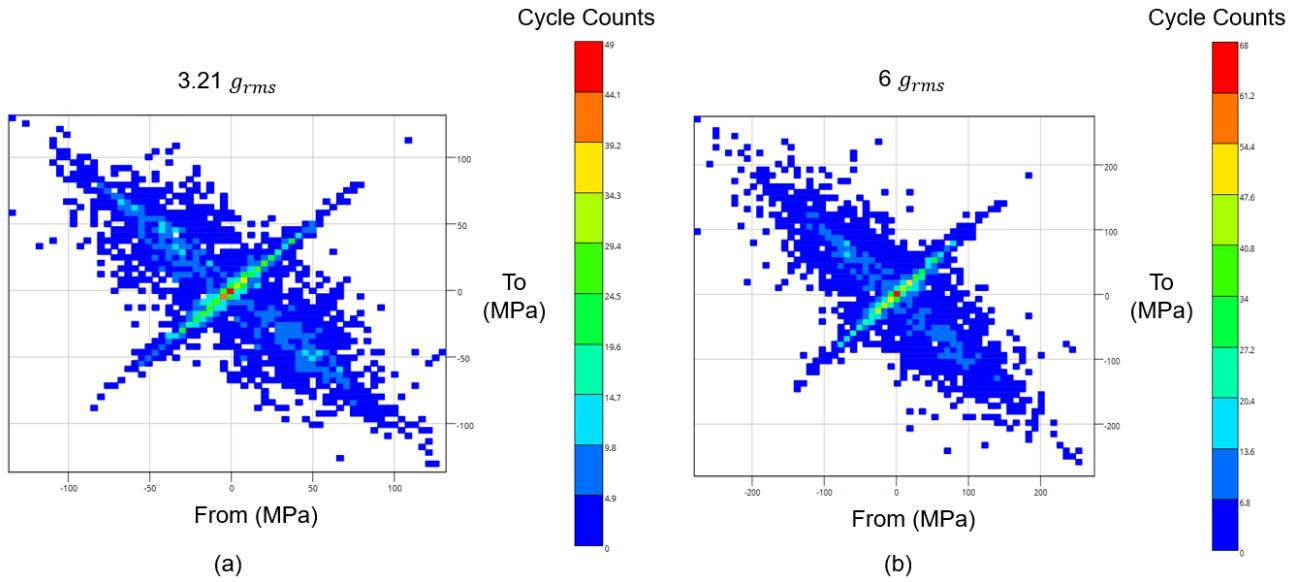

Source: Author

The total number of cycles for a given stress amplitude (or range) is given by the number of cycles Rainflow cycle counted multiplied by a time factor k_1 as:

$$n_{i\ total} = n_{i\ 25s} \cdot k_1 \tag{131}$$

k_1 is defined as:

$$k_1 = \frac{t_{random}}{t_{synth}}, \tag{132}$$

where t_{random} is total time that the component is subjected to the random vibration profile and t_{synth} the total time where signal was synthesized. A summary of the scale factors applied to the rainflow cycles is shown in Table 8.

Table 8 – Time scale factor

Vibration Profile	t_{random}	t_{synth}	k_1
3.21 g_{rms}PSD	7800	25	312
6 g_{rms}PSD	2500	25	100

The total number of cycles per stress amplitude for each input excitation is shown in Figure (56).

Figure 56 - Total number of cycles for the two vibration profiles

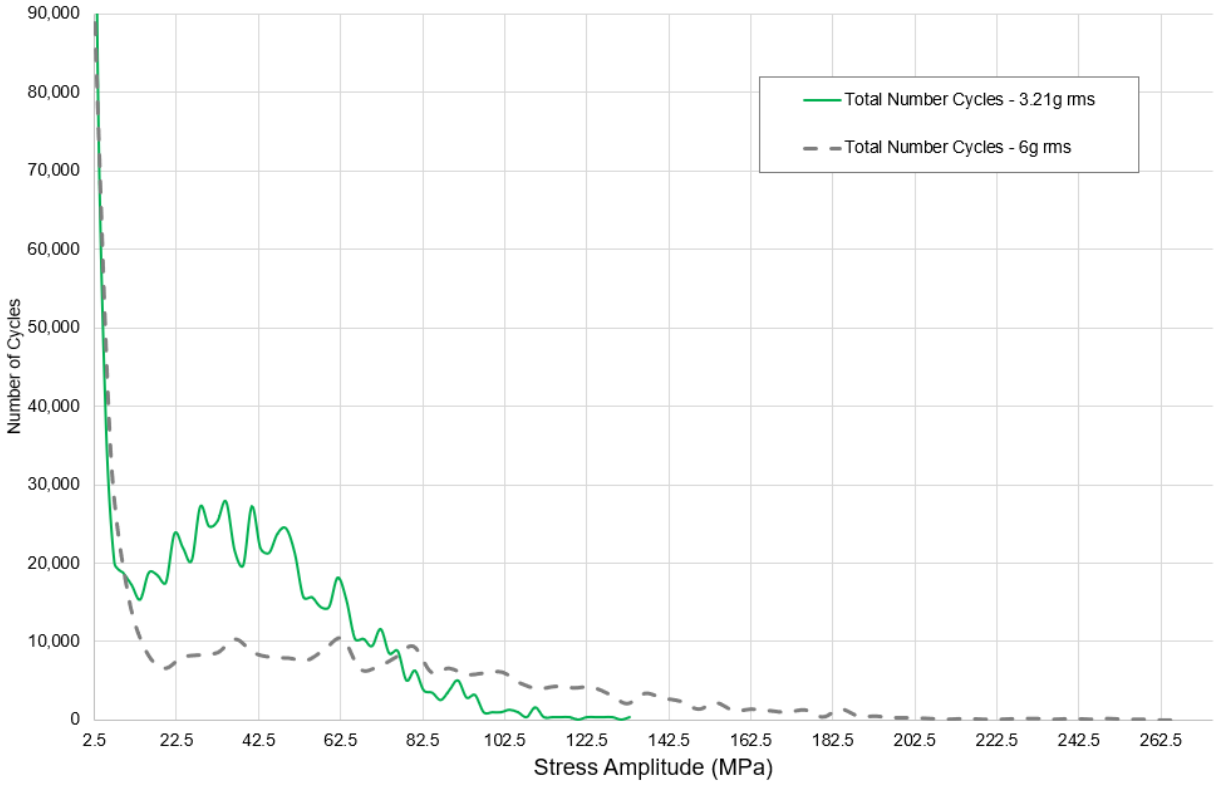

Source: Author

The life is given in terms of repeats of the vibration profile, the TTF has units of time because is relative to the duration that the component is subjected to the vibration profile. In step 1 a life greater than one represents that the component is likely to complete the test and

no failures (NF) are expected for the given test duration, therefore the TTF is shown as "NF". In column "Total", when a failure occurs, the correspondent "NF" cell is replaced by the test duration for TTF estimation. A cumulative damage greater than one, represents the component is not able to withstand one repeat of the vibration profile.

Values of damage greater than one and life smaller than one are highlighted in red. The linear cumulative damage is then calculated for the S-N percentiles p=0.01, p=0.5 and p=0.99, the summary of the cumulative damage, life and time to failure (TTF) are presented in Table 9.

Table 9 – Cumulative damage, life and time to failure

	Step 1 - 3.21 g_{rms}			Step 2 - 6g_{rms}			Total		
S-N	p=0.01	p=0.5	p=0.99	p=0.01	p=0.5	p=0.99	p=0.01	p=0.5	p=0.99
Damage	0.057	0.009	0.002	7.15	1.34	0.14	7.21	1.35	0.14
Life (repeats)	17.4	109.7	728.1	0.13	0.74	6.90	0.14	0.74	6.84
TTF (s)	NF	NF	NF	329	1847	NF	8129	9647	NF

Failure was predicted using the time domain during second vibration profile (step 2) for the S-N percentiles p=0.01 and p=0.5, no failure is expected for the specimens with fatigue properties at p=0.99. In fact, p=0.99 does not predict a failure until 6.84 repeats of the 6 g_{rms} vibration profile.

4.2 FREQUENCY DOMAIN

In the frequency domain, the number of cycles was estimated from the duration of the input PSD, the probability density function and the number of positive peaks per second which were derived from combined stress response PSD. The PDF models of Dirlik and Lallane were used to estimate the component fatigue life, the results from both models were then compared to the results in the time domain and test results.

The spectral moments were then computed from the response stress PSD, the number of positive peaks, upward zero crossings per second, central frequency, irregularity factor and standard deviation are summarized in Table 10.

Table 10 – Spectral moments and properties of the Stress Response PSD

Parameter	Description	Value
m_0	0th spectral moment	4574
m_1	1st spectral moment	3.51e5
m_2	2nd spectral moment	3.35e7
m_4	4th spectral moment	6.2e11
$\mathrm{E}[0]$	Upward zero crossings per second	85.6
$\mathrm{E}[\mathrm{P}]$	Peaks per second	136.1
γ	Irregularity factor	0.629
f_{mean}	Mean frequency	0.56

A comparison of the probability density functions modeled using Dirlik's and Lallane's formulation for the 3.21g_{rms} and 6g_{rms} inputs per stress amplitude are shown in Figure (57).

The correspondent number of cycles are shown in Figure (58), a comparison of the two probability density functions with the results from the rainflow cycle counts in the time domain is shown in Figure (59) for the 3.21g_{rms} and in Figure (60) for the 6g_{rms}.

Figure 57 - Lallane's and Dirlik's PDFs

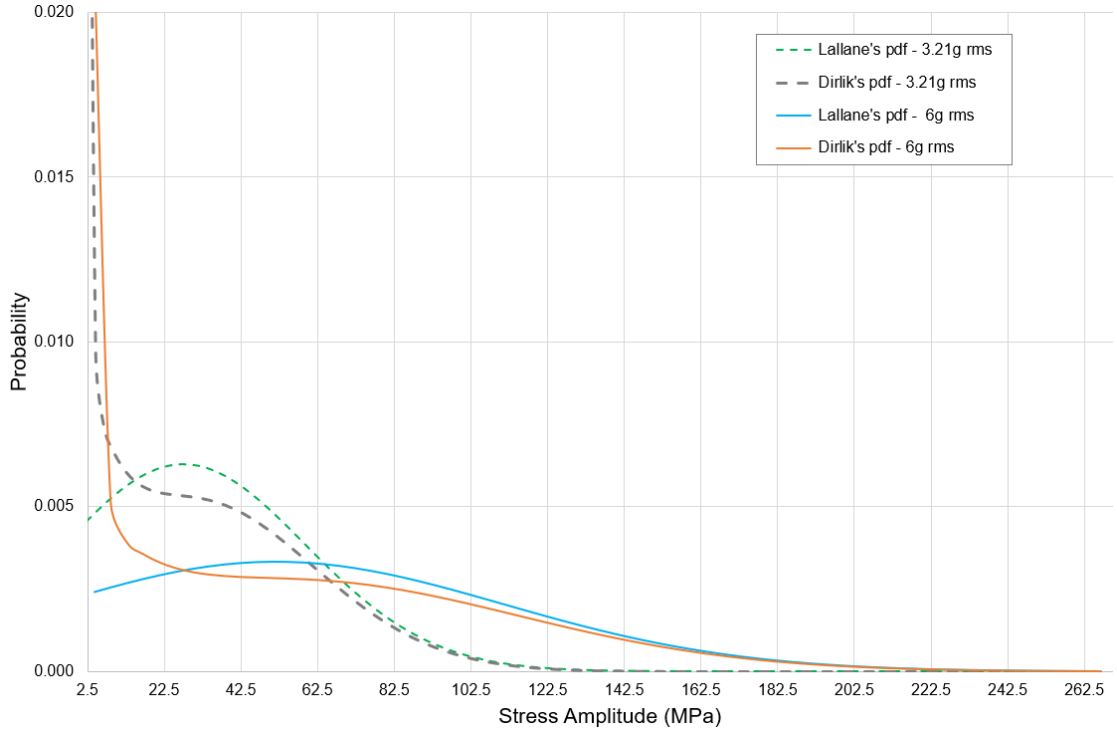

Source: Author

Figure 58 - Lallane's and Dirlik's number of cycles for each input acceleration

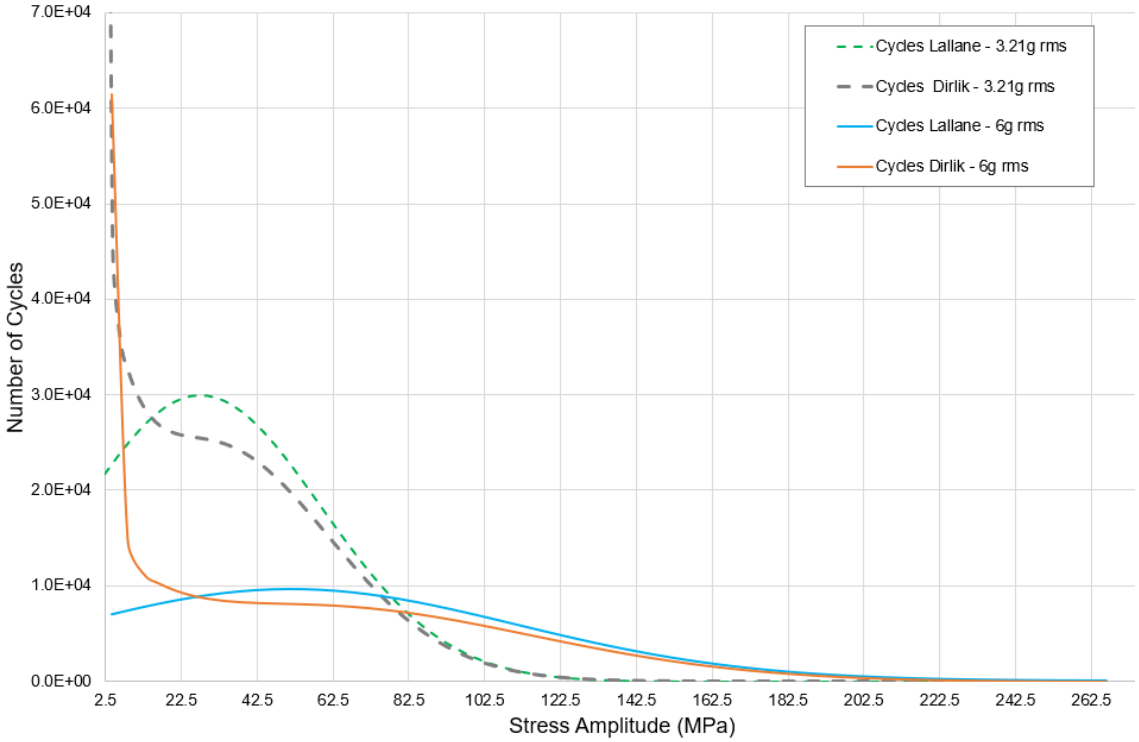

Source: Author

Figure 59 - Lallane's, Dirlik's and Rainflow number of cycles - 3.21g_{rms} input

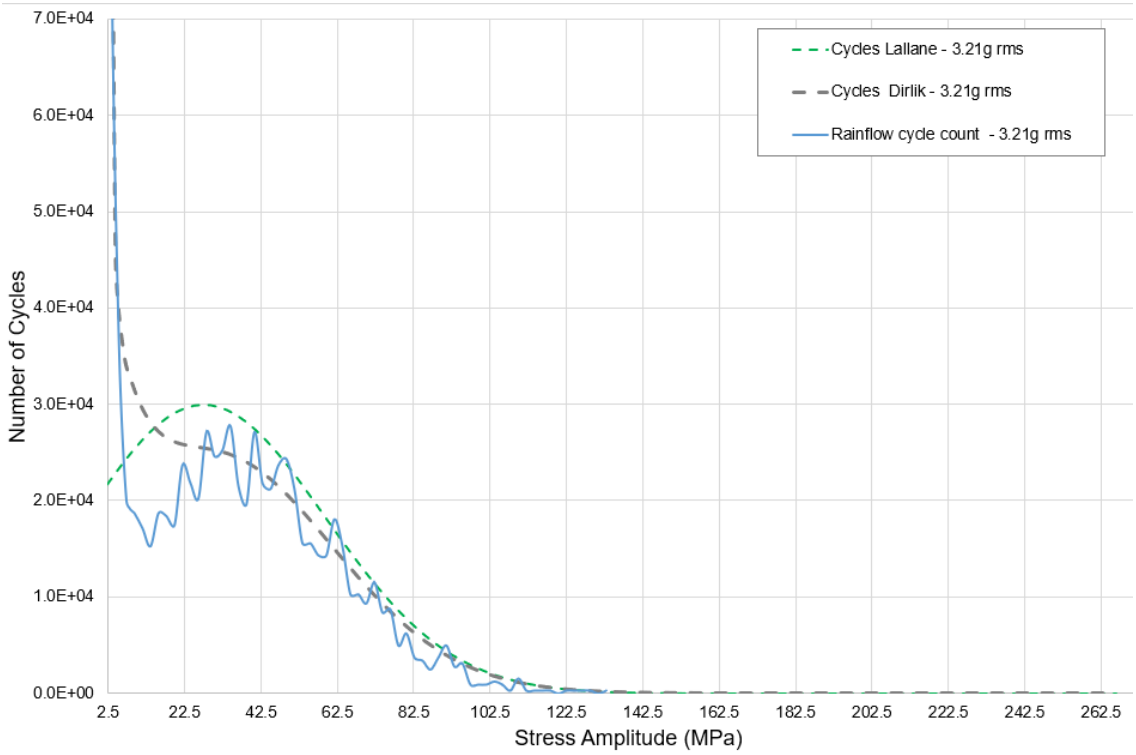

Source: Author

Figure 60 - Lallane's, Dirlik's and Rainflow number of cycles - 6g_{rms} input

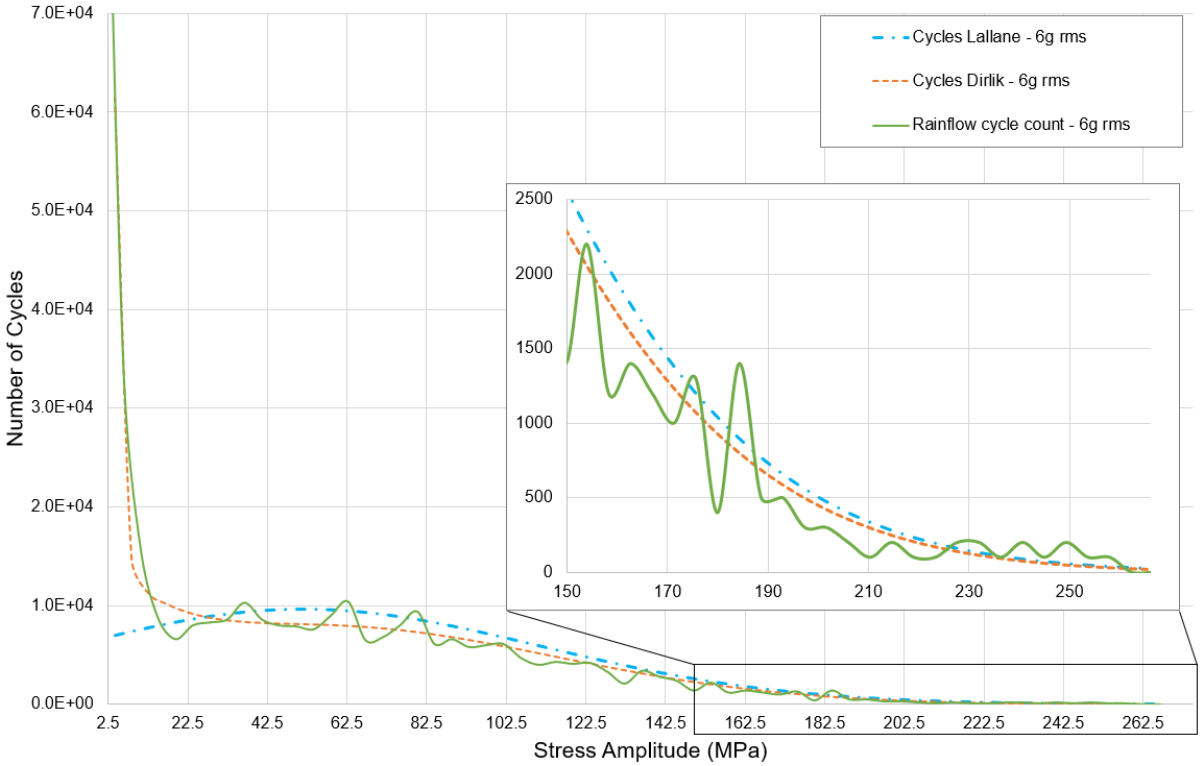

Source: Author

Figures (57) and (58) show the different stress amplitude areas excited by the different input vibration profiles, the difference between the two models are evident at lower stress amplitudes, which are less of concern, compared to the more damaging high amplitude cycles given the observation of the behavior of the S-N curve. Both models agree at the high amplitude stresses. The comparison with the number of cycles from the time domain time history rainflow cycle counts in Figures (60) and (61) show good agreement between the cycles counts obtained from both time and frequency domains. Lallane's PDF creates an envelope capturing the peaks of determined stress levels, except at lower stress amplitudes. Dirlik's PDF, however, models an average curve in which the rainflow curve fluctuates around it, good agreement is obtained at low stress amplitudes. Figure (60) also shows an augmented detail of the of the number of cycles for stress amplitude over 150MPa.

In general, despite the evident difference at low stress amplitudes, which is not the critical region for the fatigue assessment, the number of cycles obtained by both frequency domain methods are in good agreement with the results from the rainflow cycles count from the stress time history, specially at the high damaging cycles.

From the number of cycles calculated at each probabilistic model, the damage, life and time to failure (TTF) can be estimated for a given S-N percentile curve. The results of the predicted number of cycles using Lallane's and Dirlik's formulation are shown in Tables 11 and 12 respectively.

Table 11 – Cumulative damage, life and time to failure - Lallane

	Step 1 - 3.21 g_{rms}			Step 2 - 6g_{rms}			Total		
S-N	p=0.01	p=0.5	p=0.99	p=0.01	p=0.5	p=0.99	p=0.01	p=0.5	p=0.99
Damage	0.10	0.02	0.003	7.28	1.34	0.15	7.38	1.36	0.15
Life (repeats)	9.3	57.6	369.2	0.12	0.73	6.69	0.13	0.73	6.59
TTF (s)	NF	NF	NF	306	1821	NF	8106	9621	NF

The damage plot at the notch area for p=0.5 is illustrated in Figure (61).

Figure 61 - Damage contour at notch area - Lallane 6g_{rms} input (p=0.5)

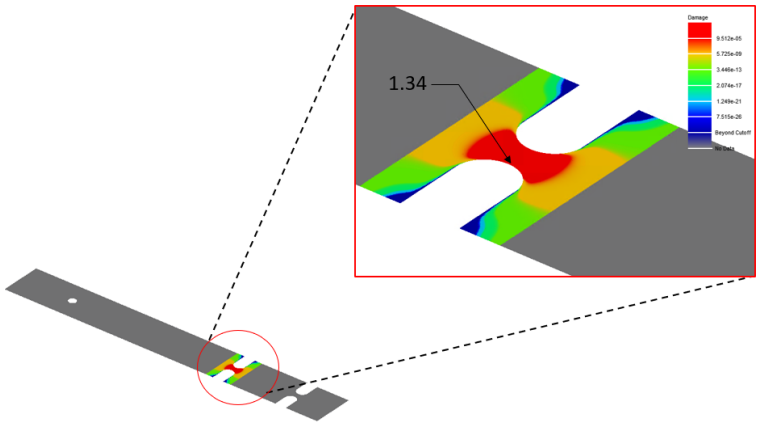

Source: Author

Table 12 - Cumulative damage, life and time to failure - Dirlik

	Step 1 - 3.21 g_{rms}			Step 2 - 6g_{rms}			Total		
S-N	p=0.01	p=0.5	p=0.99	p=0.01	p=0.5	p=0.99	p=0.01	p=0.5	p=0.99
Damage	0.09	0.015	0.002	6.53	1.21	0.13	6.62	1.35	0.14
Life (repeats)	10.4	64.2	441.9	0.14	0.81	7.47	0.15	0.74	6.84
TTF (s)	NF	NF	NF	346	2035	NF	8146	9835	NF

The damage plot at the notch area for p=0.5 is illustrated in Figure (62).

Figure 62 - Damage contour at notch area - Dirlik 6g_{rms} input (p=0.5)

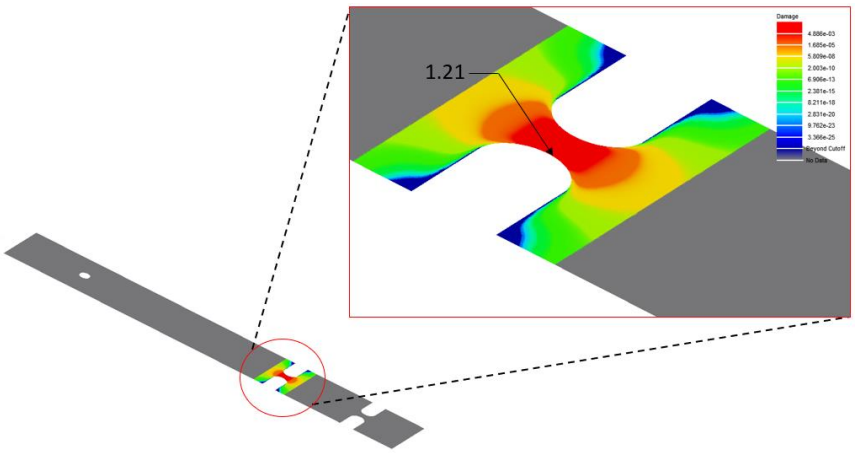

Source: Author

The contour plot shown in Figures (61) and (62) illustrates the areas of the part that are likely to initiate a crack.

For all percentile curves considered, step 1 loading does not create significant damage into the component, therefore, for the time duration defined, no failures are expected.

The step 2 loading, however, create fatigue damage at the notch which is higher than the threshold criteria of one for the percentile curves 0.01 and 0.5 using both Lallane and Dirlik models. The failure is not predicted if the fatigue properties of the specimen are within the 0.99 percentile.

The results presented in Tables 11 and 12 are important because the scatter in the fatigue properties could lead to results in testing which not necessarily correlating with the estimations if only the p = 0.5 is used. The large difference of the expected damage between the different percentiles also indicates the sensitivity of the studied notched specimen design for the vibration profile requirement in step 2.

Observing the total damage results for p = 0.5, Lallane's method was 10.52% more conservative than the Dirlik's method under step 2 loading, the higher number of cycles predicted of the mid-range stress amplitude resulted in overall higher cumulative damage

4.3 TESTING RESULTS

Due to characteristic of the test, the failure was defined when the complete fracture has occurred based on the assumption that takes most of the fatigue life to initiate the crack. The time to failure of each specimen in seconds is summarized in Table 13.

The samples are identified as follows:

- Sample 1 – “Input 3”
- Sample 2 – “Input 4”
- Sample 3 – “Input 5”

Table 13 – Testing time to failure summary

	Step 1 – 3.21 g_{rms}	Step 2 – 6 g_{rms}	
Specimen	Exposure time (s)	Exposure time (s)	Total time to failure (s)
Sample 1	7800 (No failure)	1772 (Failure)	9572
Sample 2	7800 (No failure)	2324 (Failure)	10124
Sample 3	7800 (No failure)	1534 (Failure)	9334

Using a weibul distribution, the statistics of the mean time to failure (MTTF) based on the testing data is shown in Table 14.

Table 14 – Testing results statistics – Mean time to failure (MTTF)

			CI 95%	
	Estimate (s)	Standard Deviation (s)	Lower (s)	Upper (s)
MTTF	9667	228.5	9230	10126

Figure 63 - Weibull distribution fit of the testing data

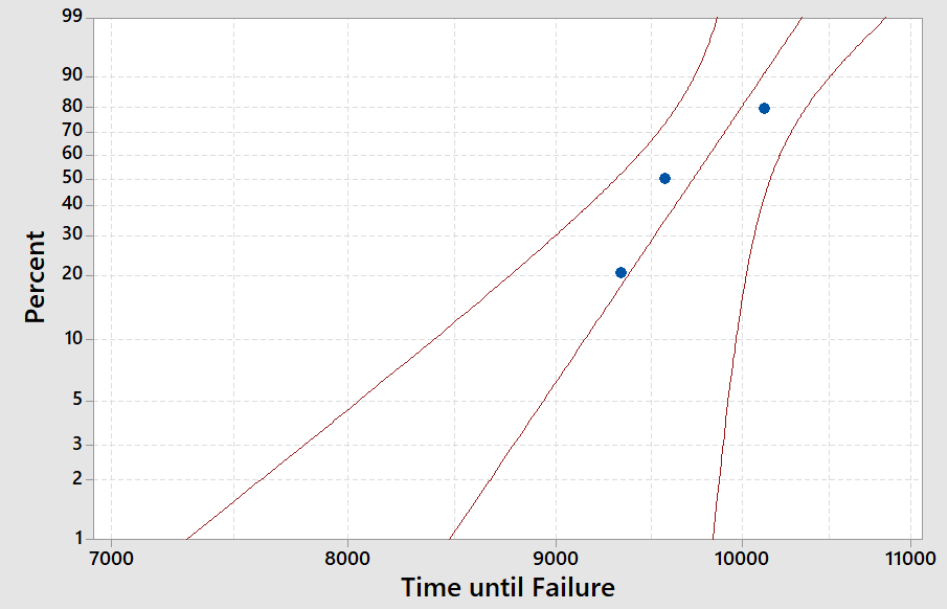

Source: Author

The three specimens failed at notch closest to the fixation point on the shaker table, the location of the failure correlates to the location predicted in the analytical models.

One of the difficulties encountered during the test was the determination of crack initiation, given the random and rapid displacement of the samples during the test. Failure was defined when the complete fracture was reached.

Nonetheless, the analysis of the failed specimens, showed that the cracks have developed from the surface of the specimens towards the bending plane through the thickness before the fast fracture.

To reduce the error in the determination of the time to failure, the test was video recorded and multiple observations of the final fracture of each specimen were made and finally compiled on Table 13.

The crack location for all the three specimens is illustrated in Figure (64).

A close-up picture of the fracture face of each specimen is shown in Figures (65), (66) and (67).

Figure 64 – Crack Location

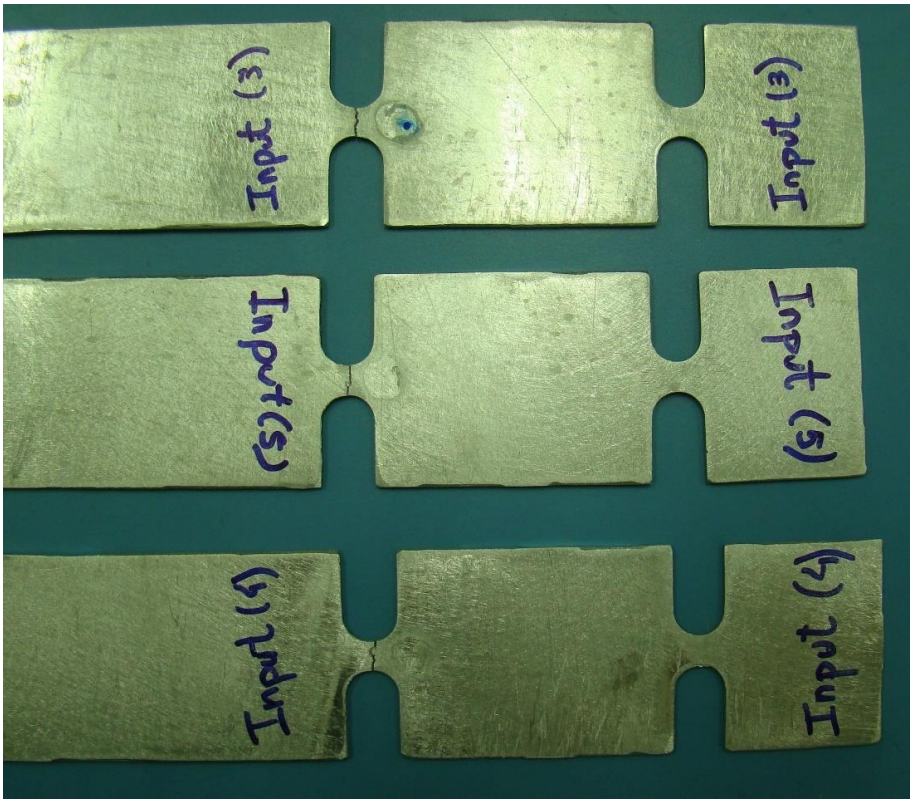

Source: Author

Figure 65 - Sample 1 fracture detail

Source: Author

Figure 66 - Sample 2 fracture detail

Source: Author

Figure 67 - Sample 3 fracture detail

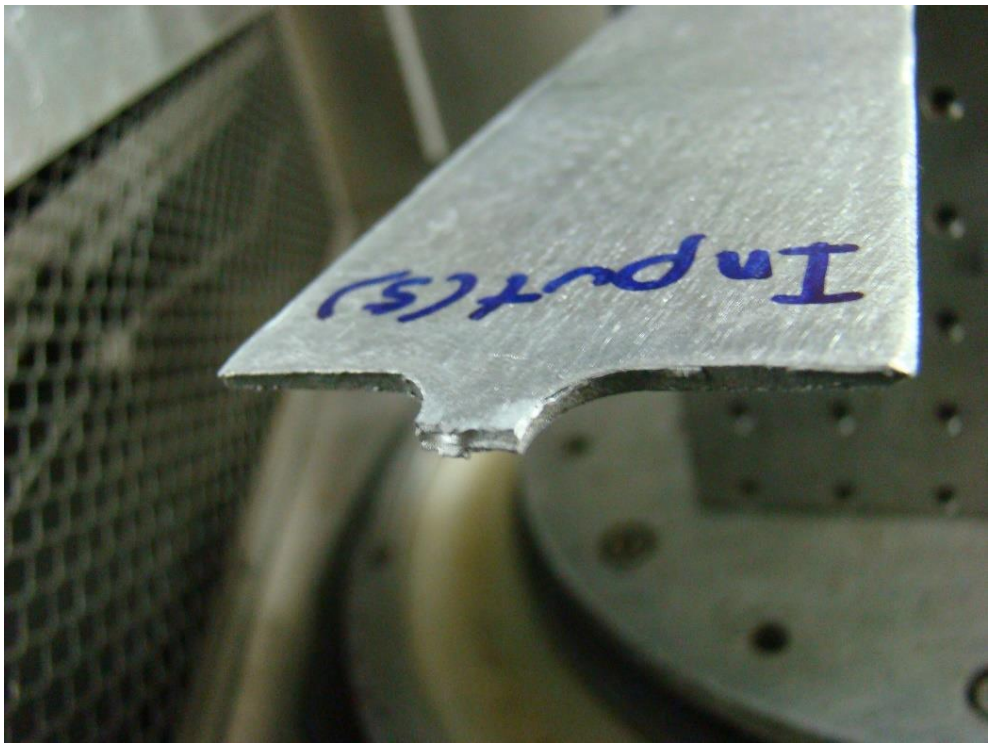

Source: Author

4.4 DISCUSSIONS

The upper limit of the S-N curve which correspond to p=0.99, is non conservative for fatigue predictions, therefore, it is not recommended to be used for design purposes, the discussion in this chapter is then focused on the results from p=0.01 and p=0.5. Furthermore, as the damage predicted during the step 1 could be neglected, to avoid skewing the results, 7800s is subtracted from the total time to failure. Table 15 summarizes the time to failure for the different models and S-N percentile curves for step 2 results only, a comparison with the testing mean time to failure as a percentage error is presented.

Table 15 – Summary of total time to failure – Step 2 – 6 g_{rms} only

	Total time to failure (s)		Error % ($\frac{N_{model}}{N_{exp}} - 1$)	
S-N	p=0.01	p=0.5	p=0.01	p=0.5
Test data	1877		Baseline	
Time Domain	329	1847	-82.5	-1.6
Lallane	306	1821	-83.7	-3.0
Dirlik	346	2035	-81.6	+8.4

As one can see, the results shown in Table 15 show good agreement between testing and analytical results, when the mean time to failure from the test results is compared to the results using the percentile 0.5 of the S-N curve in both time and frequency domains. The predictions using p=0.01 S-N are conservative in all cases as one would expect.

In the time domain the maximum stress amplitude was found to be 258MPa, as the S-N approach was used, the validity of the models in the frequency domain was defined to be the yield stress of the 6061-T6 aluminum (σ_y = 266MPa).

The total number of cycles for the different random amplitudes from the different models are shown in Table 16.

Table 16 – Total number of cycles

	Step 1 – 3.21 g_{rms}	Step 2 – 6 g_{rms}	Grand Total
Time Domain	1,052,688	358,400	1,411,088
Lallane	851,090	272,665	1,123,755
Dirlik	978,058	313,528	1,291,586

The number of cycles when observed from the perspective of Figures (59) and (60) reiterates the cumulative nature of the fatigue damage, however, the observation of data shows that for the load case step 2 in the time domain, stresses below 0.85 σ_y contributed to 99.72% of the number cycles but to only 50.2% of the overall damage. In the frequency domain Lallane and Dirlik presented similar percentage of the number of cycles, but with slightly over 67% contribution to the overall damage.

In a random phenomenon the tail of the distributions shown in Figures (59) and (60) are critical for the fatigue prediction, as the damage increases significantly at these stress levels. A comparison of the damage as function of the stress amplitude for the p=0.5 S-N curve is shown in Figure (68) and (69). The cumulative damage is shown is Figure (70).

Figure 68 - Damage as function of stress amplitude (p=0.5) - 3.21g_{rms} input

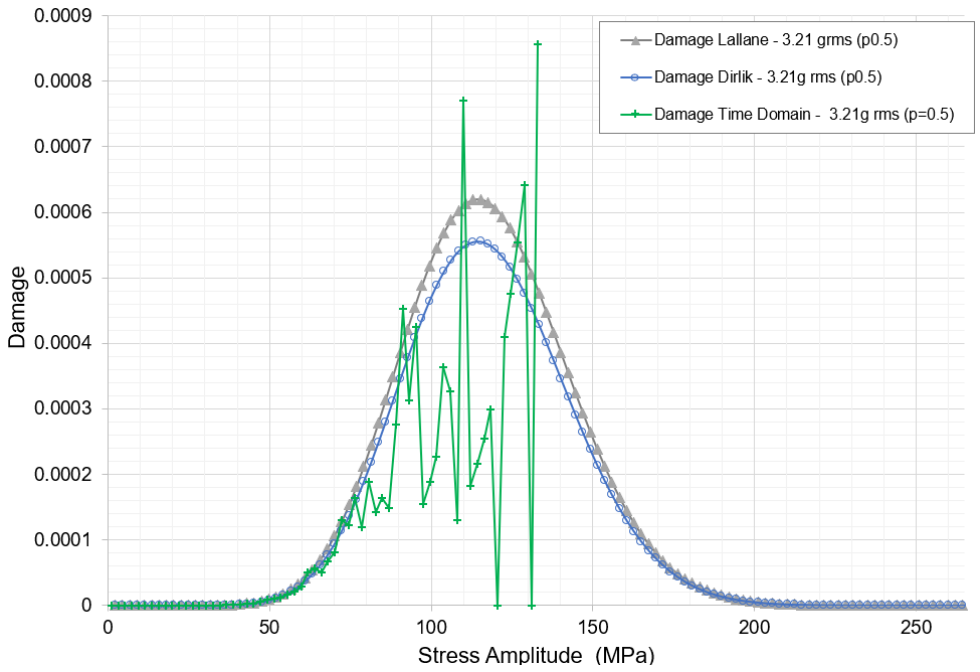

Source: Author

Figure 69 - Damage as function of stress amplitude (p=0.5) - 6g_{rms} input

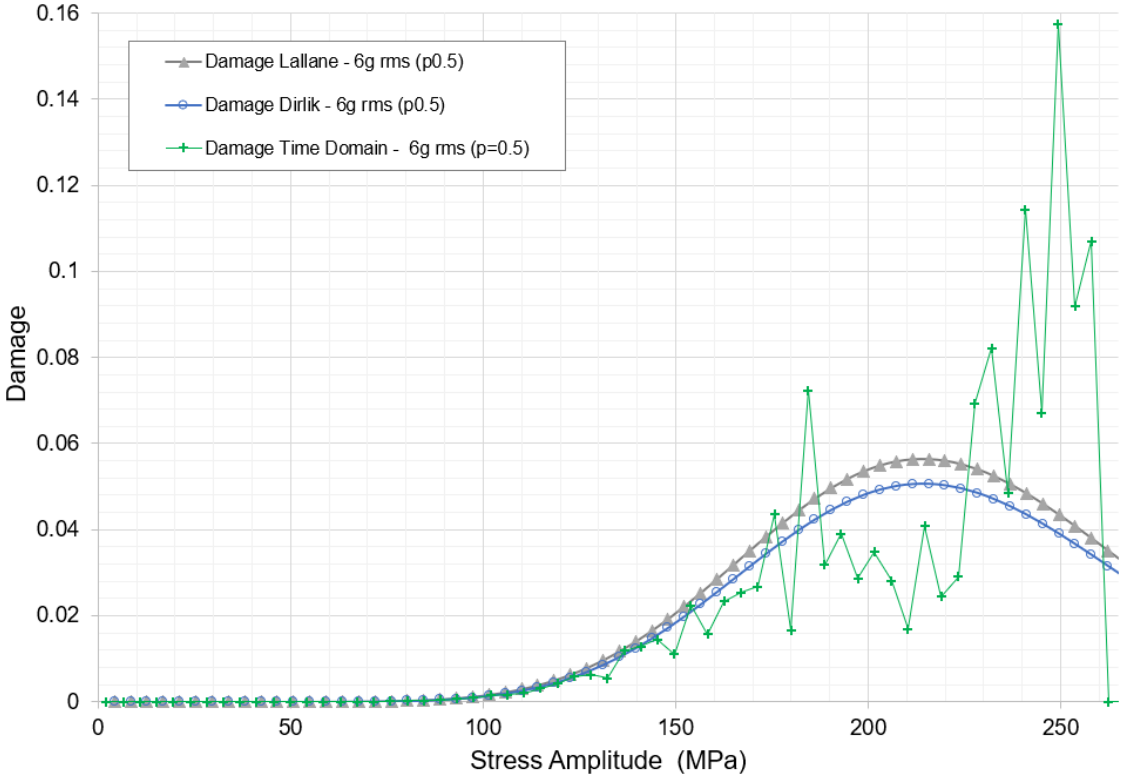

Source: Author

Figure 70 - Cumulative Damage as function of stress amplitude (p=0.5)

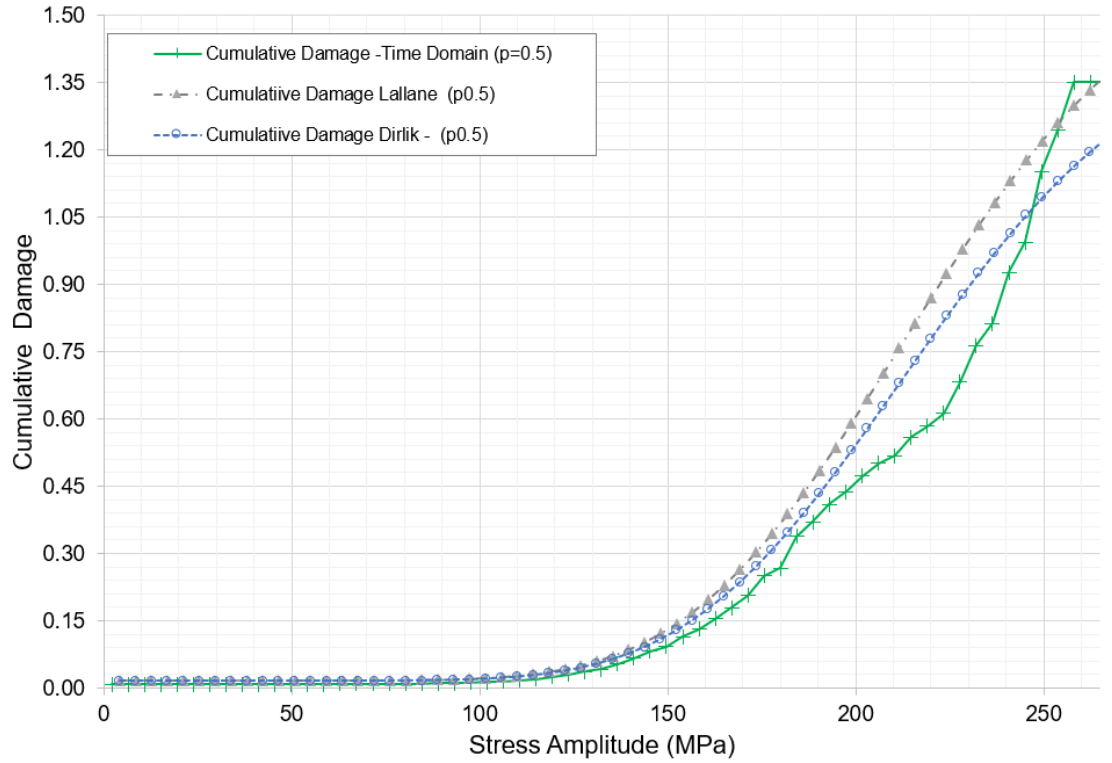

Source: Author

Despite the well-known limitations of the linear cumulative damage, the proper dynamic characterization of the structure via a representative damping modeling and the consideration of geometrical factors which affects the fatigue behavior were found in this work to significantly influence the fatigue life prediction under random vibration environment.

Considering the advantages in computational time of the frequency domain, the contribution of each factor in the fatigue life prediction was evaluated using the input $6g_{rms}$ input PSD with a 2500s duration and Lallane's method.

The baseline for comparison was defined based on the results from step 2 in Table 11. The time to failure for the $6g_{rms}$ input PSD considering constant damping ratio and unnotched S-N curve are shown in Table 17.

Table 17 –Time to failure estimation - $6g_{rms}$ input PSD – Modeling Factors

	Rayleigh damping k_f=1.14 (p=0.5)	Damp. Ratio ζ = 1% Unnotched S-N curve	Damping Ratio ζ = 1% k_f=1.14 (p=0.5)
Damage	1.34	0.4	1.27
Life (repeats)	0.73	2.5	0.79
TTF (s)	1,821	6,250	1,969
TTF Error (%)	Baseline	243	8.1

The modeling of the notch effect on the fatigue strength reduction has reduced the estimated time to failure in 68.5%. The Rayleigh damping contributed to additional 7.52% reduction in the predicted time to failure. Considering fatigue strength reduction correction and constant damping ratio, the TTF is 8.1% higher than the predicted in the time domain, resulting in a non-conservative prediction.

There are various sources of variation when modeling fatigue in a random environment, however, using the linear cumulative damage with p=0.5 produced results in good agreement with testing, after the appropriate characterization of the effect of the notch and modeling of the damping. Another fact that contributed for the good agreement of the predictions, is the primarily uniaxial behavior of the stress tensor, which approximates the material response to the one obtained in the standard S-N test.

5 CONCLUSIONS AND RECOMMENDATIONS FOR FUTURE WORK

In this work the fatigue life of a notched component subjected to random vibration was estimated using the frequency domain alongside with the statistical modeling of the material S-N fatigue curves.

The fatigue life estimation based on the well-known time domain was used as the benchmark solution. The fatigue strength reduction in the presence of a notch was estimated based on the volumetric approach. The proper correction of the base S-N curve (p=0.5) had an influence in the fatigue life estimation of approximately 69%, thereafter, including the effects of geometric discontinuities is critical to the accuracy of the prediction.

The probabilistic modeling of S-N curves aimed the model of the inherent scatter observed in the fatigue testing data. If the material behavior can be modelled using Basquin's relation, the ordinary least square method can be used to determine the percentile curves. For materials that exhibit strong curvature caused by the fatigue limit, the Random Fatigue Limit model is recommended.

The observation of the harmonic excitation response from the physical testing of the AL 6061-T6 specimen showed a frequency dependency of the damping ratio. Based on the testing results a Rayleigh damping model was used improving the accuracy of the dynamic response of the structure in the simulation model. The fatigue life using Rayleigh damping compared to a constant damping ratio produced results approximately 8% more conservative.

Based on Palmgreen-Miner's rule, the probabilistic linear cumulative damage was proposed to account for the damage at specific S-N percentile. In the probabilistic approach not only the commonly used percentile 50% (p=0.5) is used to calculate the fatigue life, but also any other quantile, resulting in a range of fatigue life rather than one unique value.

Between the two methods that have been used for the cycles count in the frequency domain, Lallane's method presented 10.5% more conservative results than the Dirlik's method. Both methods are in good agreement with the results obtained from the time domain.

Once the main modeling parameters were refined, the fatigue life prediction from the frequency domain were in good agreement with both time domain and average physical testing TTF for the percentile 0.5.

Even though the fatigue life estimations using the percentile 0.99 are non-conservatives and are not recommended to be used for design purposes, the visualization of

the envelope created over the data alongside with the range of life predictions could be used in the evaluation and determination of safety factor as well as interpretation of physical testing results.

Finally, for the notched specimen model presented in this work, the total calculation time to solve the model in the time domain was 42 hours, in comparison to 2.5 hours in the frequency domain, this great advantage in terms of computational time allows the application of the frequency domain method to solve much larger and complex problems using finite element analysis, thus, efforts to improve its accuracy are worthwhile.

A suggestion for future work would be to explore the application of the probabilistic linear cumulative damage using Random Fatigue Limit Model for the high cycle fatigue problems.

Another area for improvement is to investigate the application of the volumetric approach to create corrected fatigue curves for stress concentration design features in complex geometries.

Moreover, the expansion of the frequency domain methods to include the mean loading could be studied.

REFERENCES

1. SURESH, S.; **Fatigue of Materials**, Cambridge University Press (Cambridge), 1991.

2. DOWLING, N. E.; **Mechanical Behavior of Materials**, Prentice Hall (Upper Saddle River, NJ), 1999.

3. FATEMI, A.; YANG, L.; **Cumulative fatigue damage and life prediction theories: a survey of the state of the art for homogeneous materials**, Int Journal of Fatigue, Vol 20, No. 1, pp 9-34, 1998.

4. CASTILLO, E.; FERNANDEZ-CANTELI, A.; ***A unified Statistical Methodology for Modeling Fatigue Damage***, Springer, 2009.

5. NELSON, W.; **Fitting of fatigue curves with non-constant standard deviation to data with runouts**, Journal of testing and evaluation,12:69-77, 1984.

6. NELSON, W.; **Accelerated Testing: Statistical Models, Test Plans, and Data Analysis**, John Wiley & Sons, 1990.

7. PASCUAL, F.G.; MEEKER, W.Q.; **Estimating Fatigue Curves with the Random Fatigue-Limit Model, *Technometrics***, 41:277-289, Nov 1999.

8. TEIXEIRA, G.M.; ***Random Vibration Fatigue Analysis of a notched aluminum Beam***, Int. J. Mech. Eng Autom. Vol 2, Number 10, pp. 425-441, 2015.

9. ASTM E 1150-1987, **Standards Definition of Fatigue, 1995 Annual Book of Standards**, ASTM, pp 753-762, 1995.

10. ASM, **Handbook Fatigue and Fracture,** Volume 19, 1996.

11. SCHIJVE, J.; **Fatigue of structures and materials in the 20th century and the state of the art**, Int Journal of Fatigue 25, pp 679-702, 2003.

12. DNVL; **DNVGL-RP-C203, Fatigue Design of Offshore Steel Structures**, Det Norske Veritas, Norway, 2016.

13. PLUVINAGE, G.; **Fracture and Fatigue Emanating from Stress Concentrators**, Kluwer Academic Publishers, 2003

14. MCKELVEY, S.A., LEE, YL.; BARKEY, M. E.; **Stress-Based Uniaxial Fatigue Analysis Using Methods Described in FKM-Guideline**, J Fail. Anal. and Preven.12, pp 445-484, 2012.

15. PETERSON, R.E., **Notch Sensitivity**, in: G. Sines and J.L Waisman (eds.), Metal Fatigue, McGraw Hill, New York, pp.293-306, 1959.

16. ADIB, H., GILBERT, J., PLUVINAGE, G.; **Fatigue Life Duration Prediction for Welded Spots by Volumetric Method**, Int. Journal of Fatigue 26, pp. 81-94, 2004.

17. ANSYS**, Theory Reference for the Mechanical APDL and Mechanical Applications**, Release 12.0, 2009.

18. MATSUISHI, M. and ENDO, T.; **Fatigue of metals subjected to varying stress**. Japan Society of Mechanical Engineers, 1968.

19. LALLANE, C., **Mechanical Vibration and Shock Analysis**, Fatigue Damage, Volume IV, Wiley, 2009.

20. BENDAT, J.S., PIERSOL, A.G., **Random Data Analysis and Measurement Procedures**, 4th edition, John Wiley & Sons, Ltd., 2010.

21. BRANDT, A., **Noise and Vibration Analysis: Signal Analysis and Experimental Procedures**, John Wiley & Sons, Ltd., 2011.

22. RICE, S.O.; **Mathematical Analysis of Random Noise**. Bell Syst. Tech. J., vol 23, pp.282-332, 1944.

23. BENDAT, J.S., **Probability Functions for Random Responses**, NASA report on Contract NASA-5-4590, 1964.

24. TEIXEIRA, G., **Random Vibration Fatigue – A Study Comparing Time Domain and Frequency Approaches for Automotive Application**, SAE Technical Paper 2014-0-0923, 2014.

25. QUIGLEY, J.; LEE, Y.; WANG, L., **Review and Assessment of Frequency-Based Fatigue Damage Models**, SAE Int. J. Mater.Manf. 9(3): 565-577, 2016

26. IRVINE, T.; **Vibrationdata Matlab Signal Analysis & Structural Dynamic Package**, ver. 14.2 release July 22nd, 2020 [Online]. Available: https://vibrationdata.wordpress.com

27. SONG, Z., SU, C., **Computation of Rayleigh Damping Coefficients for the Seismic Analysis of a Hydro-Powerhouse**, Shock and Vibration. 2017, Article ID2046345,11 pages, 2017.

28. MILES, J. W.; **On structural Fatigue under random loading**. Journal of the Aeronautical Sciences, vol. 21, pp.753-762, 1954.

29. RYCHLIK, I; **On the narrowband approximation for expected fatigue damage**. Prob. Engineering Mechanics, 8,1-7, 1993a.

30. DIRLIK, T.; **Application of Computers in Fatigue Analysis**. PhD thesis, The University of Warwick, 1985.

31. HALFPENNY, A.; **A frequency domain approach for fatigue life estimation from Finite Element Analysis**. In M. D. Gilchrist, J. M. Dulieu Barton, and K. Worden, editors, DAMAS 99: Damage Assessment of Structures, volume 167-1 of Key Engineering Materials, pages 401–410, 1999.

32. SCHNEIDER, C.R.A., MADDOX, S.J, **Best Practice Guide on Statistical Analysis of Fatigue Data**, International Institute of Welding, document number Doc IIW-XIII-WG1-114-03, 2003

33. EVANS, M., NICHOLAS H., PEACOCK, B., **Statistical Distributions**, 2nd ed, New York, J. Wiley, 1993.

34. POLLAK, R.D.; **Analysis of methods for determining high cycle fatigue strength of a material with investigation of Ti-6AL-4V gigacycle fatigue behavior**. PhD thesis, Air Force Institute of Technology, 2005.

35. PASCUALINOTTO JUNIOR, V.; BURGOS, DFS. **Fatigue Life Estimation Using Frequency Domain Technique and Probabilistic Linear Cumulative Damage Model**." Proceedings of the. Volume 3: Design and Analysis. Virtual, Online. August 3, 2020. V003T03A045. ASME, 2020.

36. MIL-HDBK-5G, Military Handbook – **Metallic Materials and Elements for Aerospace Vehicles Structures**, Vol. 1 and 2, 1994.

APPENDIX A – MATLAB ROUTINE

This appendix presents the implementation of a MATLAB routine to calculate the fatigue strength reduction factor k_f based on the volumetric approach discussed in section 2.3.

```
% Fatigue Strength Reduction Factor - Volumetric Approach
% By Vagner Pascualinotto Junior,  v1.0 - Feb, 2021
% vagnerpj@gmail.com
clc
clear all
disp(' Select file input       ');
disp('   1=external ASCII file        ');
file_choice = input('');
%
      if(file_choice==1)
      [filename, pathname] = uigetfile('*.*');
      filename = fullfile(pathname, filename);
      fid = fopen(filename,'r');
      SCANFILE = fscanf(fid,'%g %g',[2 inf]);
      SCANFILE=SCANFILE';
      end

size(SCANFILE);
x=SCANFILE(:,1);
y=SCANFILE(:,2);

Fx=gradient(x)
Fy=gradient(y)

dFy=gradient(y,x)
Qsi=(1/(max(y)))*dFy
Qsi1=abs(Qsi)

index = find(Qsi==min(Qsi))
xeff=x(index)
SigmaN=mean(y)

      for i=1:index
       Integral(i)=y(i)*(1-(x(i)*Qsi1(i)))*Fx(i)
      end

cintegral = cumtrapz(Integral)
cintegral=cintegral'
Intergral=Integral'
Sigmaeff=(1/(xeff))*cintegral

kf0=Sigmaeff/SigmaN

kf=(1/(xeff*SigmaN))*cintegral

semilogx(x,y)
grid on
yyaxis right,
semilogx(x,Qsi)
grid on
```